NASA TM- 84419

NASA Technical Memorandum 84419

NASA-TM-84419 19830013983

An Atlas of November 1978 Synthetic Aperture Radar Digitized Imagery for Oil Spill Studies

H. E. Maurer

W. Oderman

and

W. F. Crosswell

February 1983

NASA

National Aeronautics and
Space Administration

Goddard Space Flight Center
Wallops Flight Facility
Wallops Island, Virginia 23337

NASA Technical Memorandum 84419

An Atlas of November 1978 Synthetic Aperture Radar Digitized Imagery for Oil Spill Studies

H. E. Maurer
NASA Goddard Space Flight Center
Wallops Flight Facility
Wallops Island, Virginia 23337

W. Oderman
Computer Sciences Corporation
Pocomoke City, Maryland 21851

W.F. Crosswell
Harris Corporation
Government Electronic Systems Division
Melbourne, Florida 32901

NASA
National Aeronautics and
Space Administration

Goddard Space Flight Center
Wallops Flight Facility
Wallops Island, Virginia 23337

N83-22254#

TABLE OF CONTENTS

LIST OF FIGURES

Figure		Page

Figure | Page

LIST OF TABLES

SYMBOLS

AOL	Airborne Oceanographic Lidar
CCTV	Closed circuit television
CCRS	Canada Centre for Remote Sensing
dB	Decibels
DCLS	Dual channel line scanner
dBSM	Decibels relative to a target with one square meter cross-section
ERIM	Environmental Research Institute of Michigan
GHz	Gigahertz
km	Kilometer
kw	Kilowatts
L	An approximate frequency range of 1.0 to 2.0 gigahertz
L_{HH}	L-Band, transmitted and received in horizontal polarization
L_{HV}	L-Band, transmitted in horizontal and received in vertical polarization
LFS	Laser fluorosensor
LLLTV	Low light level television
m	Meter
MS	Microwave scatterometer
MSS	Multispectral scanner
NOAA	National Oceanic and Atmospheric Administration
R_g	Ground range
RCS	Radar cross-section
R_L	Reference gain for L-Band digital image formation
RSA	Canadian DC-3 aircraft (Registration C-GRSA)
RSC	Canadian CV-580 aircraft (Registration C-GRSC)
R_X	Reference gain for X-Band digital image formation
SAR	Synthetic aperture radar
SCR	Surface Contour Radar
X	An approximate frequency range of 8.0 to 12.5 gigahertz
X_{HH}	X-Band, transmitted and received in horizontal polarization
X_{HV}	X-Band, transmitted in horizontal and received in vertical polarization
x	Difference, in slant range, of an arbitrary point P and far range
σ_0	Radar cross-section of target
σ_X	Radar cross-section of target at X-Band
σ_L	Radar cross-section of target at L-Band
θ_X	Depression angle, the angle the range vector makes with the horizontal

AN ATLAS OF NOVEMBER 1978 SYNTHETIC APERTURE RADAR DIGITIZED IMAGERY FOR OIL SPILL STUDIES

H. E. Maurer
NASA Goddard Space Flight Center
Wallops Flight Center
Wallops Island, VA 23337

W. Oderman
Computer Sciences Corporation
Pocomoke, MD 21851

W. F. Croswell
Harris Corporation
Government Electronic Systems Division
Melbourne, FL 32901

SUMMARY

A data set is described which consists of digitized synthetic aperture radar (SAR) imagery plus correlative data and some preliminary analysis results. This data set should be of value to experimenters who are interested in the SAR instrument and its application to the detection and monitoring of oil on water and other distributed targets. The SAR imagery was acquired during field experiments conducted during November 2 and 3, 1978.

INTRODUCTION

A set of synthetic aperture radar (SAR) digitized imagery as well as its correlative (supporting) data was acquired during a November 1978 series of experiments which were conducted to study the spreading and dispersal of crude oil on the sea. The November experiments were supported by the American Petroleum Institute in cooperation with the Environmental Protection Agency. The oil spills were made from the Research Vessel Annandale in the test area shown in Figure 1. This area (dump site 106), 30 miles off

the coast of New Jersey, conformed to the requirements of an EPA permit. The spills were in a quadrangle bounded by:

Latitude: 39°40'00" to 40°10'00" N
Longitude: 73°10'00" to 73°40'00" N

A total of four separate spills were conducted but SAR imagery was acquired only for the first two spills, i.e., the spills of November 2 and 3, 1978.

Remote sensors on aircraft platforms were assembled under the operational control of NASA. The sensors were selected on the basis of being candidate sensors for future satellite systems. These candidate sensors included both L-band and X-band SAR systems which were flown aboard medium altitude aircraft. See Table I for nominal specifications of these SAR systems. These systems acquire imagery simultaneously in the X and L-bands (see Reference 1).

TABLE I. NOMINAL SPECIFICATIONS FOR SYNTHETIC APERTURE RADAR

	X-Band	L-Band
Frequency (wavelength)	9.350 GHz (3.2 cm)	1.315 GHz (22.8 cm)
Transmitter Peak Power	1 kW	5 kW
Antenna Gain	28 dB	16.5 dB
Along Track Beamwidth	1.1°	7°
Depression Angle	0° to 90°	0° to 90°
Maximum Range	24.1 Km	24.1 Km
Pulsewidth	3 μsec	2 μsec
Resolution		
Range	1.5 m	2.3 m
Azimuth	2.1 m	2.1 m
Delay	38 μsec	38 μsec

Although the SAR has shown promise for use as a spacecraft sensor for surveillance and monitoring of the ocean for pollutants, SAR imagery is not currently admissible as courtroom evidence. Ships, waves, wind slicks, and radar shadows can all produce radar images that appear similar to those of oil. Also, the specific methods of image processing can produce artifacts which result in ambiguity. If machine processed oil detection systems based on SAR images are to be practical, then: optimum operating frequencies, polarizations, and incidence angles need to be determined; improved methods of

image analysis and precision calibration need to be developed; and higher power transmitters need development.

This research activity is in response to the United States Congress and its NASA Authorization Act of 1978 which directed NASA to investigate the potential of satellite systems and space technology to detect and monitor oil spills and ocean waste disposal in the United States waters. The goal is the development of a space system which would acquire pollutant information for and distribute it to the proper regulatory agencies.

DATA SET DESCRIPTION

The data set described in this report consists of digitized SAR imagery and correlative data acquired by in-situ and remote sensors of research oil spills on November 2 and 3, 1978. Remote sensors on aircraft platforms were assembled under the operational control of NASA. The sensors were selected on the basis of being candidate sensors for future satellite systems. The focus here is on the digital SAR imagery.

While a total of four separate spills were conducted, SAR imagery exists only for the first two spills. These spills of November 2 and 3, 1978, were allowed to spread and age for about two hours at which time a dispersant was applied by helicopter. Each spill consisted of 440 gallons of crude oil.

Digitized SAR Imagery

The Environmental Research Institute of Michigan (ERIM) SAR mounted on a CV-580 aircraft was used to acquire imagery of the oil spills. Both X-band and L-band SARs were flown aboard this medium altitude aircraft. See Table I for the nominal specifications of this SAR system. This SAR is ordinarily capable of transmitting either horizontal or vertical polarization and receiving both like and orthogonal polarization. However, during the oil spill experiment the vertical polarization transmitter malfunctioned. The SAR system produces four independent strip maps of the recorded echo on film for post flight processing by the ERIM optical processing facility. The recorded scenes are approximately six kilometers wide. The SAR geometry for a nominal 18,000 foot (5.486 km) altitude is illustrated in Figure 2.

At an altitude of 18,000 feet, a round trip propagation velocity of 490 feet (149.4 meters) per microsecond, and a delay time to the start of the image of 38 microseconds, then the distance to the near-edge of the image is 18,690 feet (5.6967 km) and the distance to the far end of the image is 37,380 feet (11.3934 km). If x represents the

difference in meters in slant range between an arbitrary point P and far range, and θ_x is the depression angle of point P, then

$$\theta_x = \text{Arc Sin } \frac{5{,}486.4}{11{,}393.4-x}$$

the depression angle is seen to vary between 29 degrees and 74 degrees. The corresponding incidence angles are 61 degrees and 16 degrees.

Figure 3 displays the two way antenna patterns for the SAR, where Figure 3a is the pattern for X_{HH} and Figure 3b is the pattern for L_{HH}. The mechanical bore site in Figure 3a is set at a depression angle of ten degrees, and the corresponding electrical bore site is at a depression angle of about four degrees. Since the depression angle entries in the flight logs refer to the position of the mechanical bore site, the "real" X_{HH} antenna depression angle is six degrees above those recorded entries. The mechanical bore site in Figure 3b is set at 180 degrees and the measurements were made in an anechoic chamber.

The SAR made six passes over the oil spill on November 2 and seven passes on November 3. In addition, the SAR made one pass over the corner reflector target range at Wallops on November 2 and two passes on November 3. A subset of this SAR imagery was chosen for digitization on the basis of its estimated potential for further analysis. This digitized SAR imagery is listed in Tables II and III and includes three passes over the oil spill and one pass over Wallops on November 2, and four passes over the oil spill and two passes over Wallops on November 3. The SAR imagery listed in Tables II and III is archived at Wallops and can be made available to interested and qualified experimenters. Figures 4 to 15 include most of the images listed in these tables. The noise files in Tables II and III were recorded at the time of digitization to provide a means to evaluate the noise injected by the ERIM image processor during the image formation and digitization process. The prints for Figures 4 to 15 inclusive were made from film transparencies written by a digital microdensitometer. The microdensitometer produces a pixel on film which was set to either a square 25 or 50 micrometer on a side. Any of these pixels can in turn represent either 1.5 or 3 meter squares depending upon the parameters set at the time of digitization.

The average altitude for these SAR passes is estimated at 18,800 feet (5.4864 km) with some passes exceeding 19,000 feet (5.7912 km). It will be necessary for a user of this imagery to make his own best estimate of altitude prior to his analysis.

TABLE II. DIGITIZED SAR IMAGERY ACQUIRED NOVEMBER 2

Time of Acquisition GMT HHMM	Scene	Pass	Mode	Pixel Size m	Tape/ File	Comments
1753	Oil	1	L_{HH}	1.5	564/1	021LHODB
	Noise	-	-	-	564/2	Noise for 564/1
1753	Oil	1	X_{HH}	1.5	632/1	021XHODB/2A&2B Includes Ship Wakes
1753	Oil	1	X_{HH}	1.5	550/1	021XHODB
1806	Oil	2	X_{HH}	1.5	550/2	022XHODB
1806	Oil	2	L_{HH}	1.5	565/1	022LHODB
	Noise				565/2	Noise for 565/1
1806	Oil	2	X_{HH}	1.5	633/1	Includes Ship Wakes 022XHODB/W2
1806	Oil	2	X_{HH}	1.5	634/1	Continuation of 633/1 022XHODB/W1
1822	Oil	3	-	-	-	No Digital Data
1834	Oil	4	X_{HH}	1.5	555/1	024XHODB
1834	Oil	4	L_{HH}	1.5	566/1	024LHODB
	Noise	-			566/2	Noise for 566/1
1848	-	5	-	-	-	Aborted - No Data
1859	-	6	-	-	-	No Digital Data
1914	-	7	-	-	-	No Digital Data
2001	Wallops	8	L_{HV}	3	572/1	W28LHVODB3PS
	Noise	-	-	-	572/2	Noise for 572/1
2001	Wallops	8	L_{HH}	3	572/3	W28LHODB3PS
	Noise	-	-	-	572/4	Noise for 572/3
2001	Wallops	8	X_{HV}	3	575/1	W28XVODB3PS
	Noise	-	-	-	575/2	Noise for 575/1
2001	Wallops	8	X_{HH}	3	575/3	W28XHODB3PS
	Noise	-	-	-	575/4	Noise for 575/3
2001	Wallops	8	X_{HH}	1.5	575/5	W28XHODB
	Noise	-	-	-	575/6	Noise for 575/5

TABLE III. DIGITIZED SAR IMAGERY ACQUIRED NOVEMBER 3

Time of Acquisition GMT HHMM	Scene	Pass	Mode	Pixel Size m	Tape/ File	Comments
1557	Oil	1	-	-	-	No Digital Data
1610	Oil	2	X-HH	1.5	546/2	Tape Problems
1610	Oil	2	L-HH	1.5	566/3	032LHODB
-	Noise	-	-	-	566/4	Noise for 566/3
1610	Oil	2	X-HH	1.5	573/1	032XHODB/2
-	Noise	-	-	-	573/2	Noise for 573/1
1622	Oil	3	-	-	-	No Digital Data
1635	Oil	4	X-HV	1.5	545/2	034XVODB
1635	Oil	4	X-HH	1.5	546/1	034XHODB
1635	Oil	4	L-HH	1.5	567/1	034LHODB
-	Noise	-	-		567/2	Noise for 567/1
1635	Oil	4	L-HV	1.5	569/1	034LVODB
-	Noise	-	-		569/2	Noise for 569/1
1656	Oil	5	X-HH	3	468/1	Preliminary, No Print OXH35D1, 6mx6m correlator resolution
1656	Oil	5	X-HH	3	468/2	Preliminary, No Print 6mx20m correlator resolution
1656	Oil	5	X-HH	3	517/1	No Print, 6m x 6m, R_X
1656	Oil	5	X-HH	3	543/1	035XHODB3PS
1656	Oil	5	X-HH	1.5	543/2	035XHODB
-	Noise	-	-		543/3	Noise for 543/2
1656	Oil	5	L-HH	1.5	544/1	035LHODB
-	Noise	-	-		544/2	Noise for 544/1
1656	Oil	5	X-HV	1.5	545/1	035XVODB
1656	Oil	5	L-HH	3	568/3	035LHODB3PS
-	Noise	-	-		568/4	Noise for 568/3
1656	Oil	5	L-HV	1.5	568/5	035LVODB
-	Noise	-	-		568/6	Noise for 568/5
1709	Oil	6	X-HH	1.5	551/3	036XHODB
1709	Oil	6	L-HH	1.5	568/1	036LHODB
1709	Noise	-	-		568/2	Noise for 568/1
1721	Oil	7	-	-	-	No Digital Data
1821	WFC	8	X-HH	3	519/1	R_X, 6m x 6m resolution, W38D63XHH300

TABLE III. DIGITIZED SAR IMAGERY ACQUIRED NOVEMBER 3 (continued)

Time of Acquisition GMT HHMM	Scene	Pass	Mode	Pixel Size m	Tape/ Tile	Comments
1821	WFC	8	X-HV	3	519/2	R_X, 6m x 6 m resolution, W38D63XHV300
1821	WFC	8	X-HH	1.5	520/1	W38D61XHH300, R_X
1821	WFC	8	L-HH	3	572/6	File 5 is Noisy
-	Noise	-	-		572/7	Noise for 572/6
1821	WFC	8	L-HV	3	572/8	W38LVODB3PS
-	Noise	-	-		572/9	Noise for 572/8
1821	Oil	8	X-HH	1.5	573/3	W38XHODB
-	Noise	-	-		573/4	Noise for 573/3
1821	Oil	8	X-HV	1.5	574/1	W38XVODB
1821	Noise	-	-		574/2	Noise for 574/1
1835	WFC	9	X-HH	3	515/1	R_X, W39D63XHH300
1835	WFC	9	X-HH	3	516/1	R_X-10dB, W39D63XHH030
1835	WFC	9	X-HH	1.5	518/1	R_X, W39D61XHH300
1835	WFC	9	X-HH	3	518/2	R_X-23 dB, W39D63XHH1.5
1835	WFC	9	X-HV	3	520/2	R_X, W39D63XHV300
1835	WFC	9	X-HH	1.5	547/1	R_X; Slant/ground range corrected, W39XHODB
1835	WFC	9	X-HH	1.5	548/1	R_X-34.3dB, W39XH-34.3DB
1835	WFC	9	X-HH	1.5	549/1	R_X-21.3dB, W39XH-21.3DB
1835	WFC	9	X-HH	1.5	549/2	R_X-11dB, W39XH-11.0DB
1835	WFC	9	X-HV	1.5	570A/1	R_X; Slant/ground range corrected, W39XVODBGR
1835	WFC	9	X-HV	1.5	570B/1	Continuation of 570A/1 W39XVODBGR/B
1835	WFC	9	L-HH	3	571/1	R_L; Slant/ground range corrected, W39LHODBGR
1835	WFC	9	L-HV	3	571/2	R_L; Slant/ground range corrected, W39LVODBGR
1835	WFC	9	L-HV	3	572/10	W39LVODB3PS
-	Noise	-	-	-	572/11	Noise for 572/9
1835	WFC	9	L-HH	3	572/12	R_L; W39LHODB3PS
1835	WFC	9	X-HV	1.5	574/3	R_X; W39XVODB
-	Noise	-	-	-	574/4	Noise for 574/3

Correlative Data for the SAR Sensor

This section discusses the supporting or correlative data which was acquired during the experiment, data which was acquired that might aid in the analysis of the SAR imagery. Although all such data is not explicitly listed here, it is intended to include enough information so that the interested experimenter can determine whether the type of data which supports his interest may exist. Correlative data was acquired by remote sensors onboard the aircraft, by measurements made from ships, and by use of a corner reflector target range at Wallops. See Reference 2 for a more complete description of the sensors. Time lines are included to indicate the potential existence of specific types of correlative data. Figure 16 and Table IV contain time line information for November 2, while Figure 17 and Table V contain time line information for November 3.

TABLE IV. SAR RELATED EVENTS DURING NOVEMBER 2

Time GMT HHMMSS	Description of Event
1653	Start Oil Spill. Murban Crude
1713	Start Sea Sample
17?	Deploy 4 Radar Markers (Corner Reflectors) with Buoys
1732	Finish Sea Sample
175316 to 175337	Overflight of Oil by Aircraft RSA. Flight Line 14
175533	SAR Image of Oil. Pass 1 of Aircraft RSC
175535 to 175602	Overflight of Oil by Aircraft RSA @ 1000 ft. Flight Line 15. Vinten Camera 4081/186-7 4080/
180531 to 180550	Overflight of Oil by Aircraft RSA. Flight Line 19. Vinten Camera 4081/214-16, 4080/214-216
180649	SAR Image of Oil. Pass 2 of Aircraft RSC
180746 to 180802	Overflight of Oil by Aircraft RSA. Flight Line 20. Cameras 4081/233-4, 4080/222-6
182331 to 182352	Overflight of Oil by Aircraft RSA. Flight Line 25. Cameras 4081/243-5, 4080/244-5
183638	SAR Image of Oil. Pass 4 of Aircraft RSC. Three Corner Reflectors Visible.
1850	Start Spray of Dispersant from Helicopter
1915	Finish Spray of Dispersant from Helicopter
1923	Start Sea Sample from Ship
1945	Finish Sea Sample from Ship
2004	SAR Image of Wallops. Pass 8 of Aircraft RSC

TABLE V. SAR RELATED EVENTS DURING NOVEMBER 3

Time GMT HHMMSS	Description of Event
151400	Start Oil Spill. LaRosa Crude
15?	Deploy 4 Radar Markers (Corner Reflectors) with Buoys from Ship
161129	SAR Image of Oil Scene. Pass 2 of RSC. Two Reflectors Visible-One in Tail of Slick
162746 to 162834	Overflight of Oil by RSA @ 1500 feet. Flight Line 2. Vinten Cameras 4081/273-275, 4080/274-276, Fluorosensor, LLTV, MSS
163248 to 163316	Overflight of Oil by RSA @ 1500 feet. Flight Line 4. Vinten Cameras 4081/283-5, 4080/284-6, Fluorosensor, LLTV, MSS
163740	SAR Image of Oil Scene. Pass 4 of RSC. No Reflectors Evident
163913 to 163939	Overflight of Oil by RSA @ 700 feet. Flight Line 5. Vinten Cameras 4081/288-290, 4080/289-290, Fluorosensor, LLLTV, MSS
1655	Start Dispersant Spray from Helicopter
165543 to 165624	Overflight of Oil by RSA @ 3500 feet. Flight Line 10. Vinten Cameras 4081/306-7, 4080/307-8, LLLTV, MSS
165935	SAR Image of Oil Scene. Pass 5 of RSC. 1 Buoy but No Reflectors Visible in SAR Imagery
165919 to 170024	Overflight of Oil by RSA @ 3500 feet. Flight Line 10. Vinten Cameras 4081/306-7, 4080/307-8, LLLTV, MSS
170559 to 170629	Overflight of Oil by RSA @ 3500 feet Flight Line 12. MSS, Vinten Cameras 4081/325 4080/325-6.
1710	Finish Dispersant Spray from Helicopter.
1711	SAR image of Oil Scene. Pass 6 of RSC
171659 to 171802	Overflight of Oil by NASA Aircraft. Flight Line 11.
171830 to 171935	Overflight of Oil by RSA @ 1000 feet. Flight Line 14. Fluorosensor, LLLTV, MSS Vinten Cameras 4081/332-4, 4080/333-4
172248 to 172353	Overflight of Oil by NASA Aircraft. Flight Line 12.
172833 to 172936	Overflight of Oil by NASA Aircraft. Flight Line 13.
173311 to 173404	Overflight of Oil by NASA Aircraft. Flight Line 14.
173758 to 173851	Overflight of Oil by NASA Aircraft. Flight Line 15.

TABLE V. SAR RELATED EVENTS DURING NOVEMBER 3 (continued)

Time GMT HHMMSS	Description of Event
174230 to 174316	Overflight of Oil by NASA Aircraft. Flight Line 16.
174731 to 174821	Overflight of Oil by NASA Aircraft. Flight Line 17.
175231 to 175338	Overflight of Oil by NASA Aircraft. Flight Line 18.
1837	SAR Image of Wallops. Pass 9 of RSC.
193008 to 193106	Overflight of Wallops by RSA @ 500 feet. Flight Line 30. MSS, Vinten Cameras 4081/443-55 4090/43-55.
193403 to 193449	Overflight of Wallops by RSA @ 500 feet. Flight Line 31. MSS, Vinten Cameras 4081/457-69, 4090/58-70.

TABLE VI. SENSOR COMPLEMENT FOR CCRS CV-580

ERIM Synthetic Aperture Radar (SAR)
Dual Channel Line Scanner (DCLS)
Wild Heerbrugg RC-10 Camera
Microwave Scatterometer (MS)
Closed Circuit Television (CCTV)
Side Looking 35 mm Cameras

The synthetic aperture radar was mounted on a CV-580 aircraft (Registration C-GRSC). This aircraft, often called RSC, had the sensor complement of Table VI. All of these sensors acquired data which was in time space coincidence with that of the SAR except for the Dual Channel Line Scanner. The Dual-Channel Line Scanner, Daedalus Model 1230, is an optical/mechanical line scanning radiometer that records energy reflected or emitted from the Earth's surface in the ultraviolet and thermal infrared bands. The Wild Heerbrugg RC-10 is a 23 cm by 23 cm format aerial mapping camera. The Microwave Scatterometer, Ryan Model 720, with a transmitter frequency of 13.3 GHz, measures absolute radar backscatter cross-section as a function of look angle from nadir.

The Canadian DC-3 aircraft (Registration C-GRSA), often called RSA, had the sensor complement of Table VII. The multispectral scanner , Daedalus Model 1260, is a multichannel, optical-mechanical, nine-scan spectrometer which records energy reflected or emitted from the Earth's surface. The CCRS MkII Laser Fluorosensor is a pulsed UV,

TABLE VII. SENSOR COMPLEMENT FOR CCRS DC-3

Multispectral Scanner (MSS)
Laser Fluorosensor MKII (LFS)
Vinten 70 mm Camera
Closed Circuit Television (CCTV)
Low Light Level Television (LLLTV)
Multiple Detector Electro-Optical Imaging Scanner (MEIS)

TABLE VIII. SENSOR COMPLEMENT FOR NASA C-54

Airborne Oceanographic Lidar (AOL)
Scanning Microwave Radiometer 22,31 GHz
Radiometer, PRT-5
TV Camera
Photography

laser-activated, range-gated fluorescence detector, where a medium resolution spectrometer allows the fluorescent return to be categorized.

The NASA Wallops C-54 (NASA 427) sensor complement is listed in Table VIII. The Airborne Oceanographic Lidar is a conically scanning pulsed laser system which operates in either the bathymetric or the fluorosense mode. In the fluorosensing mode a short pulsed dye laser is used to stimulate waterborne oils, chlorophyll, or dyes which in turn emit characterisitc radiation that is spectrally resolved into forty (40) spectrometric channels spanning from 350 nm to 800 nm. The dual channel (22 and 31 GHz) scanning microwave radiometer has been used by Hollinger to infer oil thickness ($\geq$0.1 mm) and oil volume (see References 3 and 4). This Naval Research Laboratory instrument was operated by LaRC staff. Additional instruments flown on the Wallops C-54 were nadir-pointed 70 mm and 35 mm photographic cameras, and a nadir-pointed black-and-white TV camera with video tape recorder.

The actual oil spills as well as in situ water column sampling runs were made from the Research Vessel Annandale. The Annandale took samples both by dipping a bucket over the side, and by use of an onboard pump sampling system. This pump system collected samples at depths of one, three, and six meters. In addition, the following in-situ data was acquired: wind speed and direction, air temperature, water temperature as a function of depth, wave height, current directions, and salinity concentrations. Also, the National Oceanic and Atmospheric Administration (NOAA) Research Vessel Kelez provided support by distributing surface radar reflector buoys and punched cards to track surface currents in the area of the spills.

Figures 16 and 17 and Tables IV and V should illustrate enough of the Experiment time lines that a potential user can identify the correlative data which might be available. These time lines do not include a United States Coast Guard C-130 which carried a real aperture X-band SLAR, and a JBF Skymaster II which monitored the oil spill with 70 mm cameras.

A set of radar reflectors was assembled at Wallops during the experiment. Figure 18 illustrates the layout of this SAR target range while Figure 19 illustrates the geometry of the individual corner reflectors. Table IX summarizes the available measurements for these targets. The numbered targets of Figure 18 correspond to those of Table IX. ERIM supplied reflectors 1-15, while Wallops supplied reflectors 16-21. The Luneberg Lens reflectors 22 and 23 belonged to Langley Research Center which was using them

TABLE IX. MEASUREMENTS OF RADAR REFLECTORS

Reflector	A Meters	B Meters	C Meters	σ_X Meter^2	σ_L Meter^2	σ_X dBsm	σ_L dBsm
1	1.652	1.169	0.826	8631	147	39.4	21.7
2	0.859	0.605	0.427	631	10.7	28.0	10.3
3	0.637	0.455	0.322	198	3.4	23.0	5.3
4	0.556	0.387	0.275	108	1.8	20.0	2.6
5	0.297	0.210	0.150	9.1	0.15	9.5	-8.2
6	1.644	1.164	0.826	8631	147	39.4	21.7
7	0.861	0.609	0.428	631	10.7	28.0	10.3
8	0.641	0.453	0.325	198	3.4	23.0	5.3
9	0.550	0.386	0.272	108	1.8	20.0	2.6
10	0.296	0.210	0.150	9.1	0.15	9.5	-8.2
11	0.299	0.210	0.150	9.1	0.15	9.5	-8.2
12	0.553	0.388	0.277	108	1.8	20.0	2.6
13	0.645	0.455	0.324	198	3.4	23.0	5.3
14	0.861	0.606	0.429	631	10.7	28.0	10.3
15	1.652	1.168	0.826	8631	147	39.4	21.7
16	0.969	0.682	0.484	1000	17	30.0	12.3
17	0.968	0.680	0.484	1000	17	30.0	12.3
18	0.968	0.681	0.483	1000	17	30.0	12.3
19	0.968	0.682	0.485	1000	17	30.0	12.3
20	0.969	0.681	0.486	1000	17	30.0	12.3
21	0.966	0.681	0.483	1000	17	30.0	12.3
22	1.405 m Circumference Luneberg						
23	Identical to Reflector 22						

for another experiment. Figures 20 and 21 are layouts of several sets of corner reflectors which are subsets of the target range. Figure 22 is a view of corner reflector 1. Figure 23 is a view, from left to right, of corner reflectors 17, 18, 19, 20, and 21. Figure 24 is a view of reflector 23. The targets were spread over enough distance so that calibration imagery would be available for several radar ranges. Also, a variety of sizes were used so as to include dynamic range effects. The SAR was to acquire imagery of the target range after completing each days passes over an oil spill. If the SAR imagery of the target range can be calibrated, then the calibration of the SAR imagery of the oil scenes could probably be inferred.

SOME RESULTS

This section describes the results of a preliminary analysis of some of the digitized SAR imagery. The results of the analysis of other individual sensor (correlative) data are available in the following references. Reference 2 includes a description of the analysis of the MSS imagery; References 5 and 6 discuss the AOL data; Reference 5 discusses the NRL microwave radiometer data; and References 2, 7, 8 and 9 discuss the results of analyzing the SAR imagery.

Table X displays the SAR X_{HH} returns for oil compared to returns from the ocean as a function of depression angle. This table indicates that the SAR X_{HH} oil/ocean contrast is not good for small depression angles (<30°). Depression angles are calculated for assumed altitudes of both 18,000 feet (5.4864 km) and 18,800 feet (5.7302 km) for this Table only. All other references to depression angles in this report assume an altitude of 18,000 feet (5.4864 km).

An examination of the SAR X and L-band imagery of this report indicates that the oil/ocean contrast is greater for the X_{HH} than for the L_{HH} imagery with the exception of Pass 6 on November 3. This single exception is probably due to the small depression angles involved. Such an examination also reveals that the oil/ocean contrast for the cross polarized X_{HV} and L_{HV} imagery are poor.

Calibration

The calibration procedure for the digital SAR imagery as supplied by ERIM is outlined in Figure 25. The uncalibrated digital SAR image is stored on a nine track magnetic tape where each pixel value relates to the relative power return. The calibration procedure includes adjustments for both the digitization process and the primary data

collection. The adjustments done because of the digitization process include terms for intensity of laser illumination and CRT response. For the SAR data itself, there is a normalization of range and the addition of a calibration constant. The final adjustment is the antenna gain correction of Figure 3. None of the SAR imagery of this section was calibrated prior to analysis, instead, all digital SAR imagery was used as it was produced by the ERIM image dissector.

Analysis results are next displayed for two examples, i.e., SAR Pass 2 on November 2 and SAR Pass 5 on November 3. The results are illustrated for Pass 2 by Figures 26-43, and for Pass 5 by Figures 44-69.

Example 1

The first example illustrates the processing and analysis of SAR imagery acquired during Pass 2 on November 2. Figures 26 to 34 are derived from the X-band imagery while Figures 35 to 43 are from the L-band imagery. Figure 26 is a contour plot of SAR X_{HH} returns processed at the reference gain, R_X, while Figure 27 is a 3D projection of these same returns. Figures 28 to 31 are across track profiles of ocean returns for SAR X_{HH} returns which should relate to the X_{HH} antenna correction of Figure 3. Figure 28 is an unfiltered, across track profile "as is" from the image dissector. Figure 29 is an across track profile in which each plotted point is the average of 500 along track pixels. Figure 30 is an across track profile in which a moving window of five pixels is passed along the plot of Figure 29. Figure 31 is an across track profile in which a moving window of 50 pixels is passed along the plot of Figure 29.

Figure 32 is an along track profile of X_{HH} returns from oil and ocean at a depression angle of 46°. A moving five pixel window is used along track. This constant range data is easier to interpret since the necessity to make range corrections is minimized.

Figure 33 is histograms of oil and ocean returns at a depression angle of 46 degrees. Figure 34 is histograms of areas of ocean and oil returns in a range of depression angles from 46 to 46.5 degrees.

Figure 35 is a contour plot of SAR L_{HH} returns processed at the reference gain, R_L, while Figure 36 is a 3D projection of these same returns. Figures 37 to 40 are across track profiles of SAR L_{HH} ocean returns which should relate to the L_{HH} antenna correction. Figure 37 is an unfiltered across track profile "as is" from the image dissector. Figure 38 is an across track profile in which each plotted point is the average of 500 along track pixels. Figure 39 is an across track profile in which a moving window of five pixels is passed along the plot of Figure 39. Figure 40 is an across track profile in which a moving window of 50 pixels is passed along the plot of Figure 38.

TABLE X. SAR X_{HH} OIL/OCEAN CONTRAST AS A FUNCTION OF DEPRESSION ANGLE

Depression Angle in Degrees		Day/Pass						
Assume Altitude of		2/1	2/2	2/4	3/2	3/4	3/5	3/6
18000'	18800'	dB	dB	dB	dB	dB	dB	dB
30.0	32.1							0.37
30.5	32.6							0.49
31.0	33.2							0.51
31.5	33.7							0.63
32.0	34.2							0.56
32.5	34.8							0.74
40.5	43.6	3.88						
41.0	44.2	4.13						
41.5	44.7	4.69					4.62	
42.0	45.3						4.43	
42.5	45.8						3.71	
43.0	46.4						3.83	
43.5	47.0						5.33	
44.0	47.5						4.73	
44.5	48.1						4.72	
45.0	48.7		1.82				4.53	
45.5	49.2		3.92				3.84	
46.0	49.8		3.55				3.21	
46.5	50.4		4.49				5.22	
47.0	51.0			3.62			4.64	
47.5	51.5			4.63	2.48		3.25	
47.9	52.0				3.17			
48.0	52.1			4.34	4.00			
48.5	52.7			4.17	3.33	4.41		
48.8	53.0				2.18			
49.0	53.3			4.74		5.61		
49.5	53.8			4.00		4.88		
50.0	54.4			4.70		5.26		
50.5	55.0			5.13		5.23		
51.0	55.6			3.33		2.79		
51.5	56.2			3.12				

Figure 41 is an along track profile of L_{HH} returns from oil and ocean at a depression angle of 46 degrees. A moving five pixel window is used along track.

Figure 42 contains histograms of oil and ocean returns at a depression angle of 46°. Figure 43 contains histograms of areas of oil and ocean returns in a range of depression angles from 46 to 46.5 degrees.

The histograms of Figures 33, 34, 42, and 43 all exhibit some of the same characteristics, i.e., that the mean value of the ocean returns is larger than the mean value of the oil returns, and that the variance of the oil returns is less than that of the ocean returns.

Example 2

The second example illustrates the processing and analysis of SAR imagery acquired during Pass 5 on November 3. Figures 44 to 56 are derived from X-band imagery while Figures 57 to 69 are from L-band imagery. Figure 44 is a contour plot of SAR X_{HH} returns processed at the reference gain, R_X, while Figure 45 is a 3D projection of these same returns. Figures 46 to 49 are across track profiles of SAR X_{HH} ocean returns which should relate to the X_{HH} antenna correction of Figure 3. Figure 46 is an unfiltered across track profile "as is" from the image dissector. Figure 47 is an across track profile in which each plotted point is the average of 500 along track pixels. Figure 48 is an across track profile in which a moving window of five pixels is passed along the plot of Figure 47. Figure 49 is an across track profile in which a moving window of 50 pixels is passed along the plot of Figure 47.

Figure 50 is an along track profile of X_{HH} returns from oil and ocean at a depression angle of 47 degrees. A moving five pixel window is used along track. This constant range data is easier to interpret since the necessity to make range corrections is minimized. Figure 51 is a repeat of Figure 50 for a depression angle of 43.5 degrees.

Figure 52 contains histograms of oil and ocean returns at a depression angle of 47 degrees. Figure 53 is a repeat of Figure 52 for a depression angle of 43.5 degrees. Figure 54 contains histograms of ocean and oil returns in a range of depression angles from 46 to 46.6 degrees. Figure 55 is a repeat, for X_{HV} returns, of Figure 50. Figure 56 is a repeat, for X_{HV} returns, of Figure 51.

Figure 57 is a contour plot of SAR L_{HH} returns processed at the reference gain, R_L, while Figure 58 is a 3D projection of these same returns. Figures 59 to 62 are across track profiles of SAR L_{HH} ocean returns which should relate to the L_{HH} antenna correction. Figure 59 is an unfiltered across track profile "as is" from the image dissector. Figure 60 is an across track profile in which each plotted point is the average of 500 along track pixels. Figure 61 is an across track profile in which a moving window of five

pixels is passed along the plot of Figure 60. Figure 62 is an across track profile in which a moving window of 50 pixels is passed along the plot of Figure 60.

Figure 63 is an along track profile of L_{HH} returns from oil and ocean at a depression angle of 47 degrees. A moving five pixel window is used along track. Figure 64 is a repeat of Figure 63 except the depression angle is changed to 43.5 degrees.

Figure 65 contains histograms of oil and ocean returns at a depression angle of 47 degrees. Figure 66 is a repeat of Figure 65 except that the depression angle is changed to 43.5 degrees. Figure 67 contains histograms of areas of oil and ocean returns in a range of depression angles from 46 to 46.5 degrees.

Figure 68 is a repeat of Figure 63 except that the polarization is changed to L_{HV}. Figure 69 is a repeat of Figure 68 except that the depression angle is changed to 43.5 degrees.

The histograms of Figures 52, 53, 54, 65, 66, and 67 all exhibit some of the same characteristics, i.e., that the mean value of the ocean returns is larger than the mean value of the oil returns, and that the variance of the oil returns is less than that of the ocean returns.

Distributed Targets

SAR images of the Wallops Flight Center corner reflector target range include areas which serve as distributed targets for the SAR, e.g., homogeneous areas of water, marsh, grass, and trees. Figure 70 and Table XI locate and define some of these targets.

Figure 70 locates the distributed targets on a SAR image of Wallops. This SAR X_{HH} image was acquired during Pass 8 on November 3 with near range on the right and the aircraft motion from top to bottom. The distributed targets are located at or near the numbered indicators. Figure 71 is an aerial photograph of Wallops taken by the RC10 camera on the CCRS CV-580 which can be used to determine ground truth such as the extent of the distributed targets.

Table XI identifies the distributed Wallops targets, while Table XII lists density measurements of these targets. The measurements were acquired by a densitometer with a one-millimeter aperture from an optically formed SAR X_{HH} image. Although the processing gain used was different than the reference gain, R_X, the results should give a qualitative indication of the differences between returns from these distributed targets.

Figure 72 is a listing of the SAR X_{HH} returns of each intensity level, from a small part of Target G2, which were acquired during Pass 9 on November 3. The SAR image was formed at the reference gain, R_X. Figure 73 is a histogram of the listing of Figure 72.

Figures 74 and 75 show the differences in radar returns between several of the distributed targets. These figures are filtered along track profiles of the SAR X_{HH} re-

TABLE XI. DISTRIBUTED SAR TARGETS AT WALLOPS FLIGHT CENTER

Symbol	Target Description	Target Location
T1	Trees	Mixed stand between pool and Tom's Cove
T2	Trees	Mixed stand near C&P Microwave Relay
T3	Trees	Conifers near Salvage Area
G1	Grass (and some shrubs)	Between Runway 04-22 & Chincoteague Causeway
G2	Grass	Between Runway 04-22 & Chincoteague Causeway
F1	Field	Across road from G houses
F2	Field	Across road from G houses
F3	Field	Middle bare field across Mosquito Creek from fuel storage area
F4	Field	Middle bare field across Mosquito Creek from fuel storage area
F5	Field	Bare field across Mosquito Creek from Sewage Plant
F6	Field	Across Mosquito Creek from Runway 17-35
F7	Field	Across Mosquito Creek from Runway 17-35
M1	Marsh	Across Mosquito Creek from Trail's End
M2	Marsh	At Trail's End
M3	Marsh	Simoneaston Bay marsh, north
M4	Marsh	Simoneaston Bay marsh, south
W1	Water	Mosquito Creek
W2	Water	Simoneaston Bay

TABLE XII. DENSITY MEASUREMENTS OF RETURNS FROM DISTRIBUTED SAR TARGETS

Target Area	Target Type	Density
W1	Water	0.48
W2	Water	0.48
W2	Water	0.48
W2	Water	0.44
M3	Marsh	1.06
G1	Grass	1.00
G2	Grass	1.03
G2	Grass	1.08
F1	Field	0.90
F2	Field	0.91
T1	Trees	0.99
T1	Trees	0.92

turns for Pass 9 on November 3. The reference gain, R_X, was used to form the SAR image. A moving along track window of five pixels was used as a filter for both figures. Figure 74 is an along track profile at 31.7 degree depression angle and Figure 75 is an along track profile at 37.1 degrees.

CONCLUSIONS

It is clear that SAR offers promise for use in the detection and areal distribution measurements of oil slicks; although, improved methods of analysis and calibration of SAR imagery are necessary if machine processed oil detection systems based on SAR satellite data are to be practical. Some of the remaining difficulties in the interpretation of SAR imagery for this application exist because wind slicks and other phenomena such as ship wakes and radar shadows can all produce radar images that in this limited analysis are indistinguishable from that due to oil slicks. These difficulties may possibly be resolved by more sophisticated analysis of this data set, but in any event, the data and analysis contained in this report add to the necessary information needed for development of improved methods of image analysis. This will, as well, contribute to SAR instrument development specifications for oil spill applications.

In the SAR imagery acquired during this experiment, the oil/ocean contrast was generally greater in the X_{HH} imagery than in the L_{HH} imagery. The cross polarized imagery did not exhibit any significant oil/ocean contrast. The SAR X_{HH} and L_{HH} returns of this experiment exhibited the following characteristics: the mean value of the ocean returns is larger than the mean value of the oil returns; and the variance of the oil returns is less than that of the ocean returns.

ACKNOWLEDGMENTS

Robert Rawson and Alex Klooster of the Environmental Research Institute of Michigan, who under Contract NAS1-15597 acquired, optically processed, and digitized the SAR imagery of this report. Robert Rawson also supplied the antenna corrections of Figure 3 and the calibration procedure of Figure 25. Dr. John D. Oberholtzer for his thorough review of the manuscript and his many helpful suggestions. Robert Swift of EG&G for generating the contour and 3D plots of SAR Pass 2 on November 2 and SAR Pass 5 on November 3. The staff of the Wallops Photolab who developed all the film based data products.

REFERENCES

1. Shuchman, R. A., R. F. Rawson and B. Drake, "A High Frequency and Dual Polarization Synthetic Aperture Radar System and Experiments in Agriculture Assessment," NAECON '75 Record, pp. 133-140.
2. "Analysis of Remote Sensing Data Collected for Detection and Mapping of Oil Spills," INTERA Environmental Consultants, Ottawa, Ontario, Canada, NASA Contractor Report 165886, May 1982.
3. Hollinger, J., R. Mennella, "Oil Spills: Measurements of Their Distribution and Volumes by Multifrequency Microwave Radiometry," <u>Science</u>, 181, 54, 1973.
4. Troy, B. and J. Hollinger, "The Measurement of Oil Spill Volume by a Passive Microwave Imager," NRL Report 3515, Naval Research Laboratory, Washington, DC, May 1977.
5. Croswell, W., J. Fedors, F. Hoge, R. Swift, J. Johnson and R. O'Neil, "Ocean Experiments and Remotely Sensed Images of Chemically Dispersed Oil Spills," soon to be published in the IEEE Transactions on Geoscience and Remote Sensing.
6. Hoge, F. and R. Swift, "Oil Thickness Measurement Using Airborne Laser Induced Water Raman Backscatter," <u>Applied Optics</u>, Vol. 19, No. 19, pp. 3269 to 3281.
7. Croswell, W., H. Maurer, R. Rawson, W. Oderman and J. Oberholtzer, "Analysis of SAR Imagery of Oil Spills on the Sea," presented at Symposium on Signature Problems in Microwave Remote Sensing of the Surface of the Earth, University of Kansas, January 1981.
8. Rawson, R. and C. Liskow, "Radar Reflectivity Measurements of Ocean Surface With and Without a Surface Coat of Oil," Proceedings of the IGARSS, June 1981.
9. Rawson, R., Final Report for Contract NAS1-15597, Environmental Research Institute of Michigan, Ann Arbor, Michigan, 1982.
10. Thomson, V., R. Neville, R. Hawkins and A. Gray, "Observation of Two Test Oil Spills with a Microwave Scatterometer and a Synthetic Aperture Radar," presented at the Workshop of the NATO-CCMS Pilot Study on the Use of Remote Sensing for the Control of Marine Pollution, Washington, DC, April 1979.

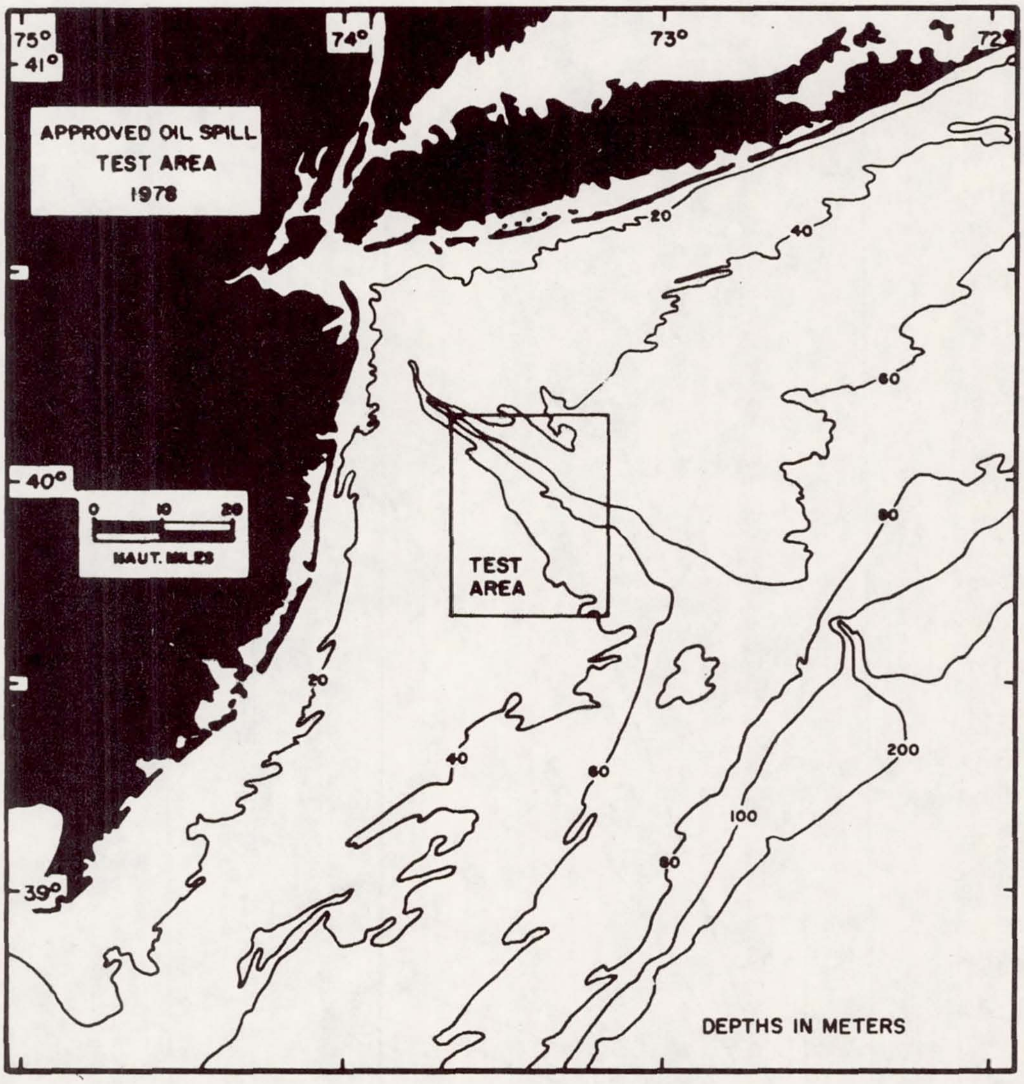

Figure 1. Test site for oil spills.

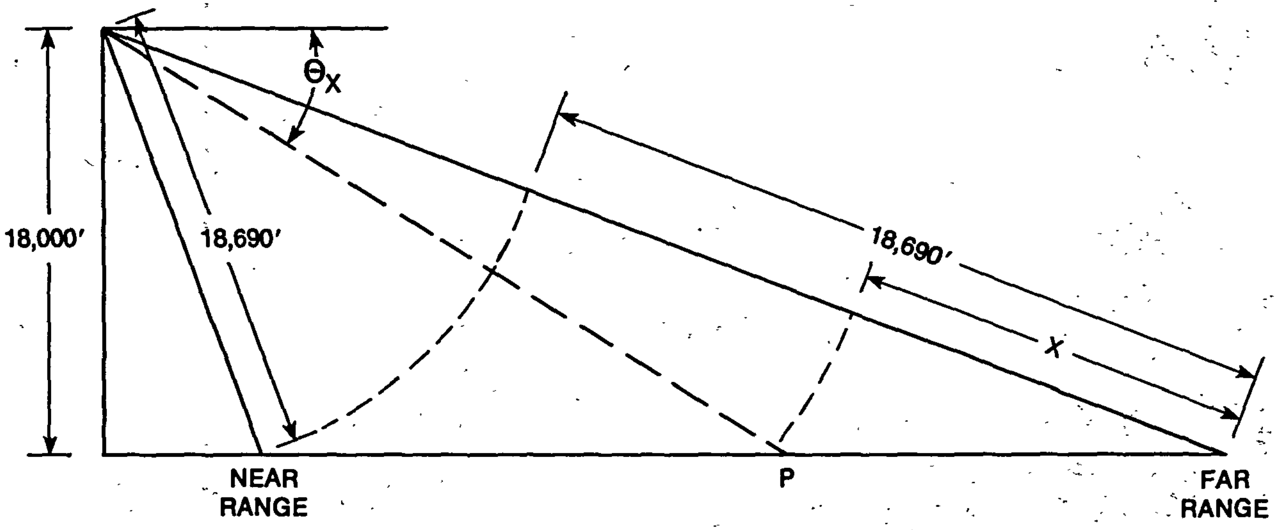

Figure 2. Nominal geometry for SAR image acquisition.

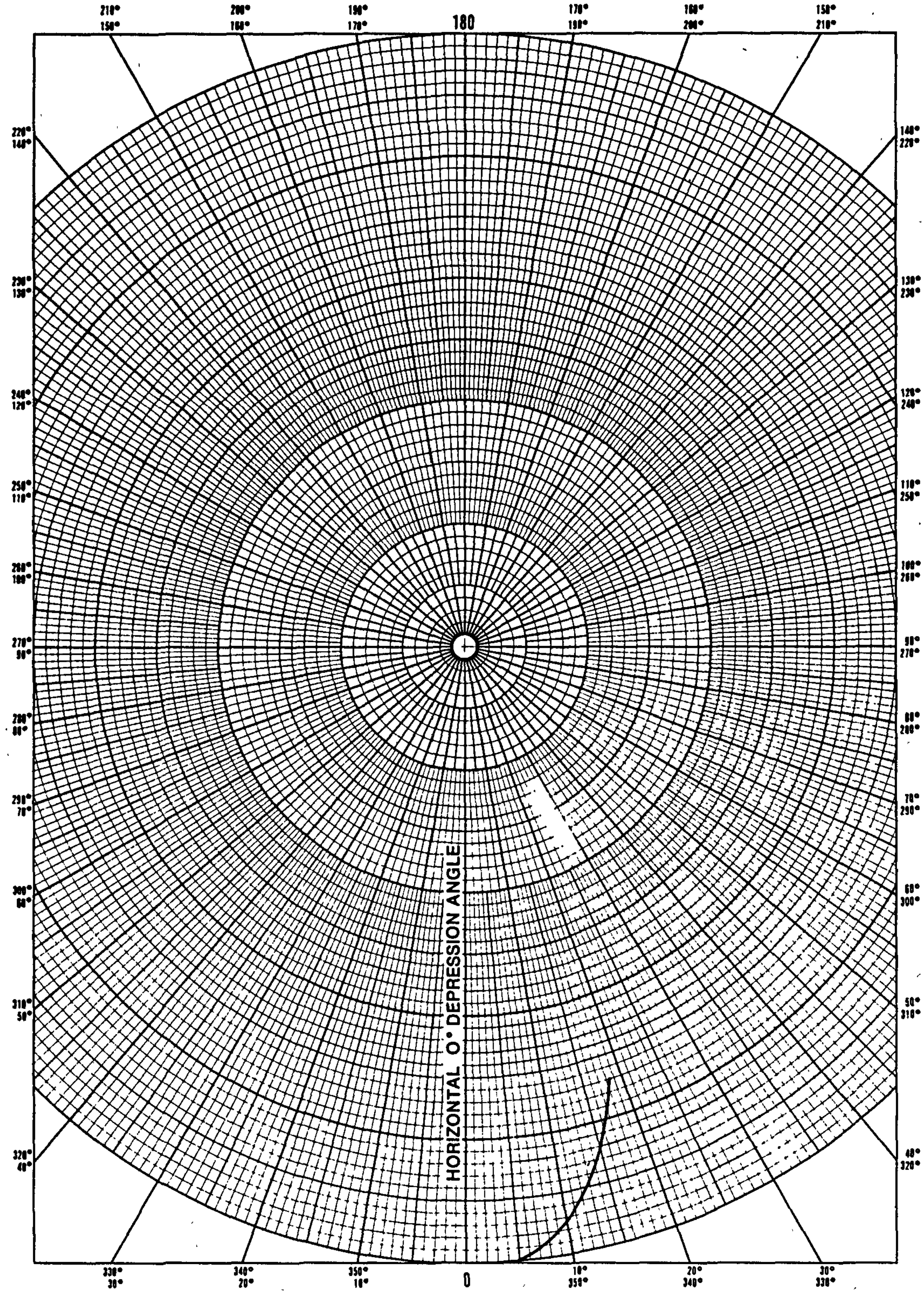

Figure 3a. Two-way antenna pattern for X_{HH}.

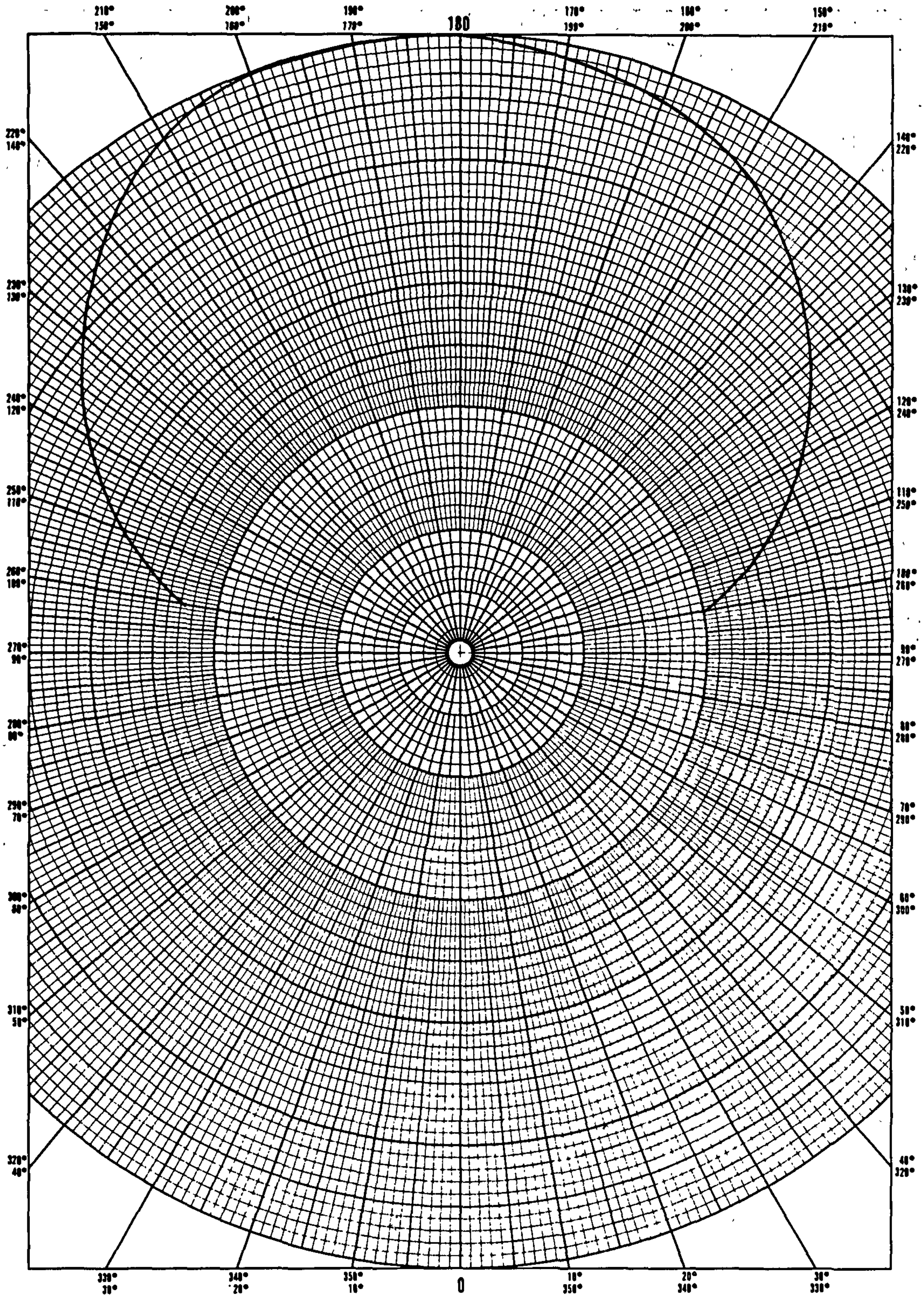

Figure 3b. Two-way antenna pattern for L_{HH}.

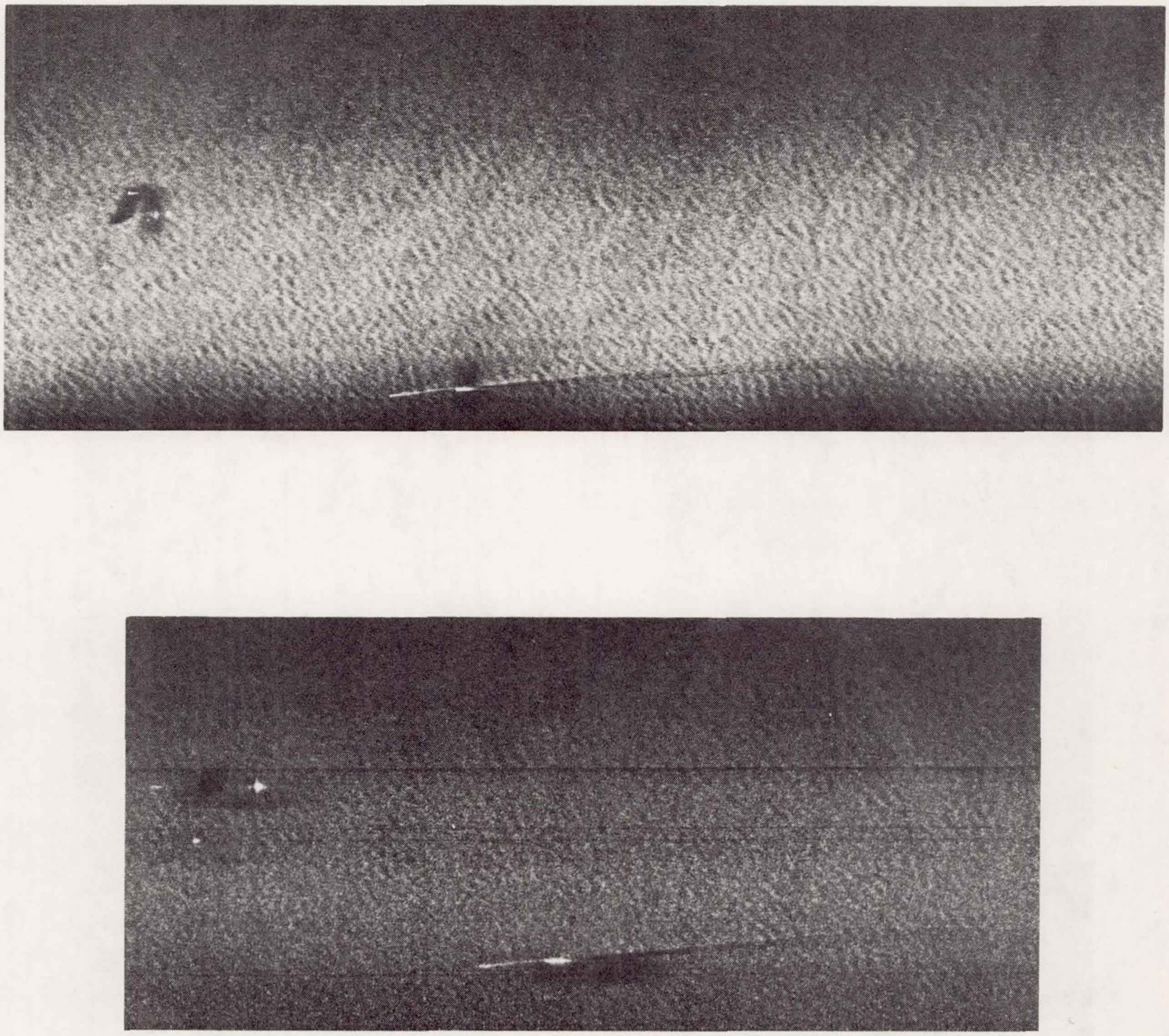

Figure 4. Pass 1 November 2, 1978.

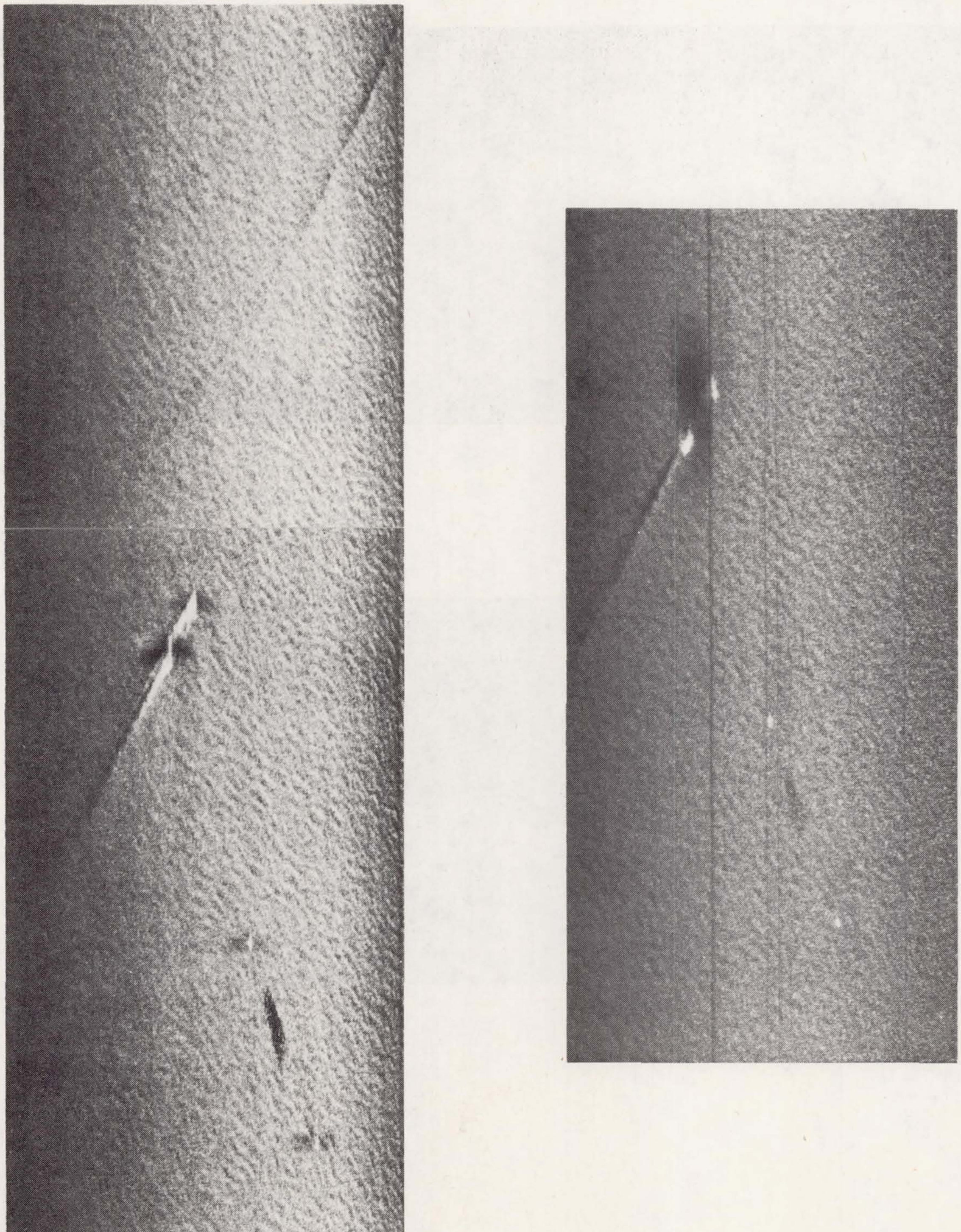

Figure 5. Pass 2 November 2, 1978.

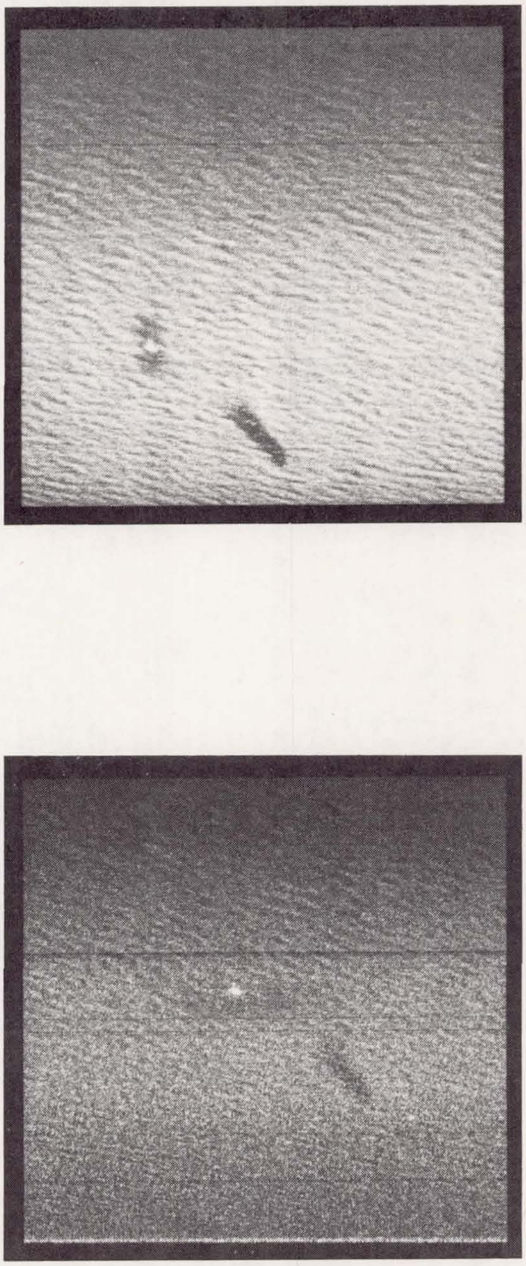

Figure 6. Pass 4 November 2, 1978.

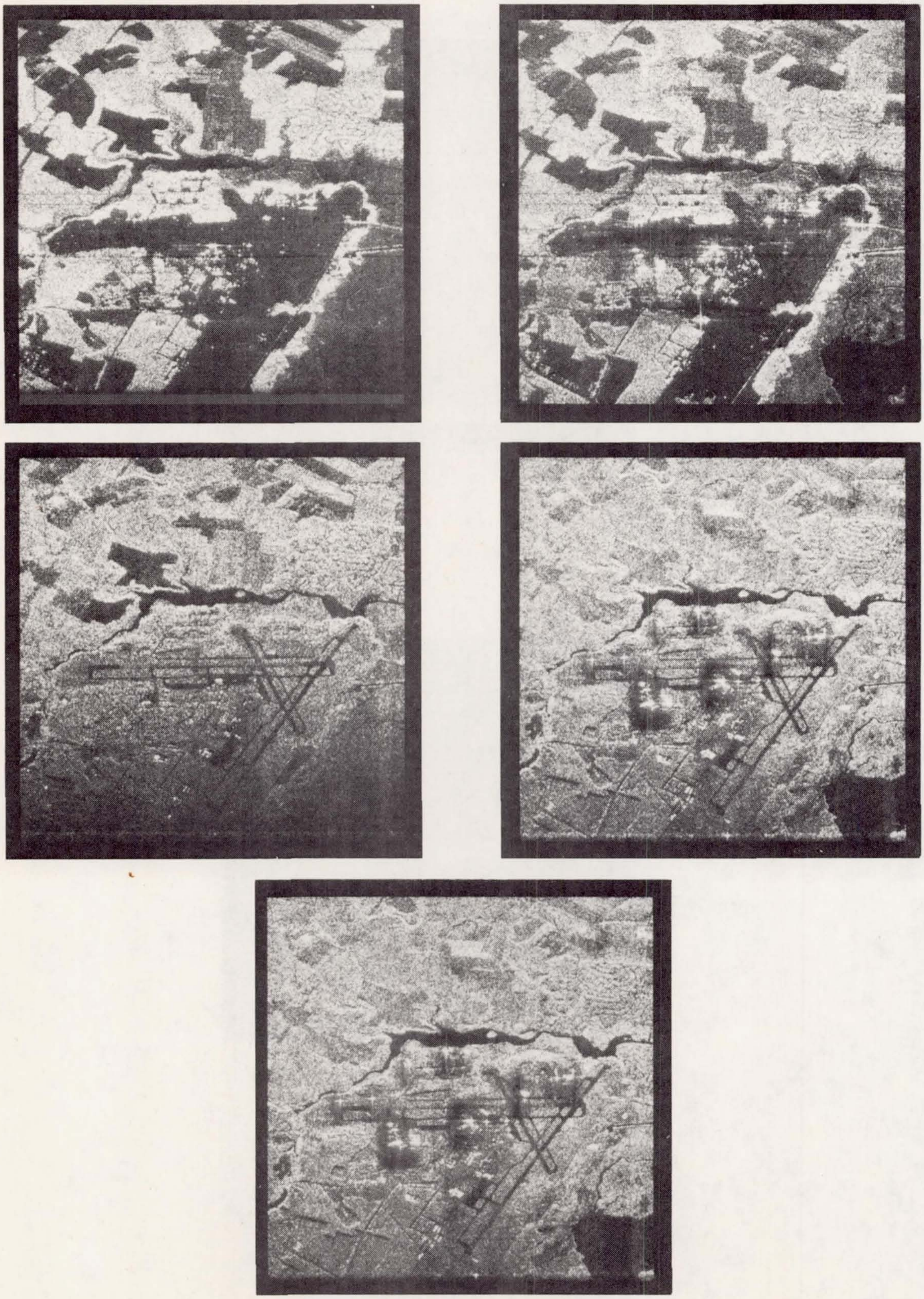

Figure 7. Pass 8 November 2, 1978.

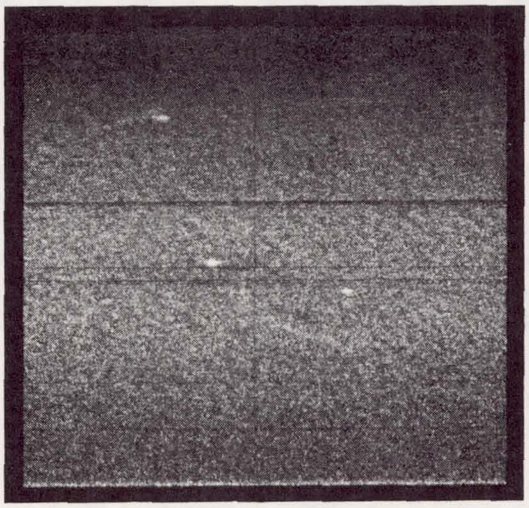

Figure 8. Pass 2 November 3, 1978.

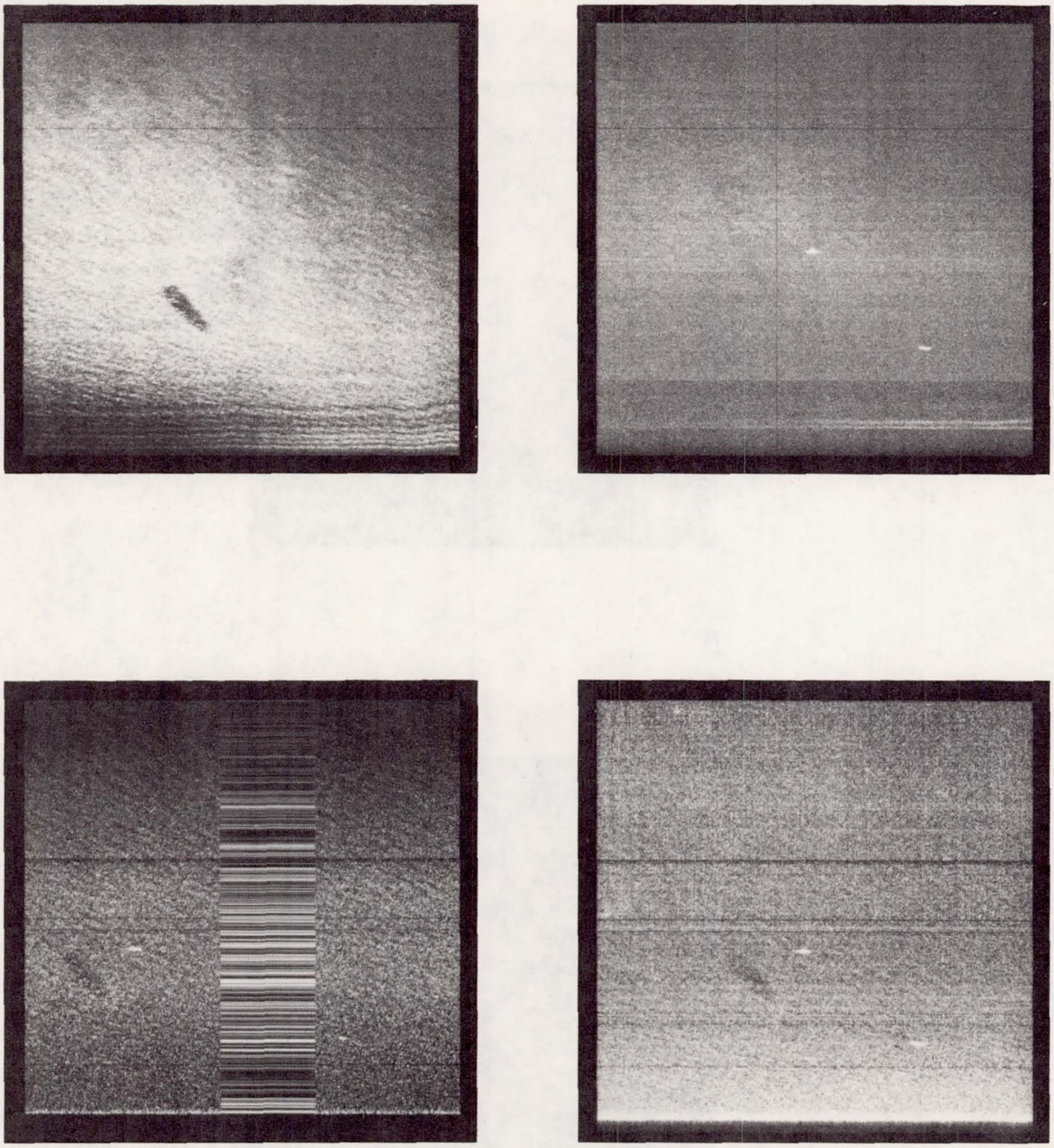

Figure 9. Pass 4 November 3, 1978.

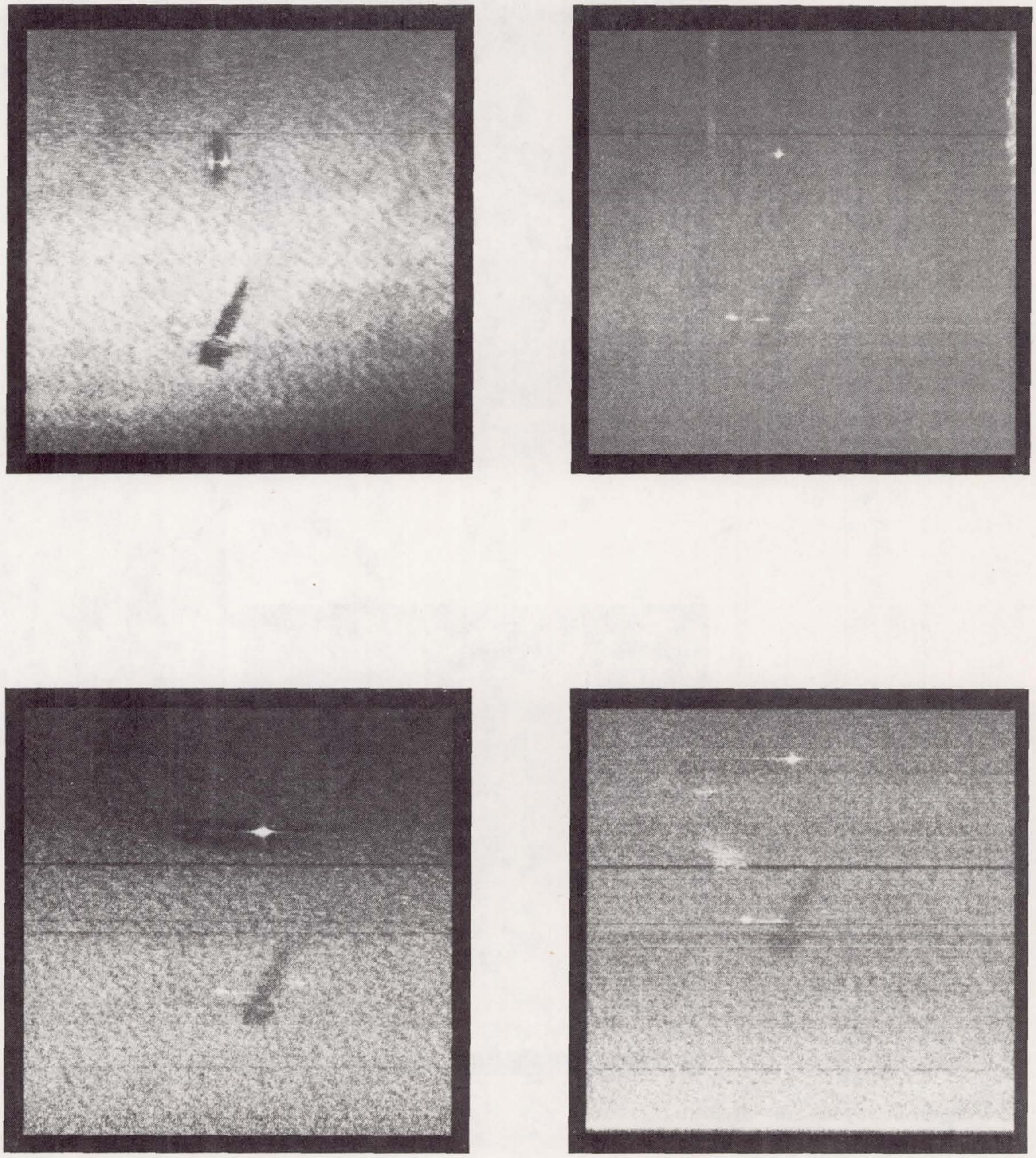

Figure 10. Pass 5 November 3, 1978.

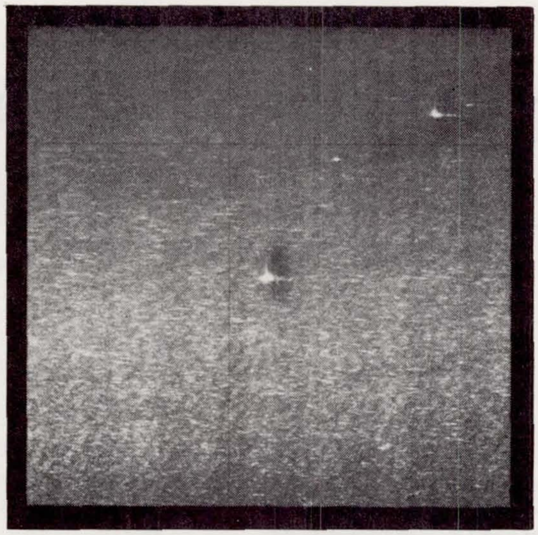

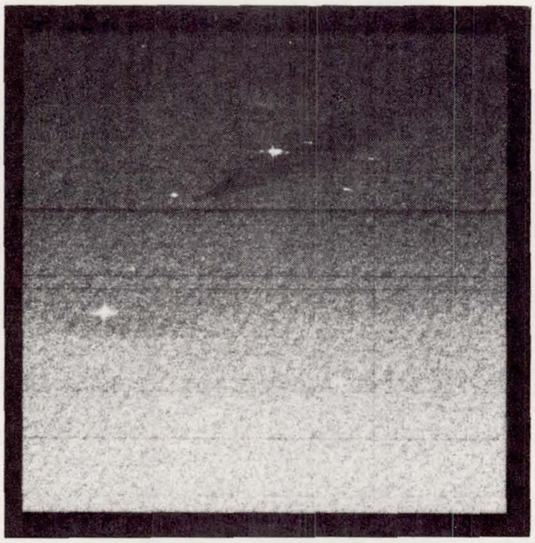

Figure 11. Pass 6 November 3, 1978.

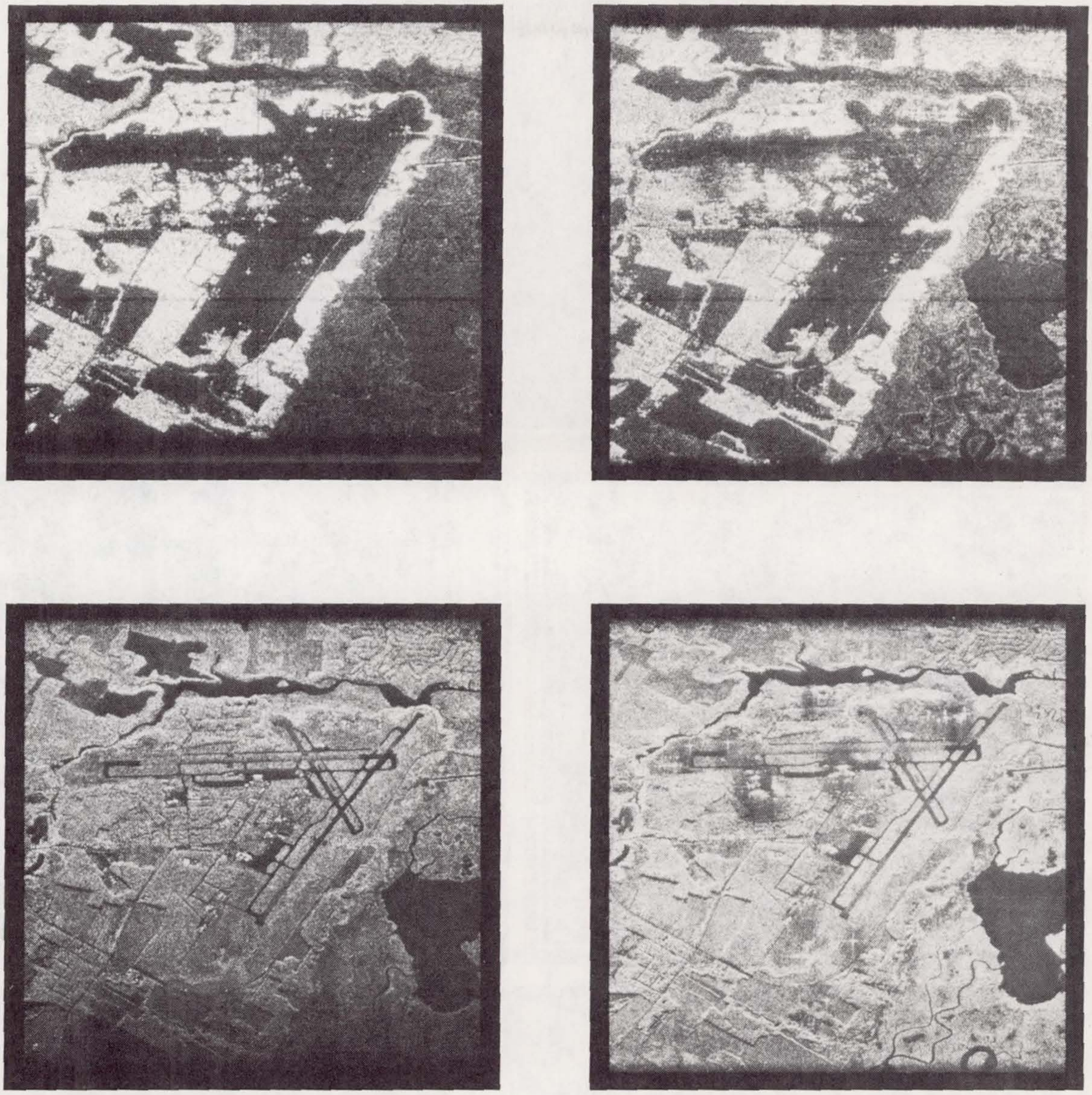

Figure 12. Pass 8 November 3, 1978.

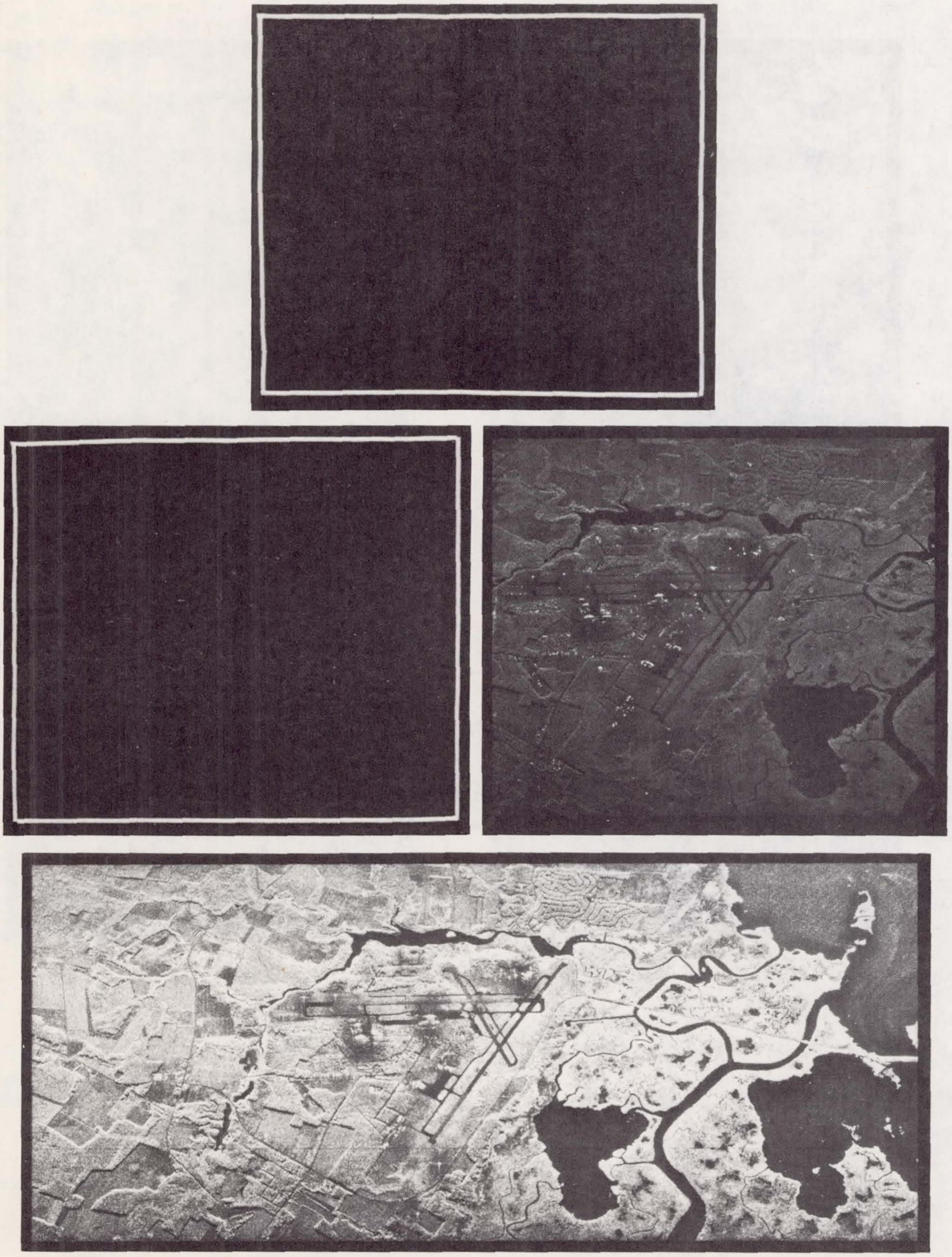

Figure 13. Pass 9 November 3, 1978 X_{HH} at several gains.

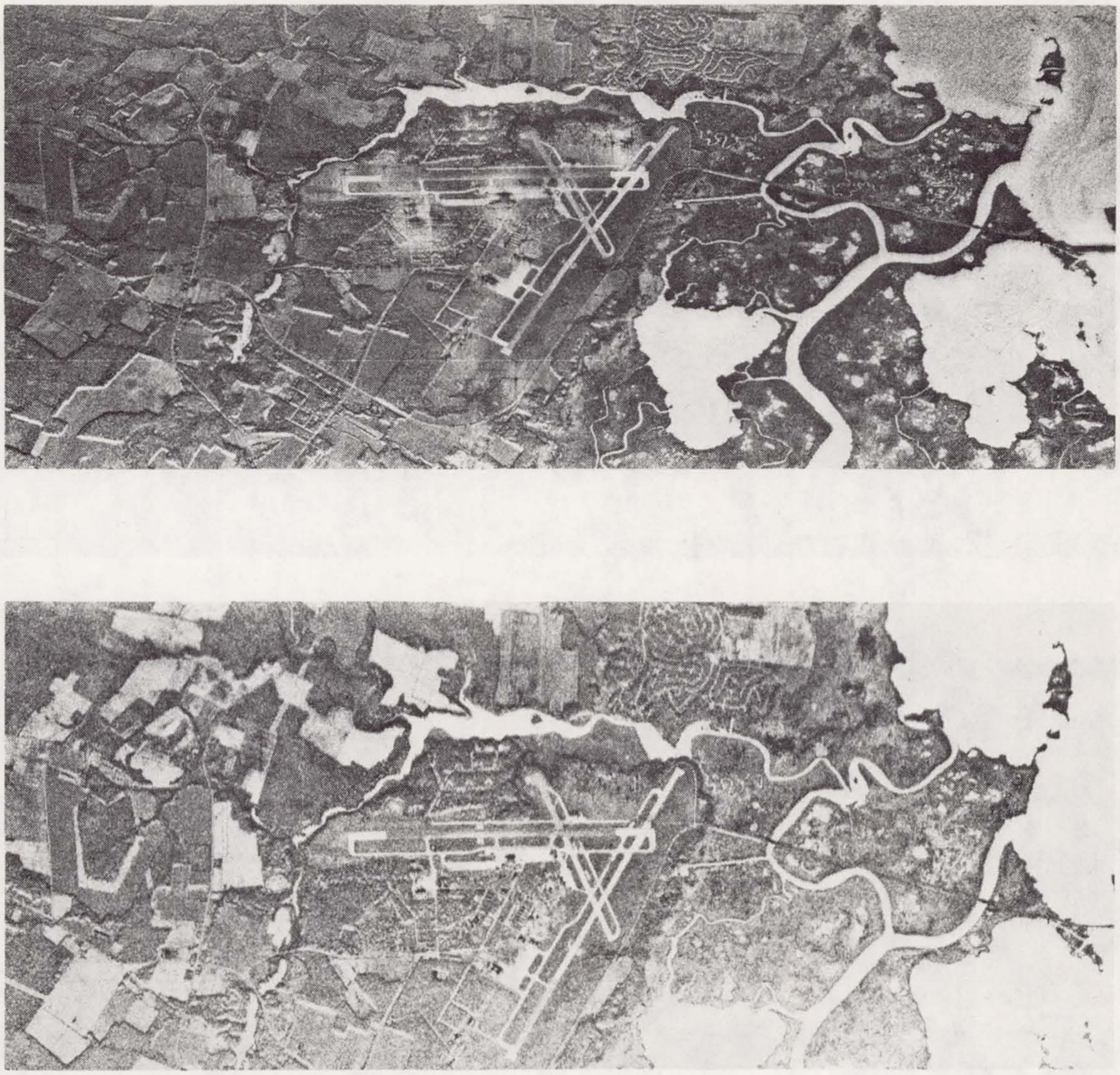

Figure 14. Pass 9 November 3, 1978, X_{HH} and X_{HV} at reference gain.

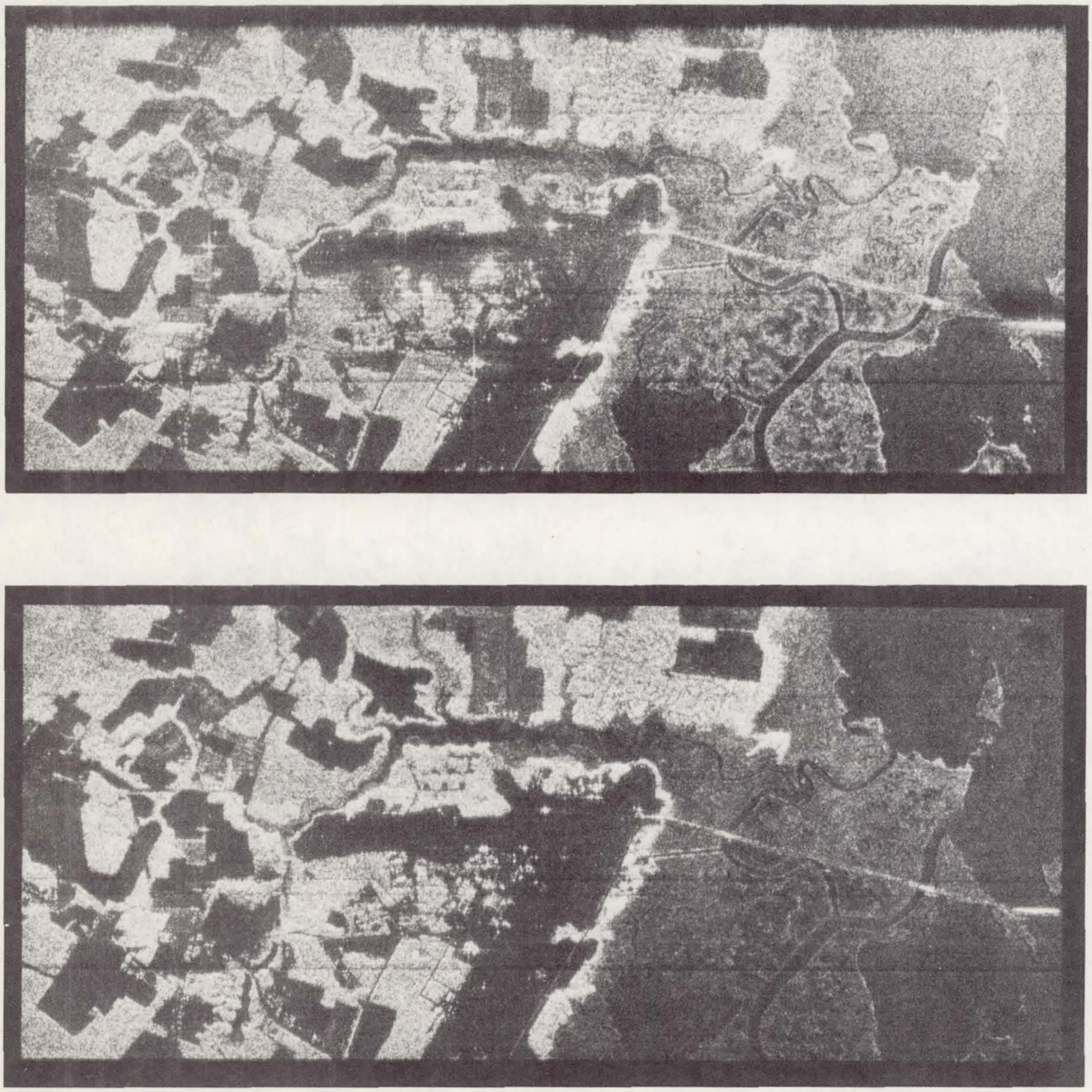

Figure 15. Pass 9 November 3, 1978, L_{HH} and L_{HV} at reference gain.

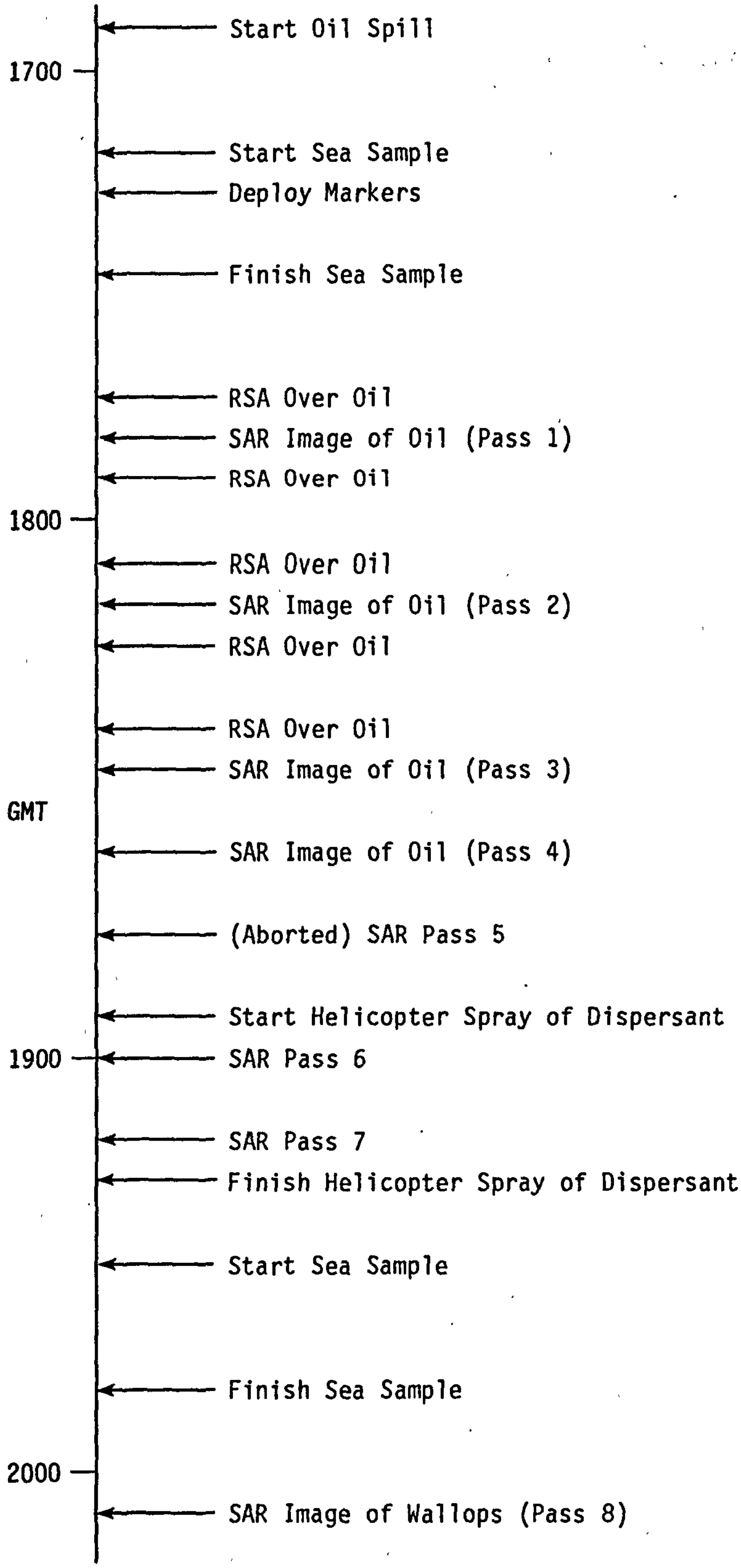

Figure 16. Time Line for SAR-Related Activities of November 2, 1978.

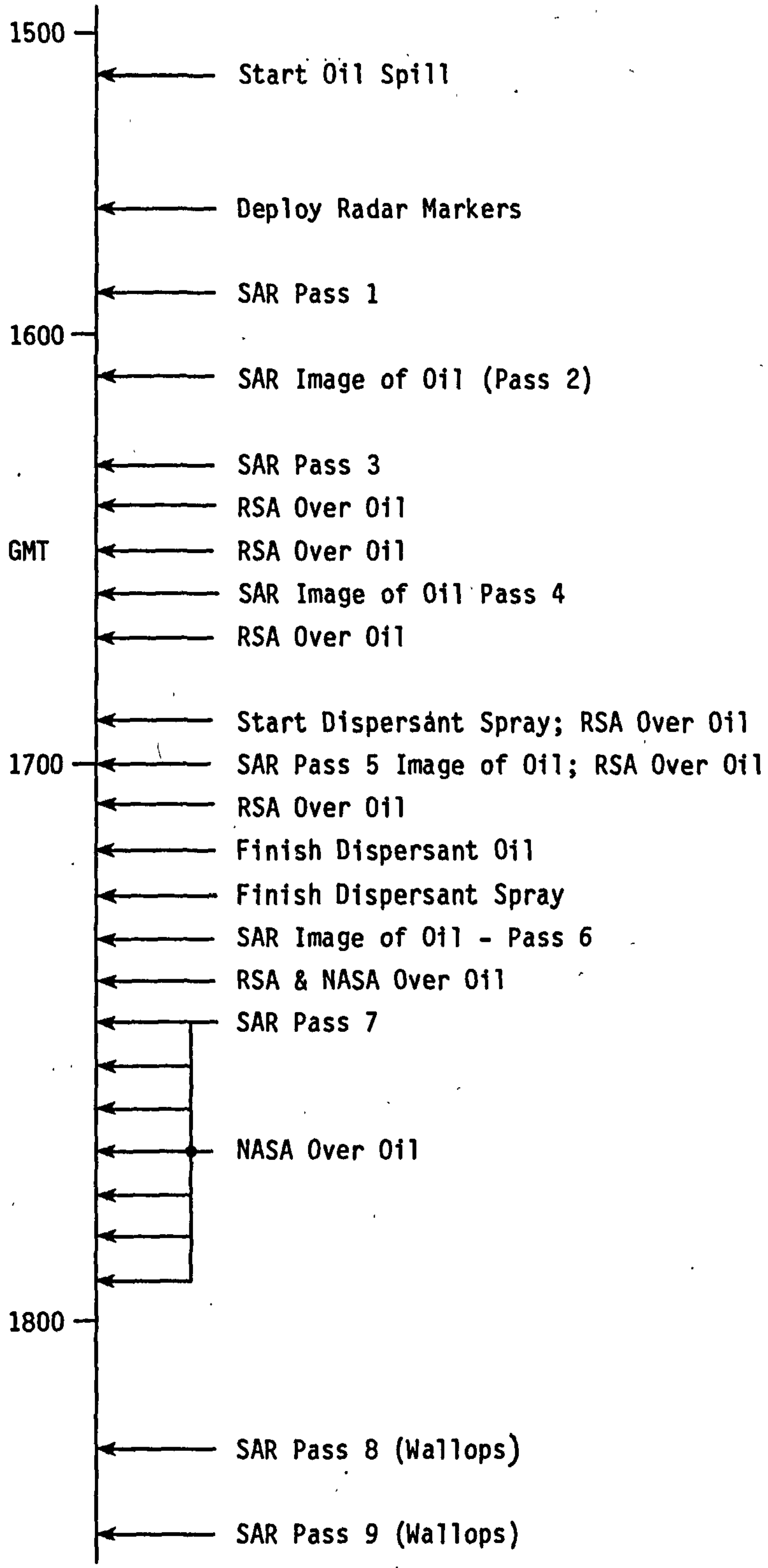

Figure 17. Time line for SAR-related activities of November 3, 1978.

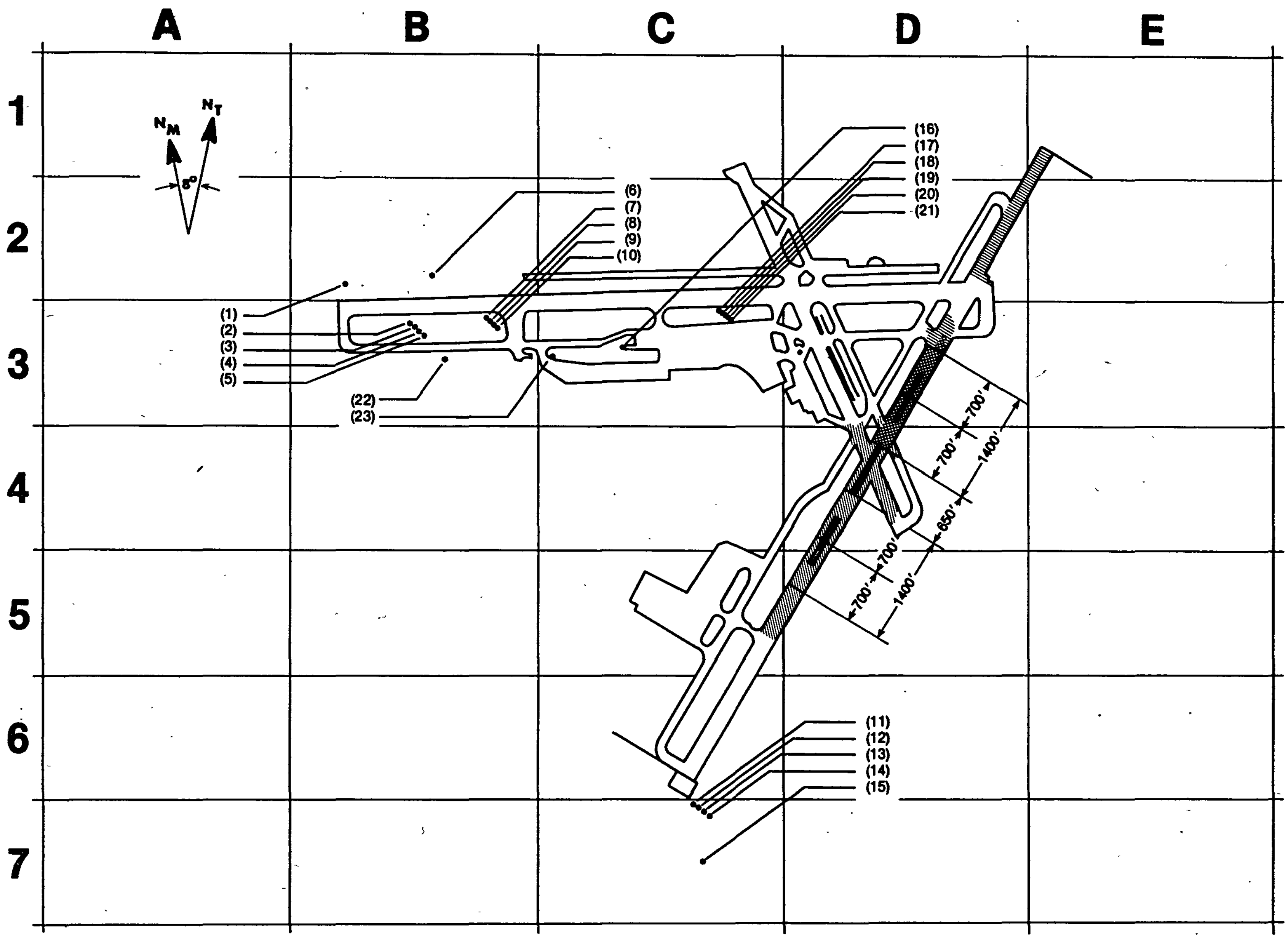

Figure 18. SAR target range at Wallops.

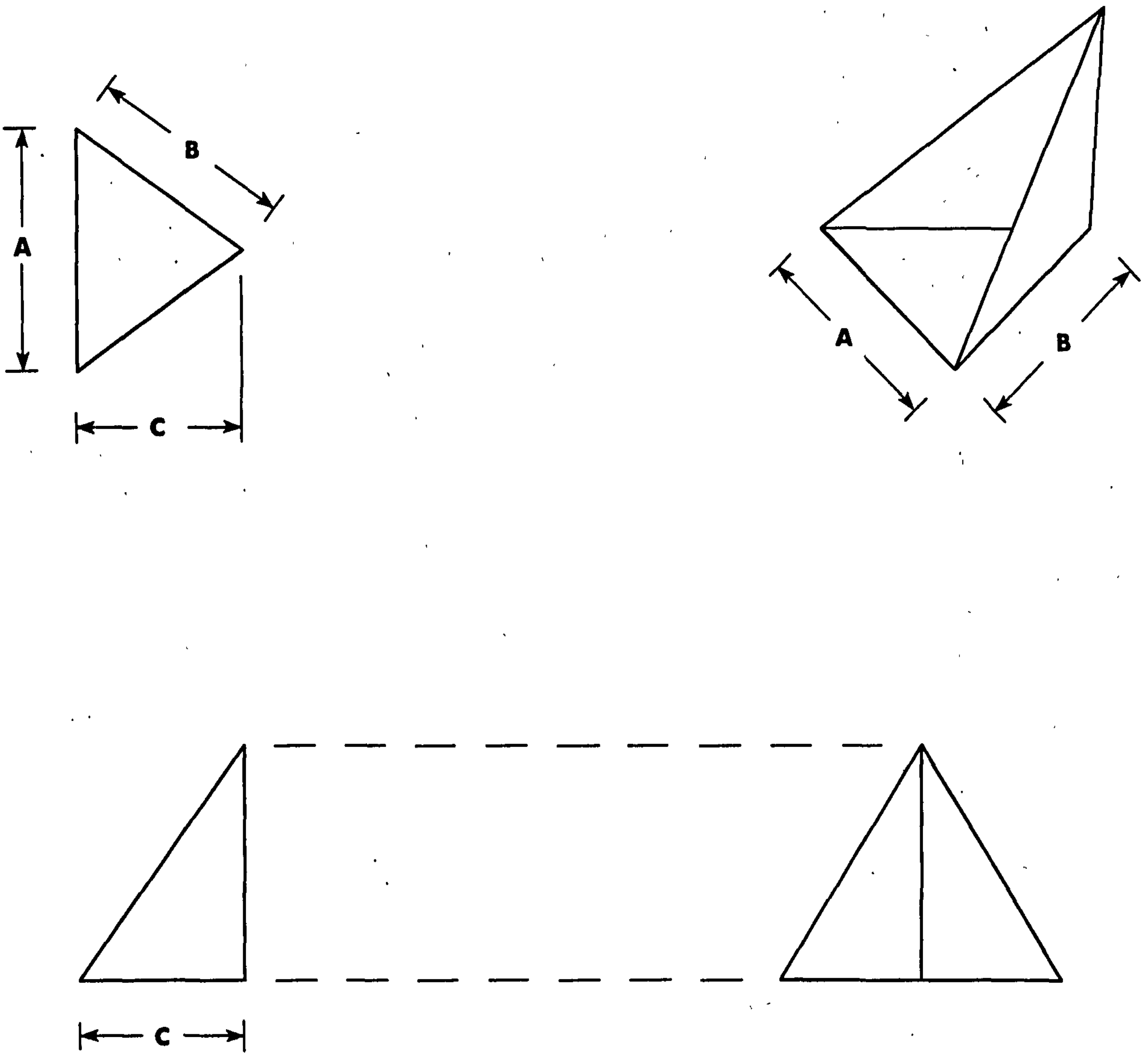

Figure 19. Geometry of corner reflectors.

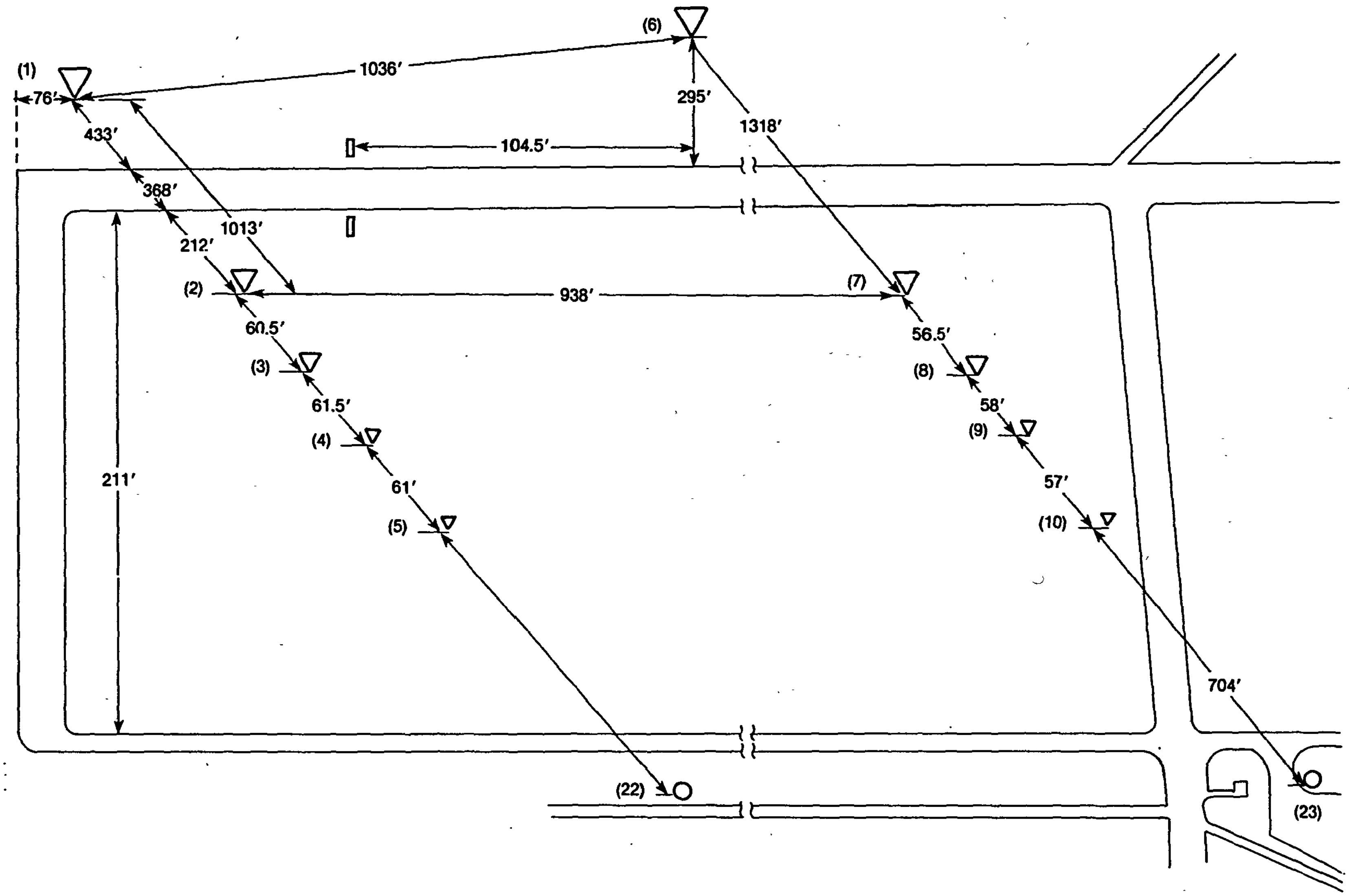

Figure 20. Subset 1 of the Wallops target range.

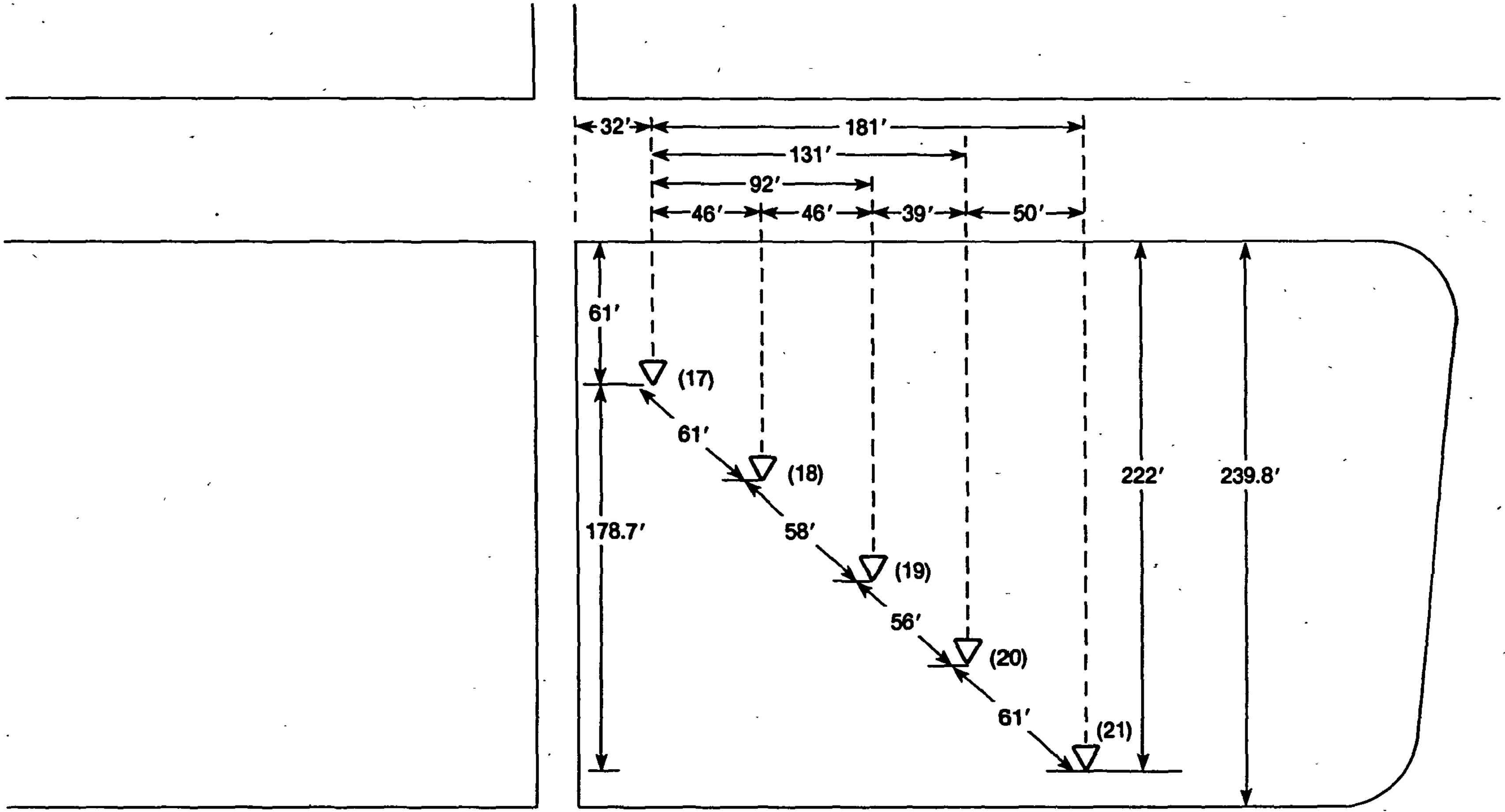

Figure 21. Subset 2 of Wallops target range.

Figure 22. Corner reflector 1.

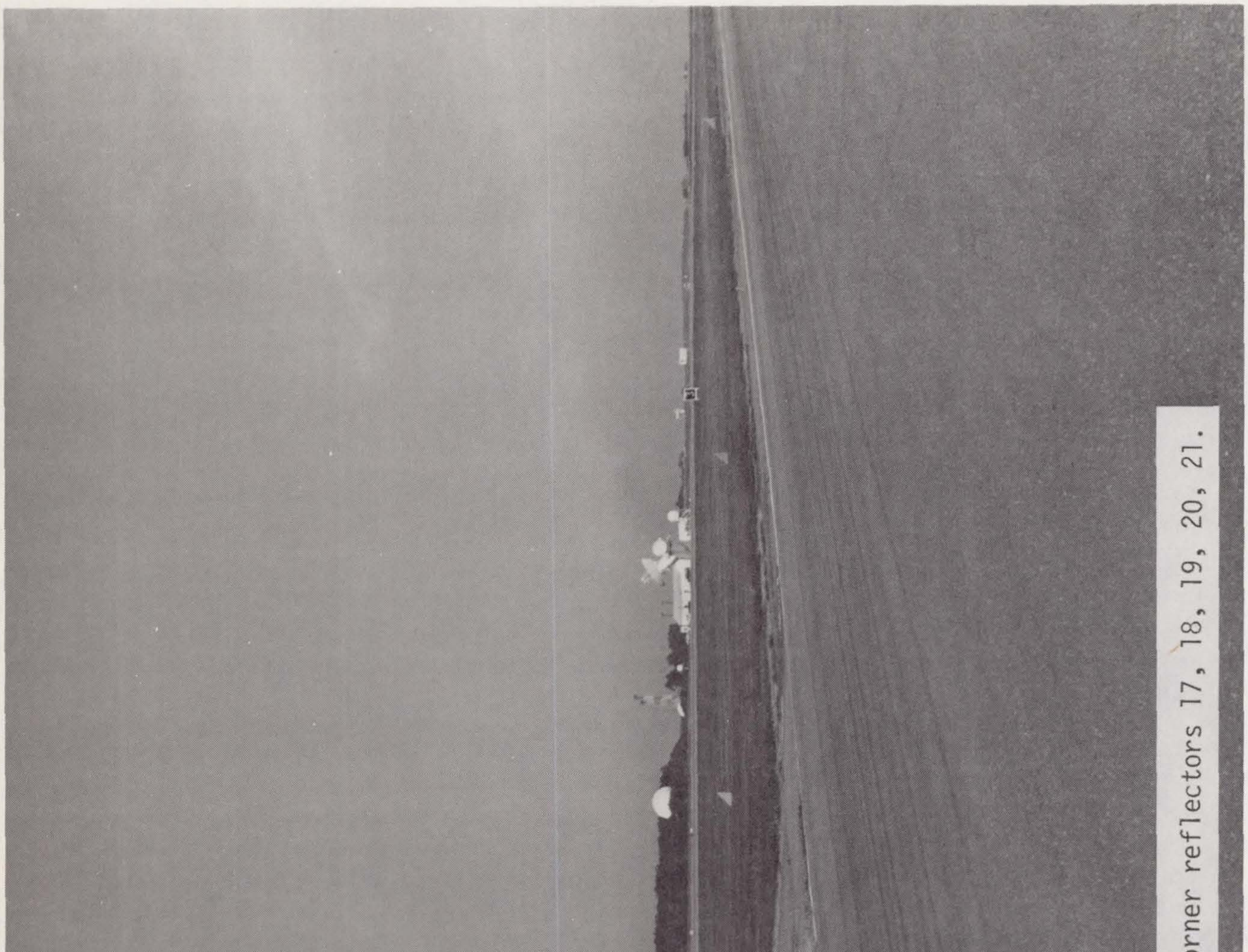

Figure 23. Corner reflectors 17, 18, 19, 20, 21.

Figure 24. Reflector 23.

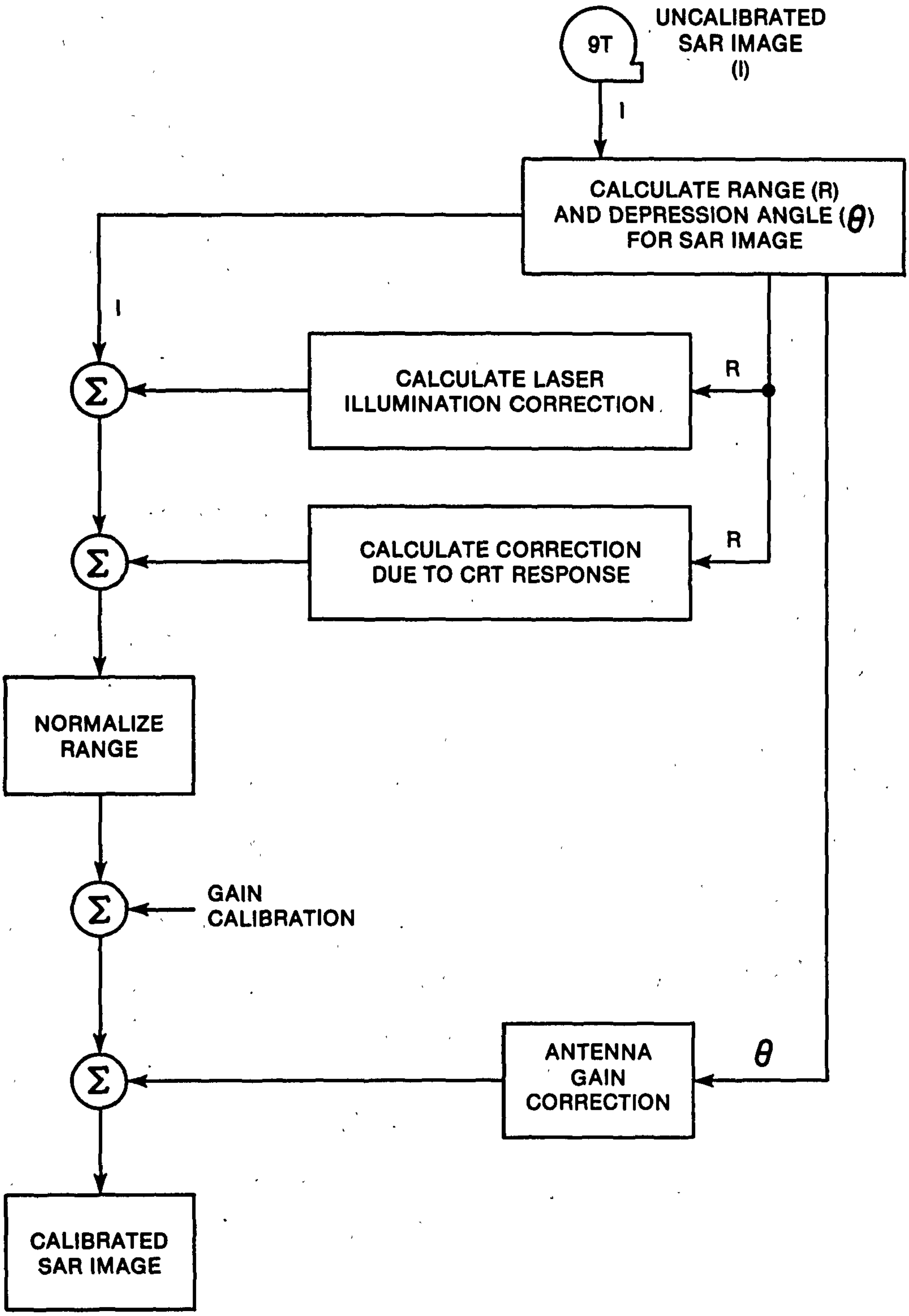

Figure 25. A calibration for the SAR imagery.

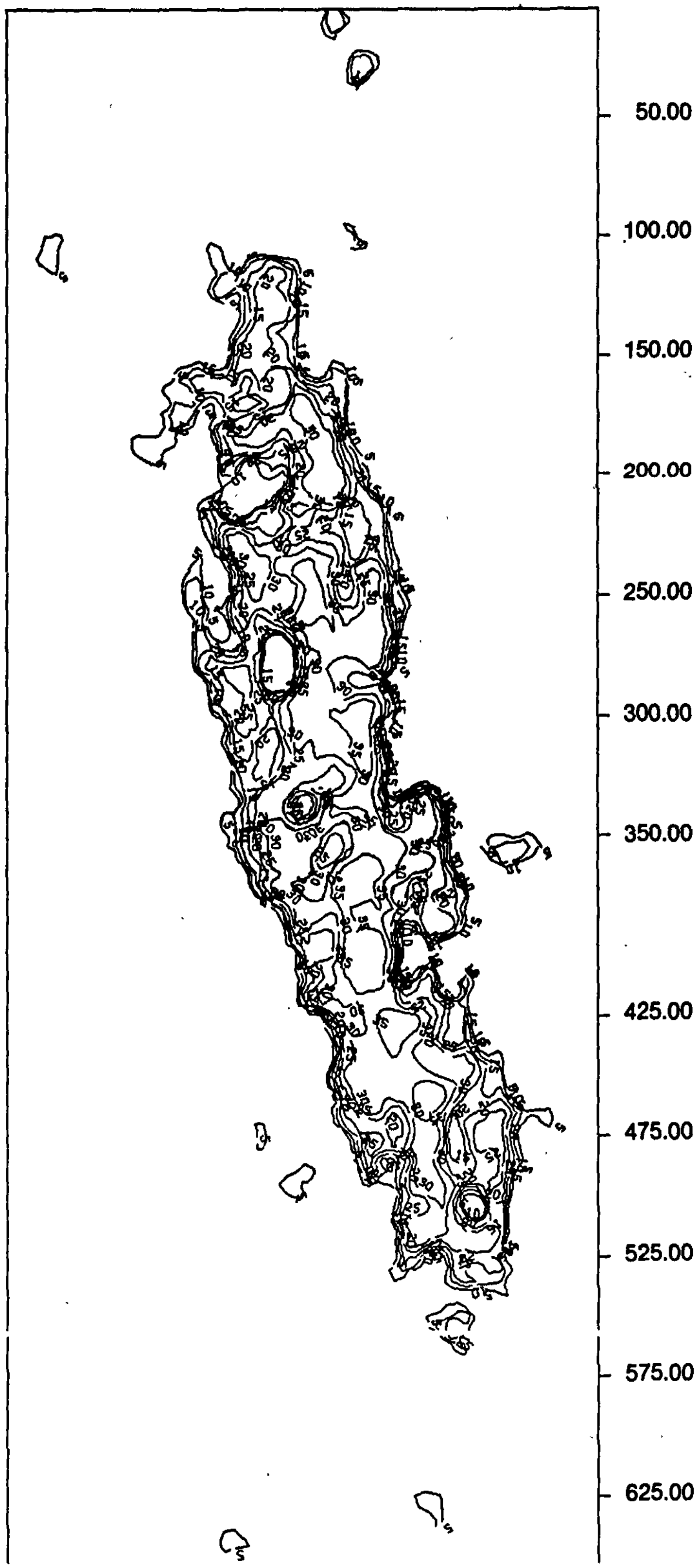

Figure 26. Contour plot of SAR X_{HH} returns of Pass 2 on November 2, 1978.

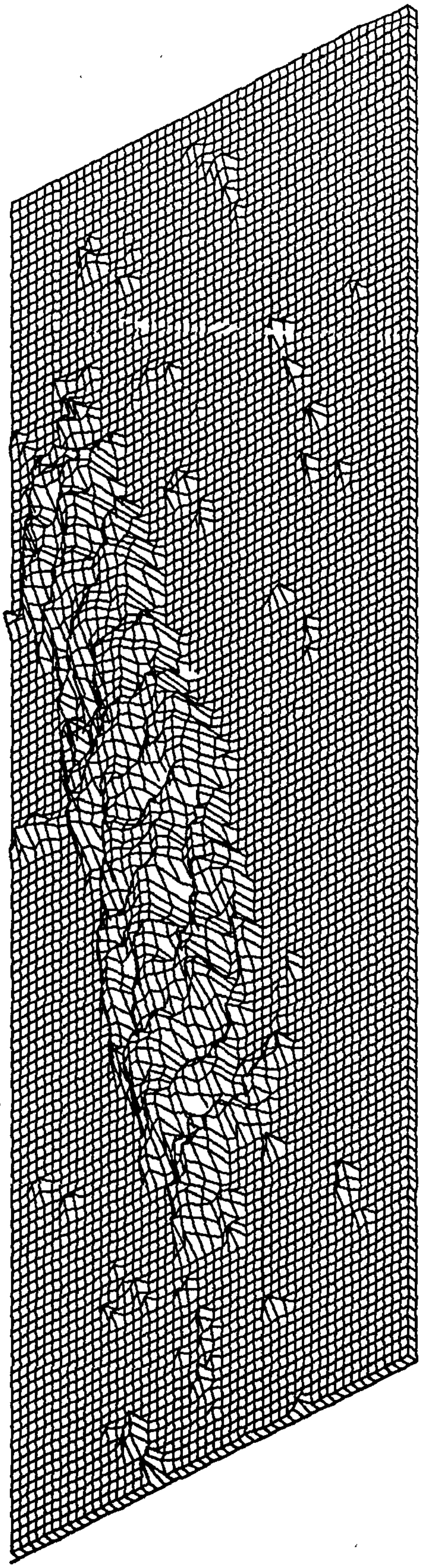

Figure 27. 3D projection of SAR X_{HH} returns of Pass 2 on November 2, 1978.

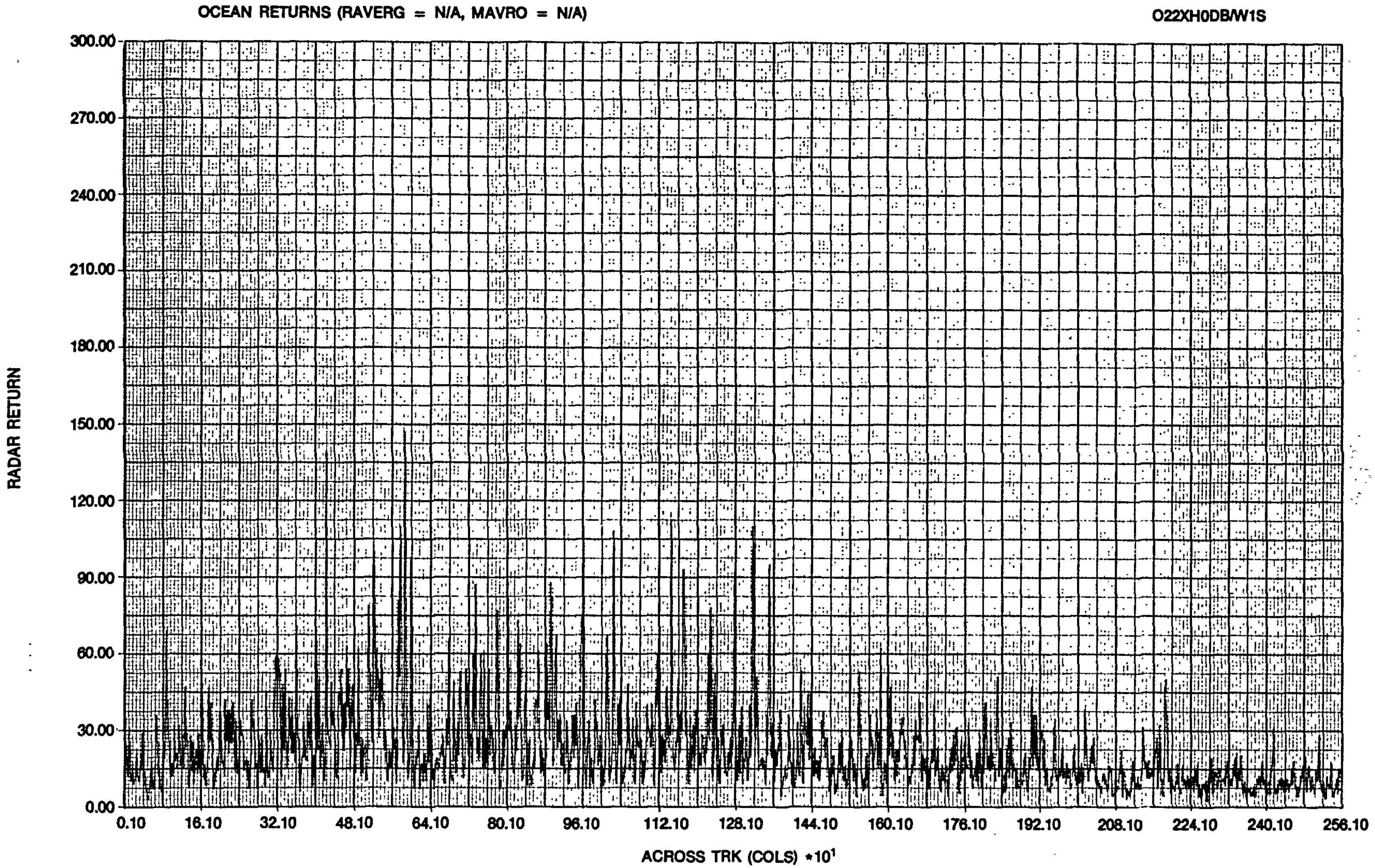

Figure 28. Unfiltered across track profile of ocean returns for SAR X_{HH} Pass 2 on November 2, 1978.

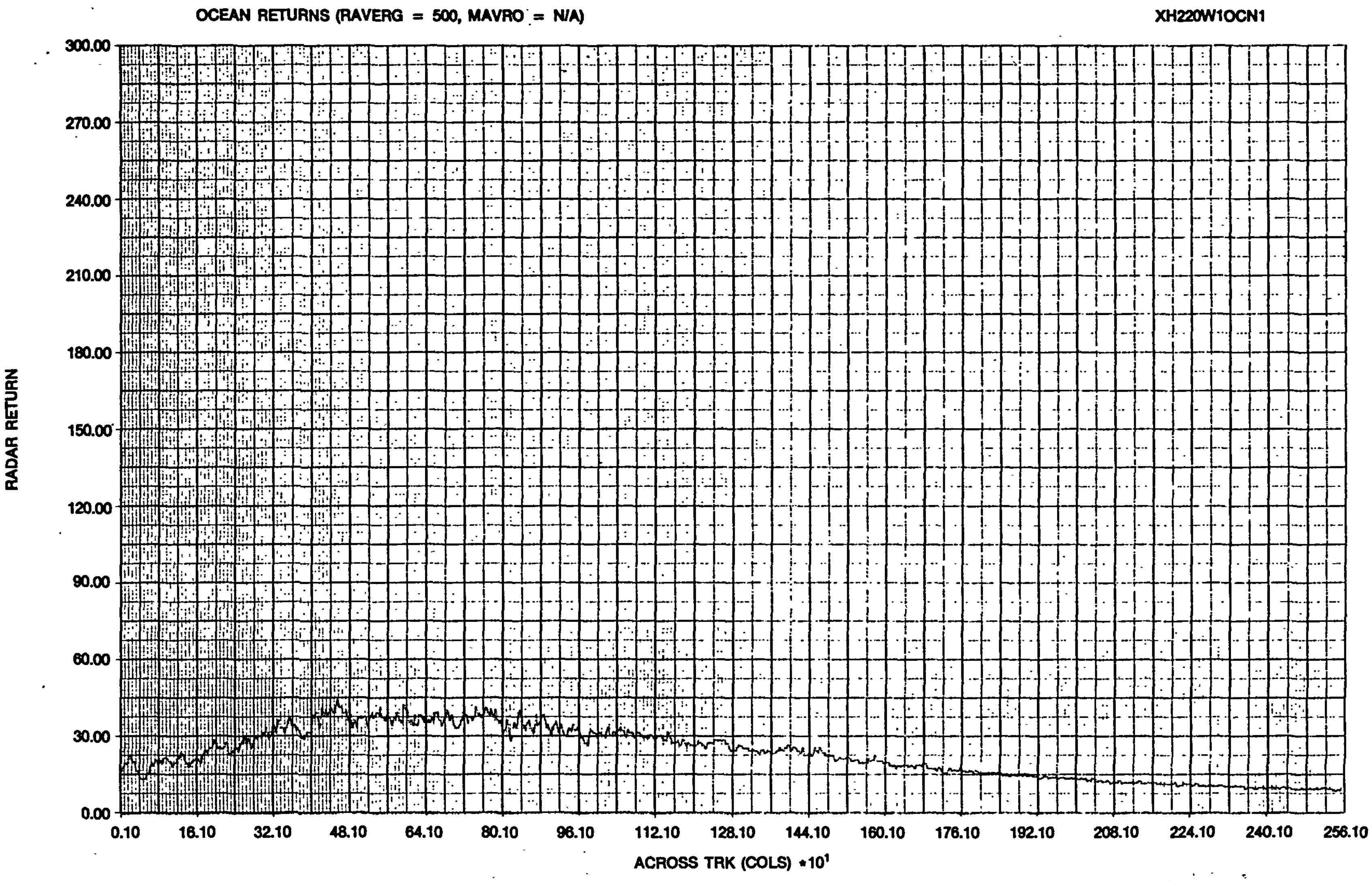

Figure 29. Filtered across track profile of ocean returns for SAR X_{HH} Pass 2 on November 2, 1978.

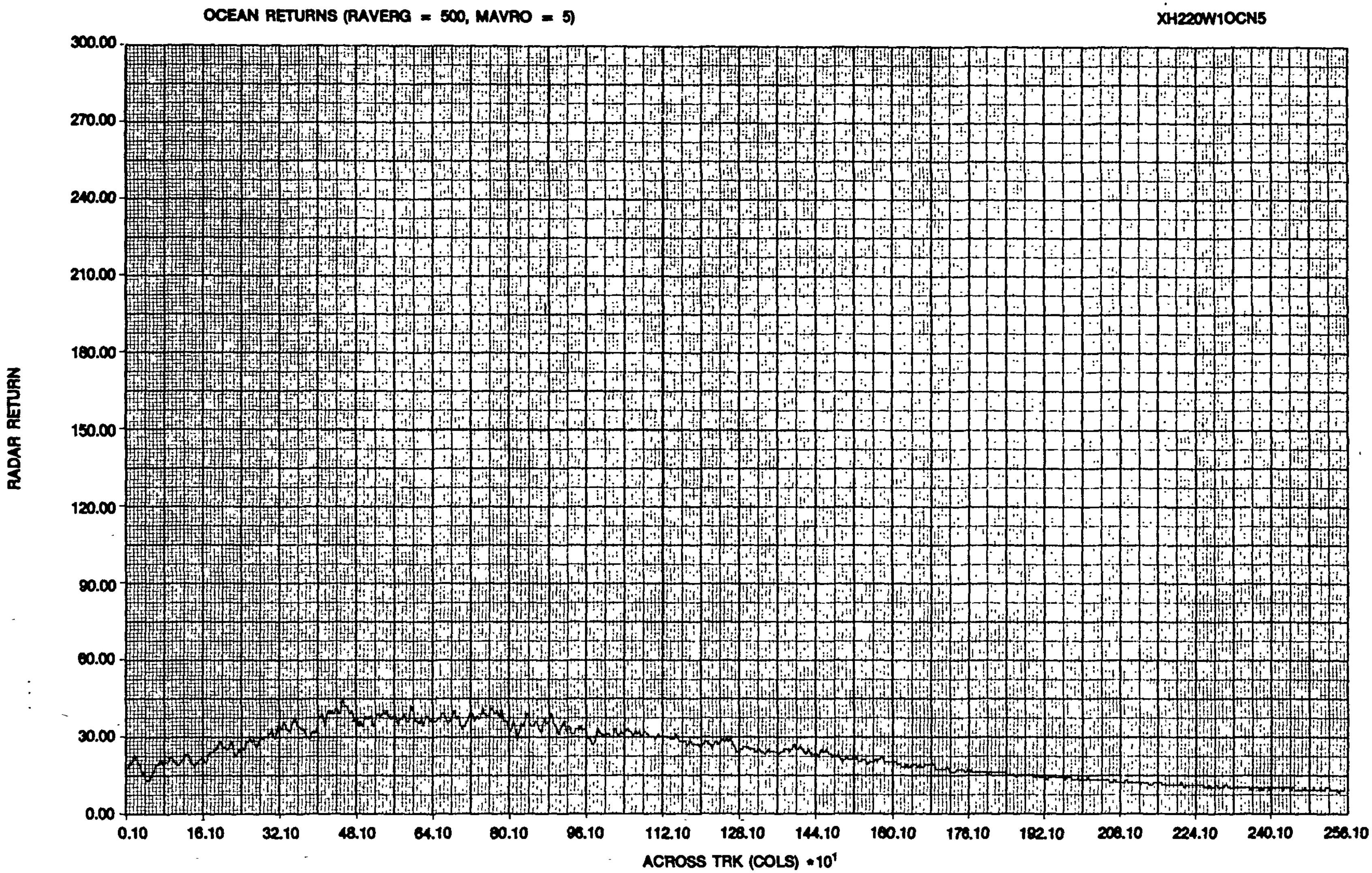

Figure 30. Filtered across track profile of ocean returns for SAR X_{HH} Pass 2 on November 3, 1978.

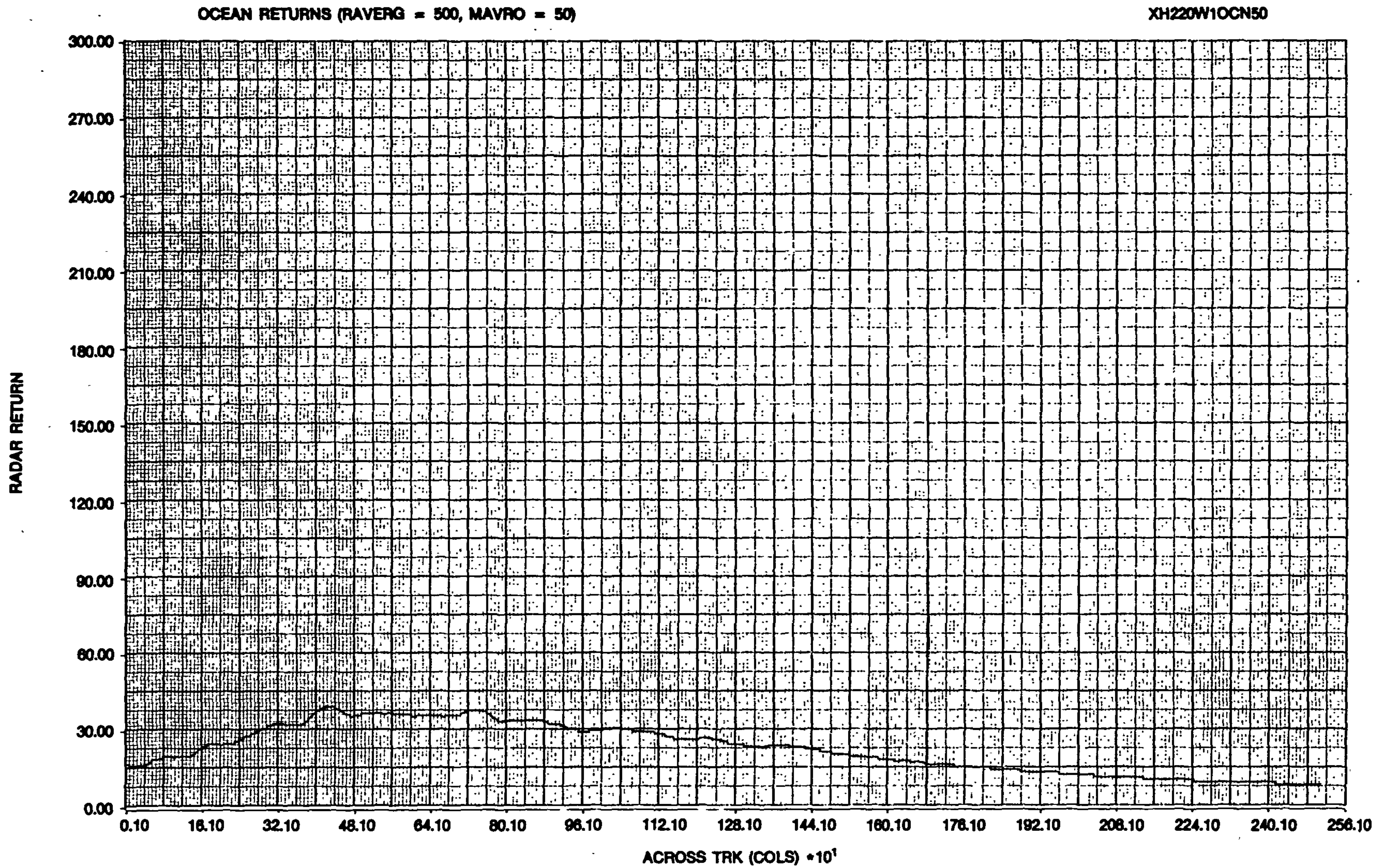

Figure 31. Filtered across track profile of ocean returns for SAR X_{HH} Pass 2 on November 2, 1978.

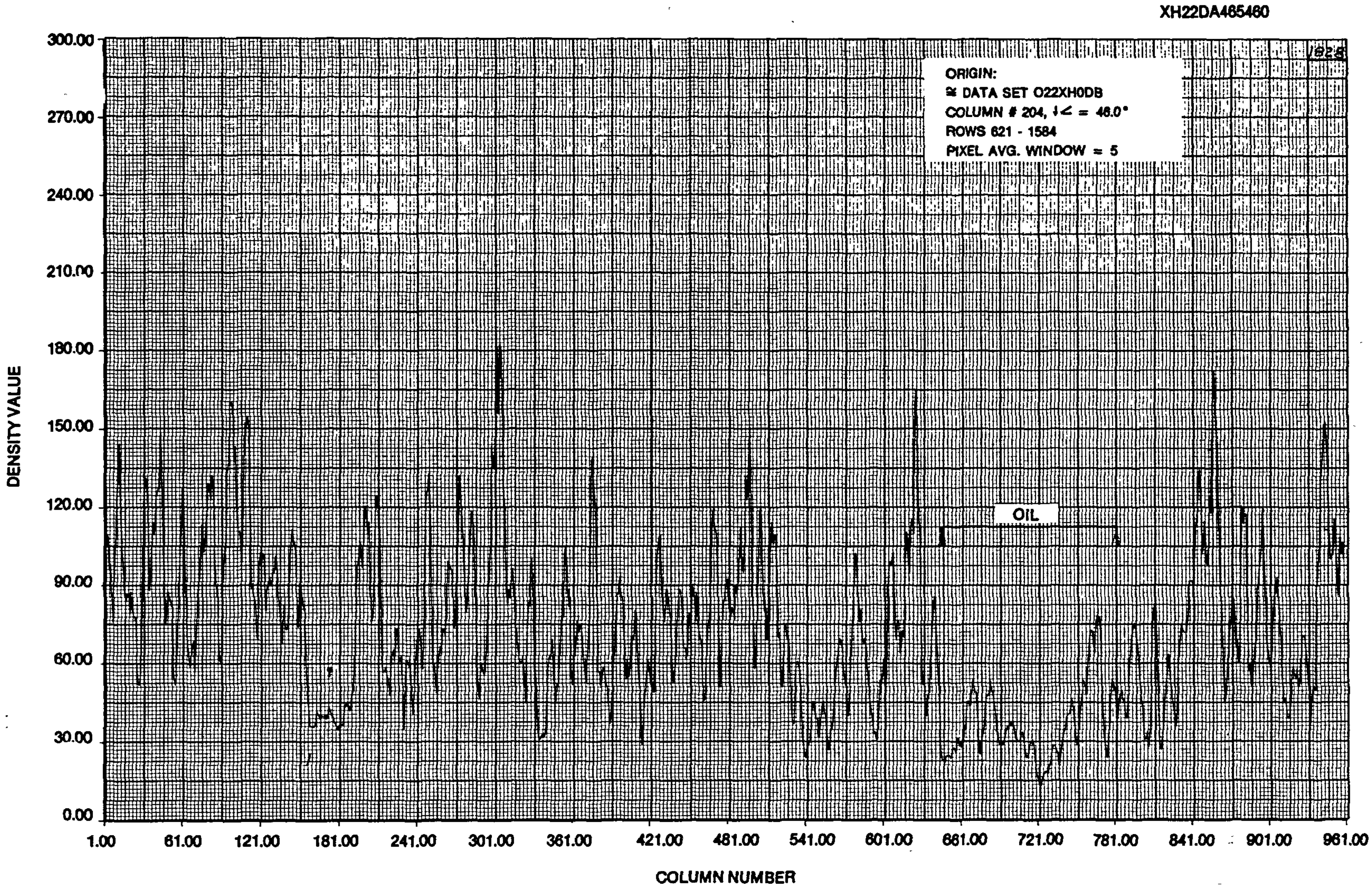

Figure 32. Filter along track profile of X_{HH} returns from oil and ocean at a depression angle of 46° for Pass 2 on November 2, 1978.

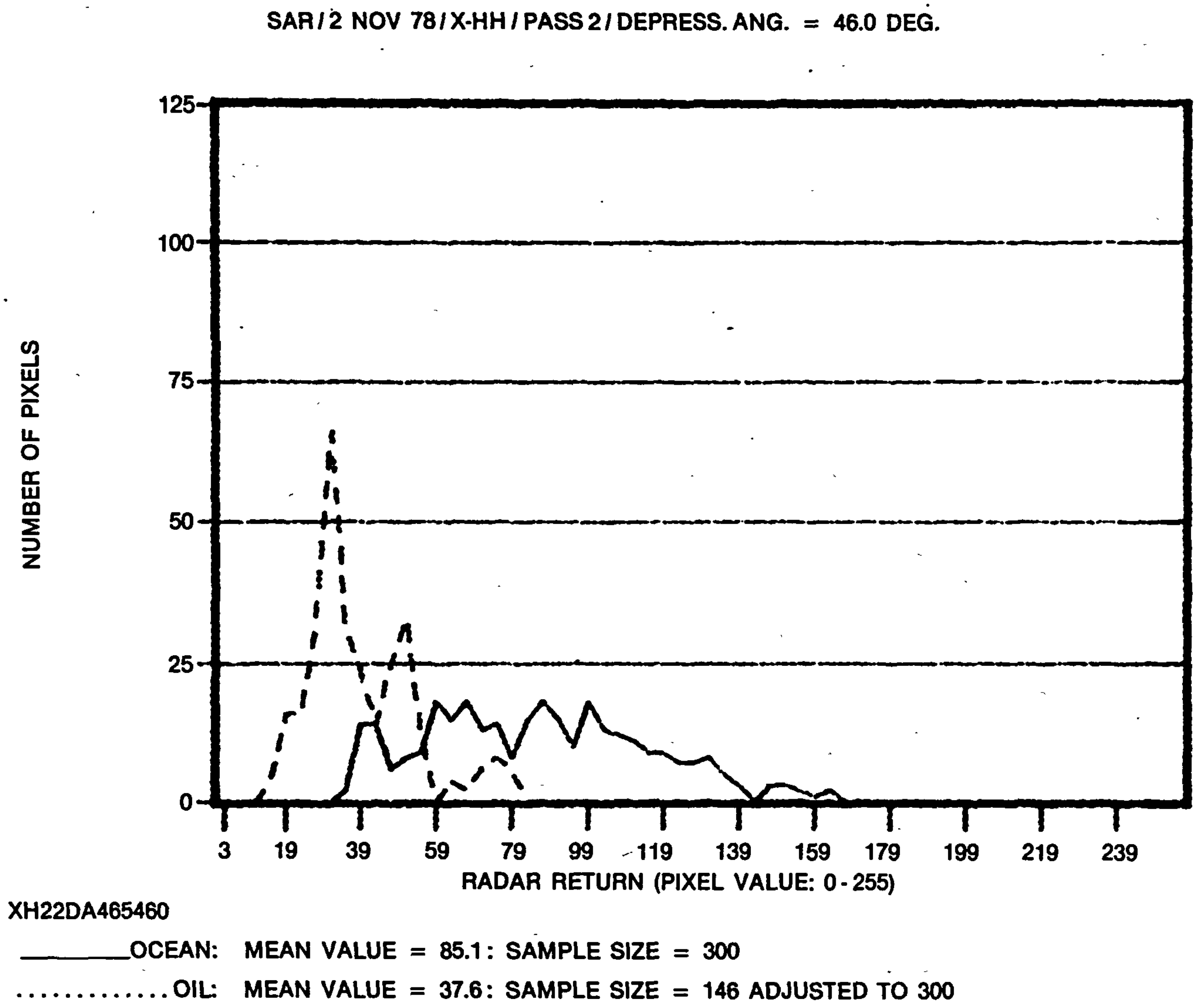

Figure 33. Histograms of SAR X_{HH} returns from ocean and oil at a depression angle of 46° for Pass 2 on November 2, 1978.

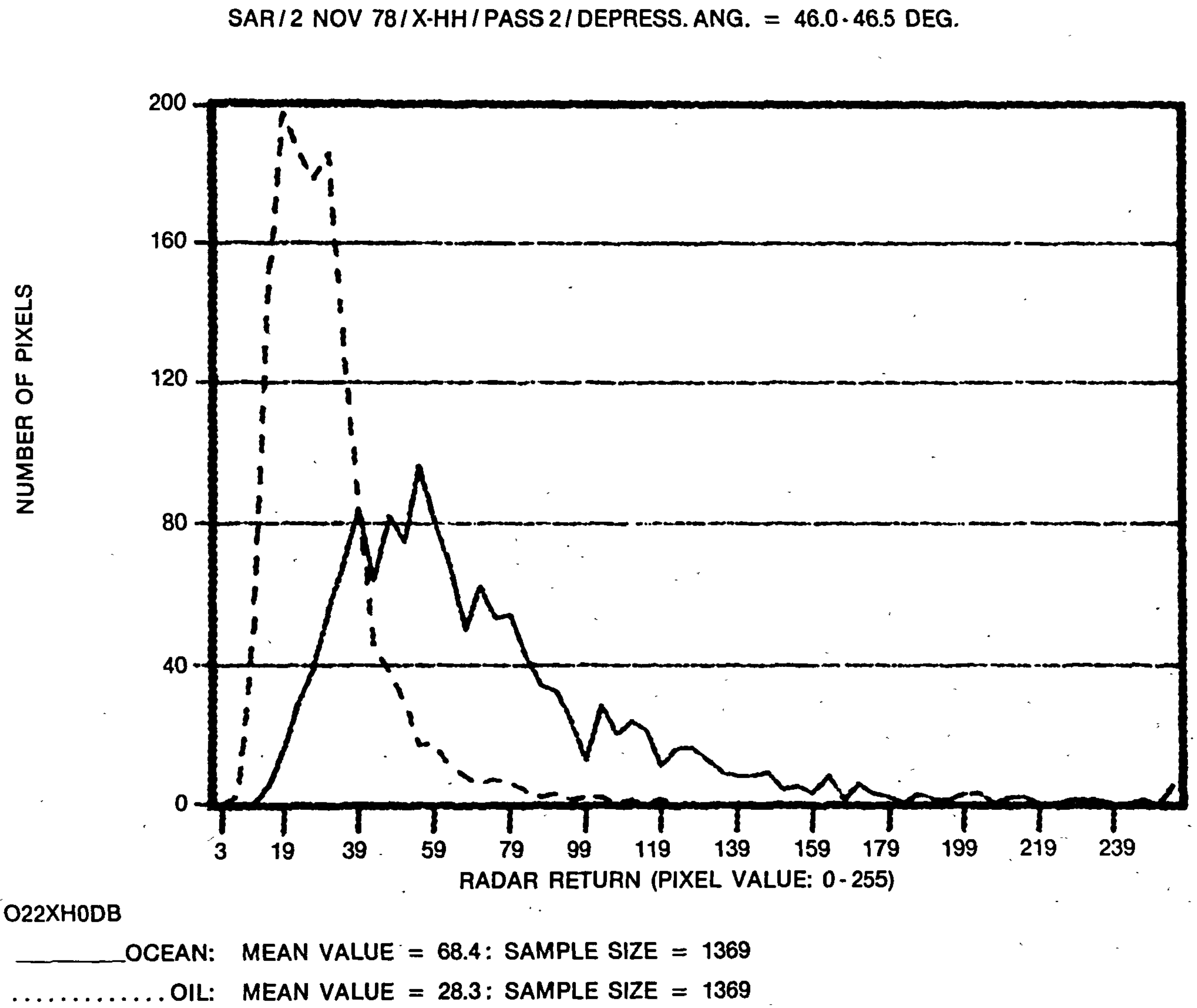

Figure 34. Histograms of SAR X_{HH} returns from areas of ocean and oil in a range of depression angles from 46° to 46.5° for Pass 2 on November 2, 1978.

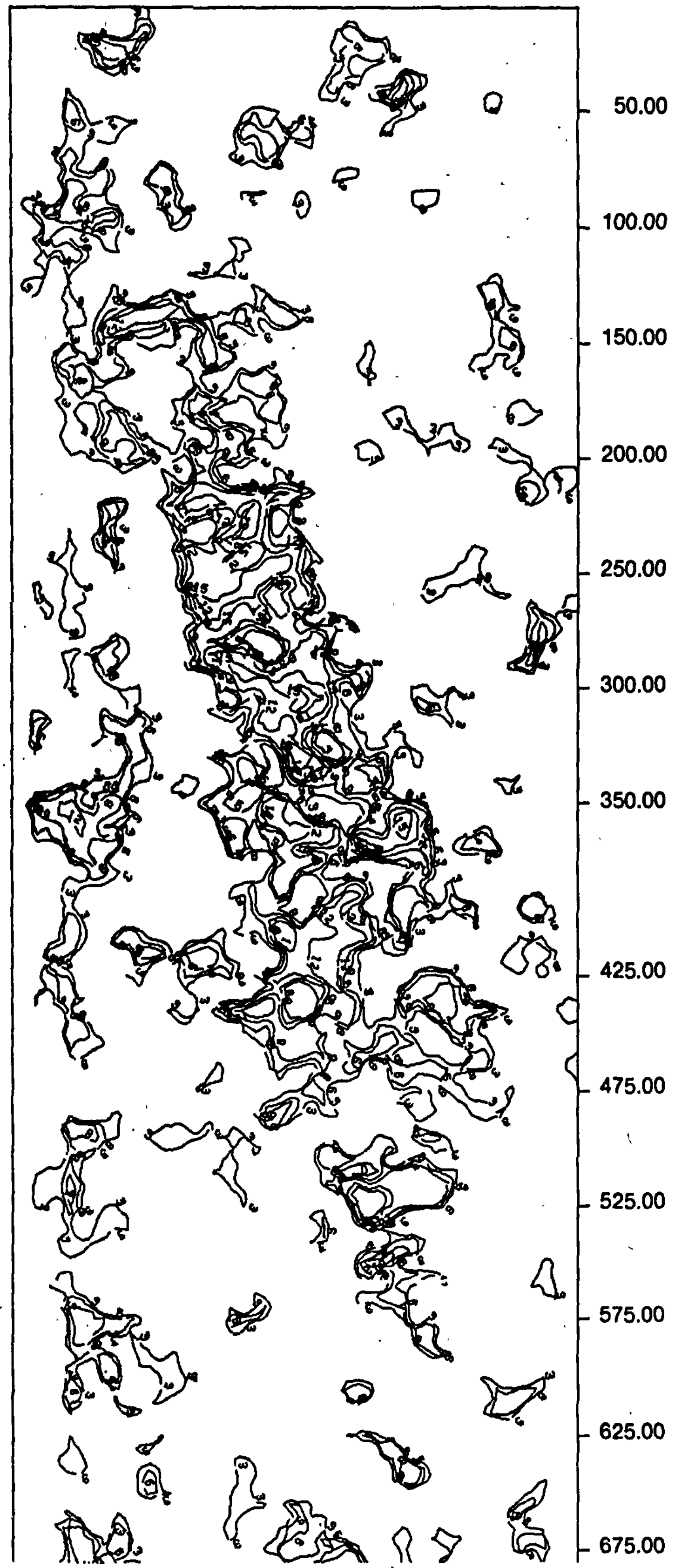

Figure 35. Contour plot of SAR L_{HH} returns of Pass 2 on November 2, 1978.

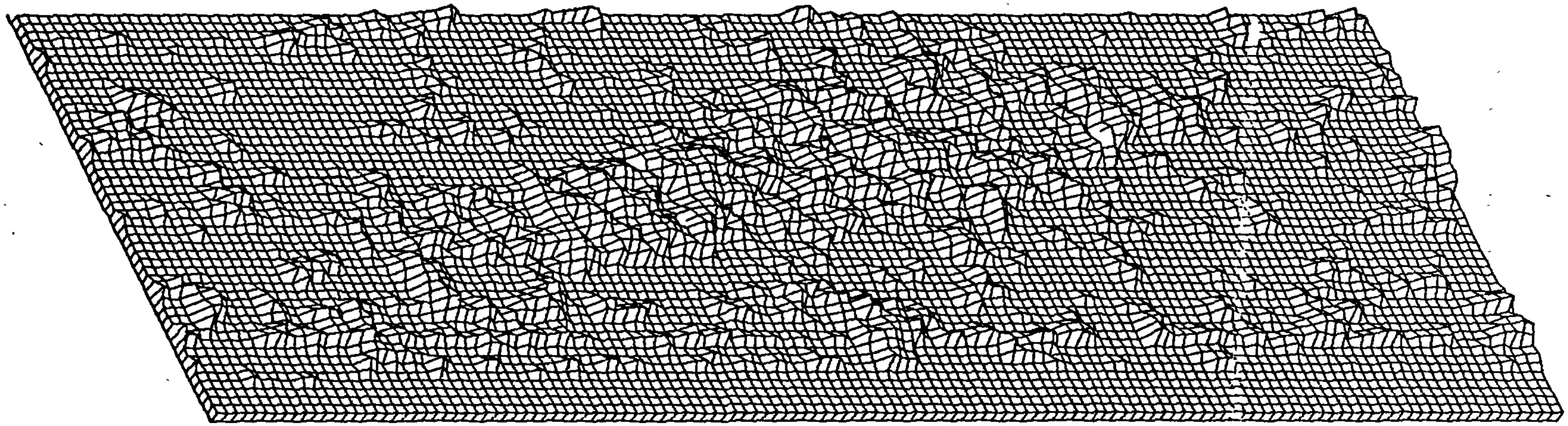

Figure 36. 3D projection of SAR L_{HH} returns of Pass 2 on November 2, 1978.

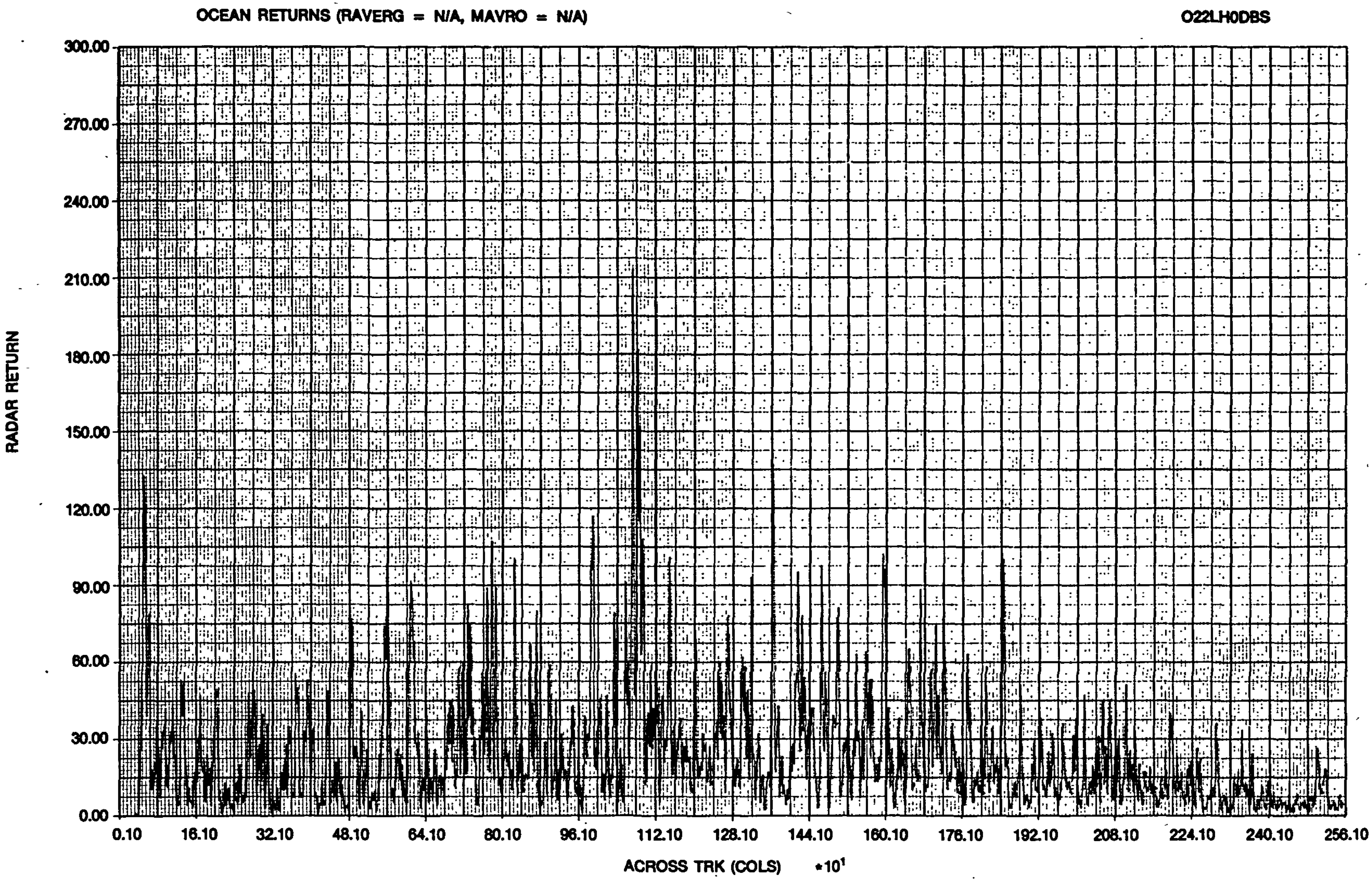

Figure 37. Unfiltered cross track profile of ocean returns for SAR L_{HH} Pass 2 on November 2, 1978.

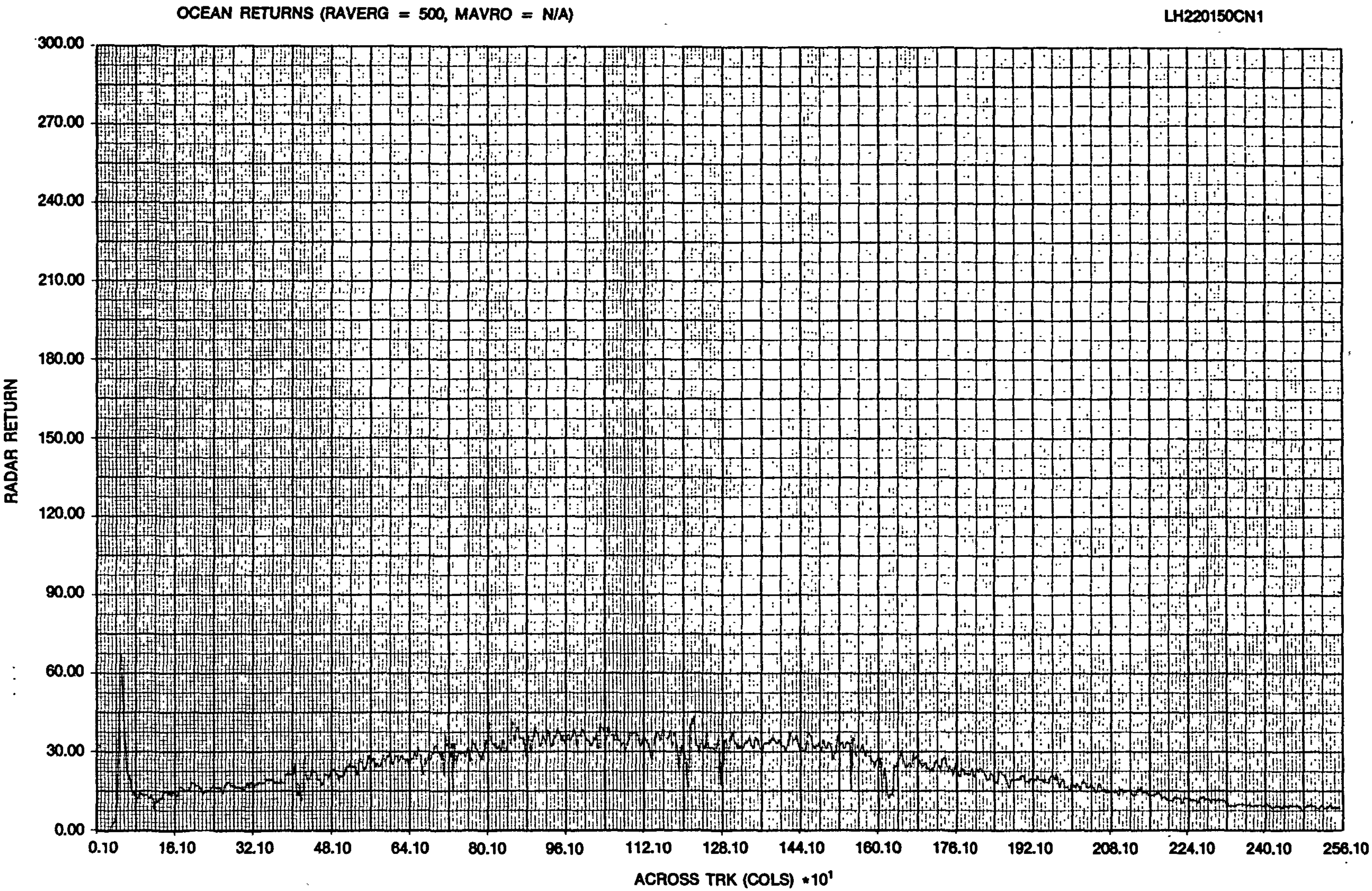

Figure 38. Filtered across track profile of ocean returns for SAR L_{HH} Pass 2 on November 2, 1978.

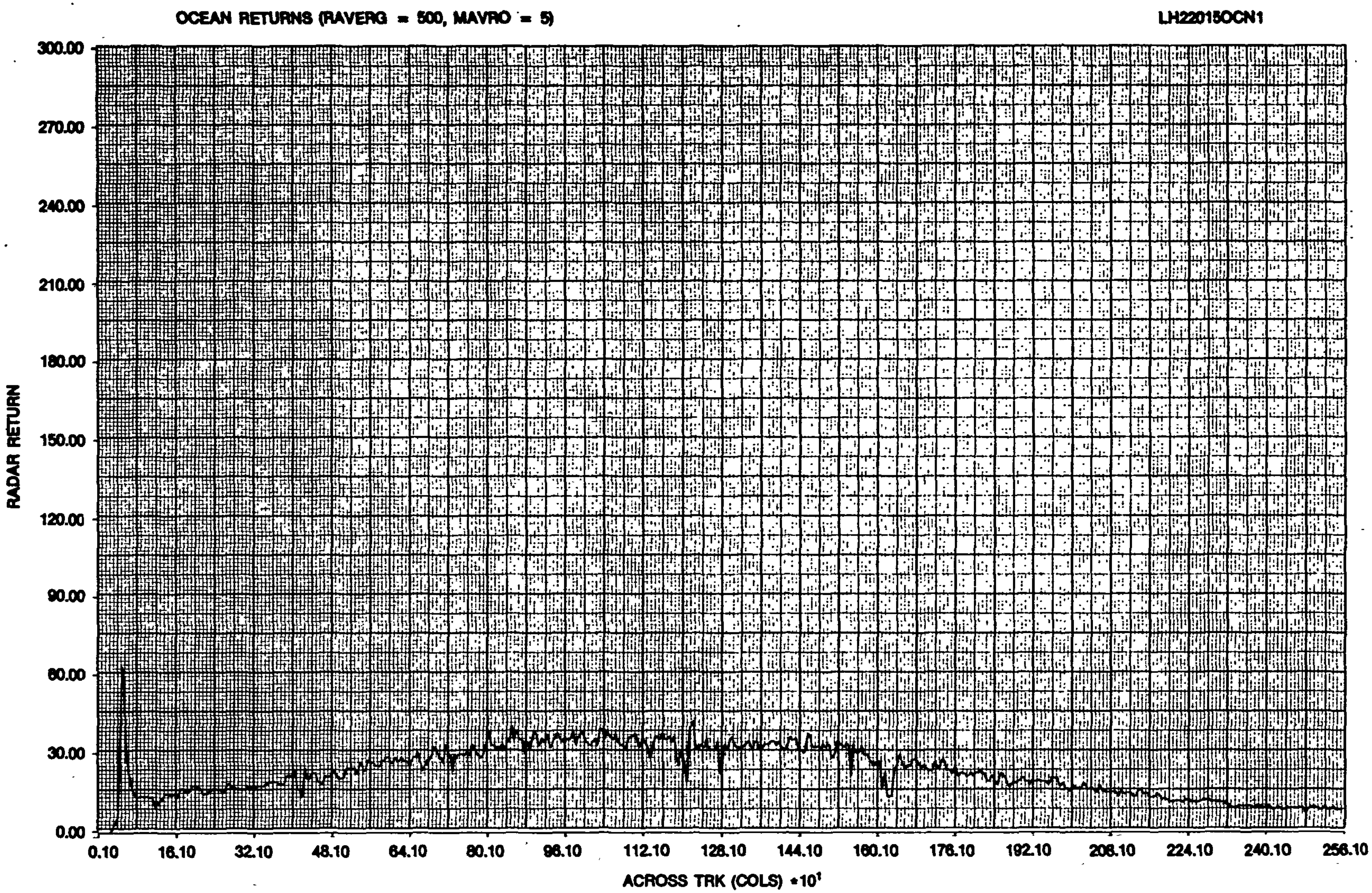

Figure 39. Filtered across track profile of ocean returns for SAR L_{HH} for Pass 2 on November 2, 1978.

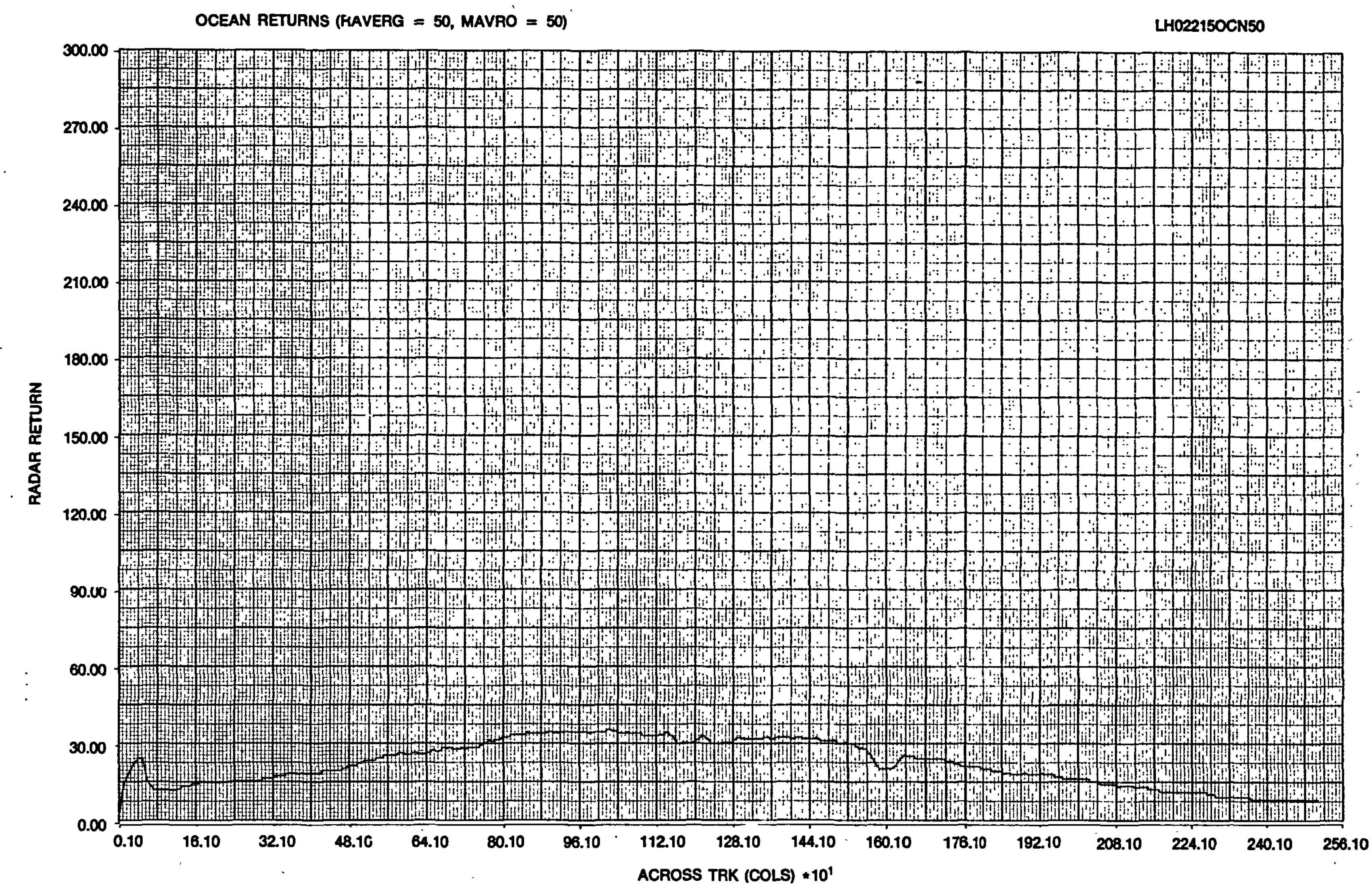

Figure 40. Filtered across track profile of ocean returns for SAR L_{HH} for Pass 2 on November 2, 1978.

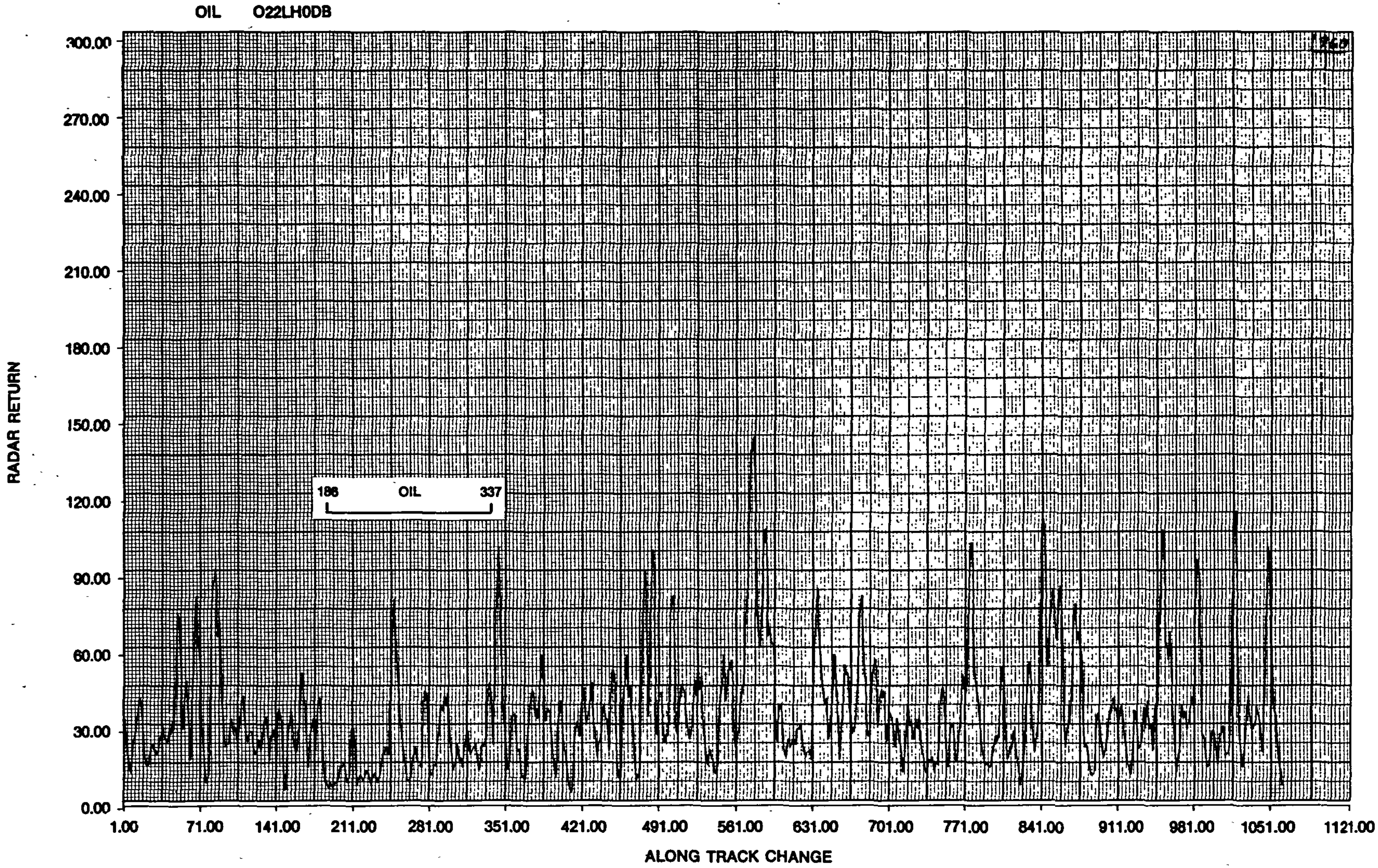

Figure 41. Filtered along track profile of SAR L_{HH} returns from oil and ocean at a depression angle of 46° for Pass 2 on November 2, 1978.

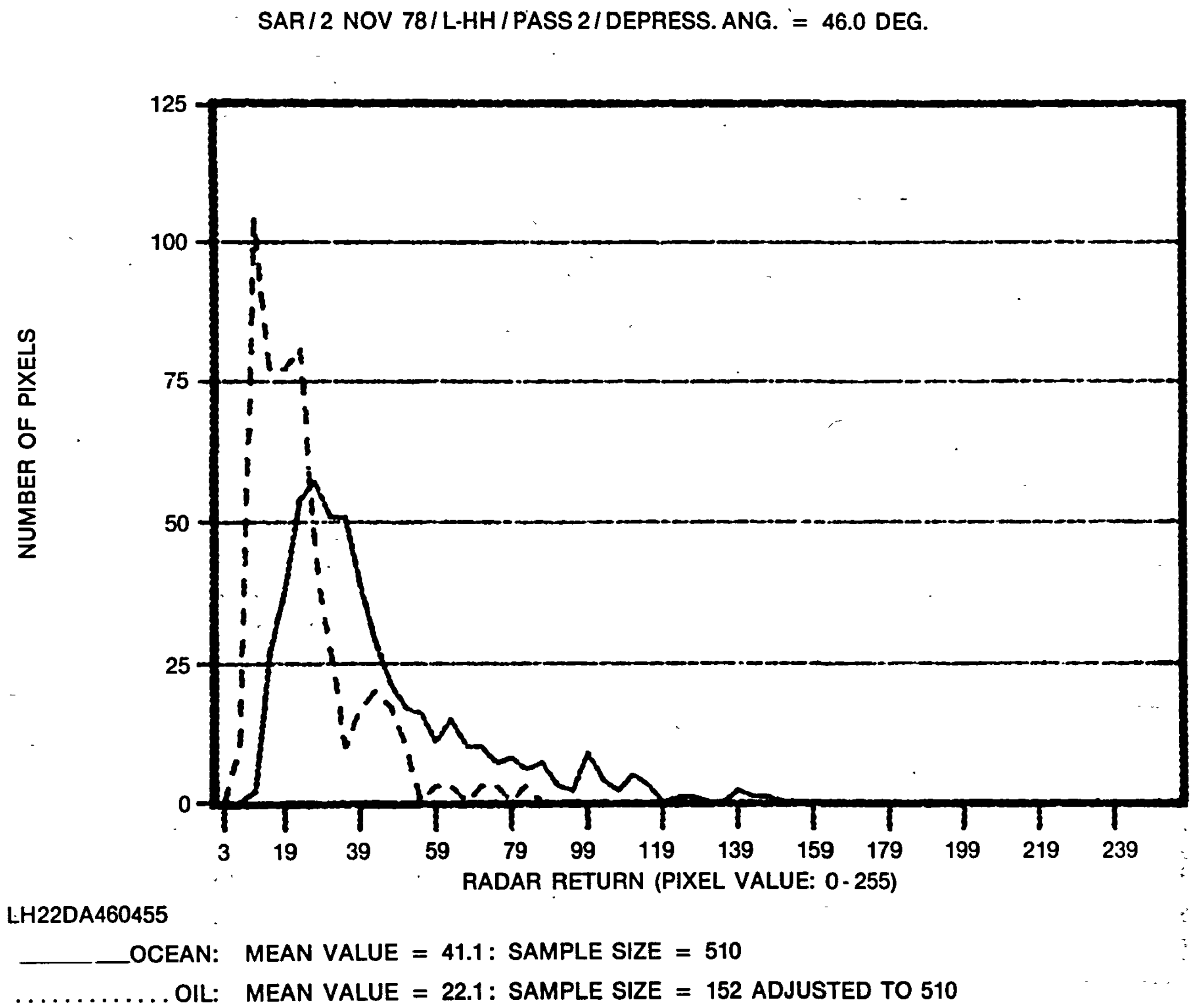

Figure 42. Histograms of SAR L_{HH} returns from oil and ocean at a depression angle of 46° for Pass 2 on November 2, 1978.

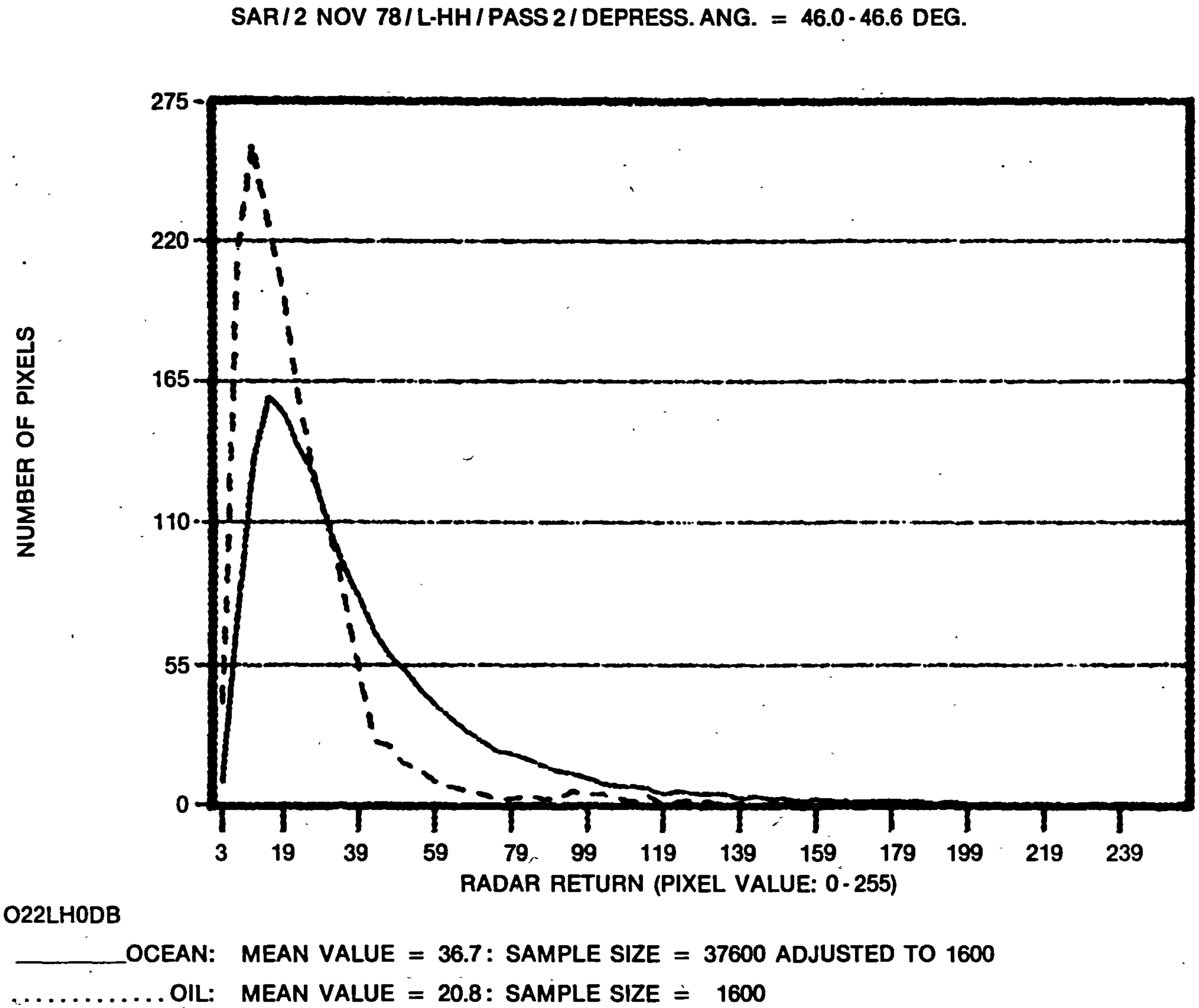

Figure 43. Histograms of SAR L_{HH} returns from areas of oil and ocean in the range of depression angles from 46° to 46.6° for Pass 2 on November 2, 1978.

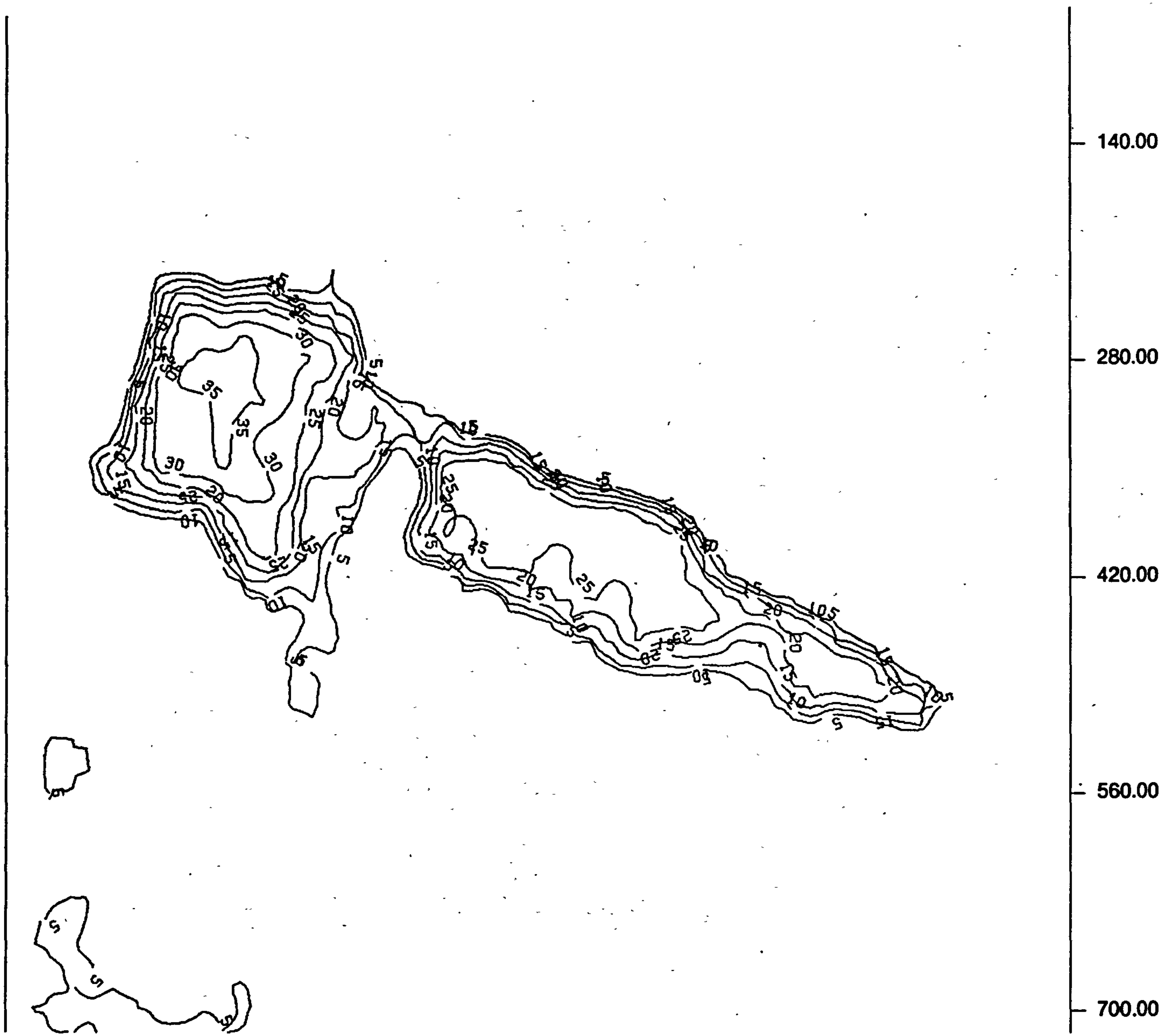

Figure 44. Contour plot of SAR X_{HH} returns of Pass 5 on November 3, 1978.

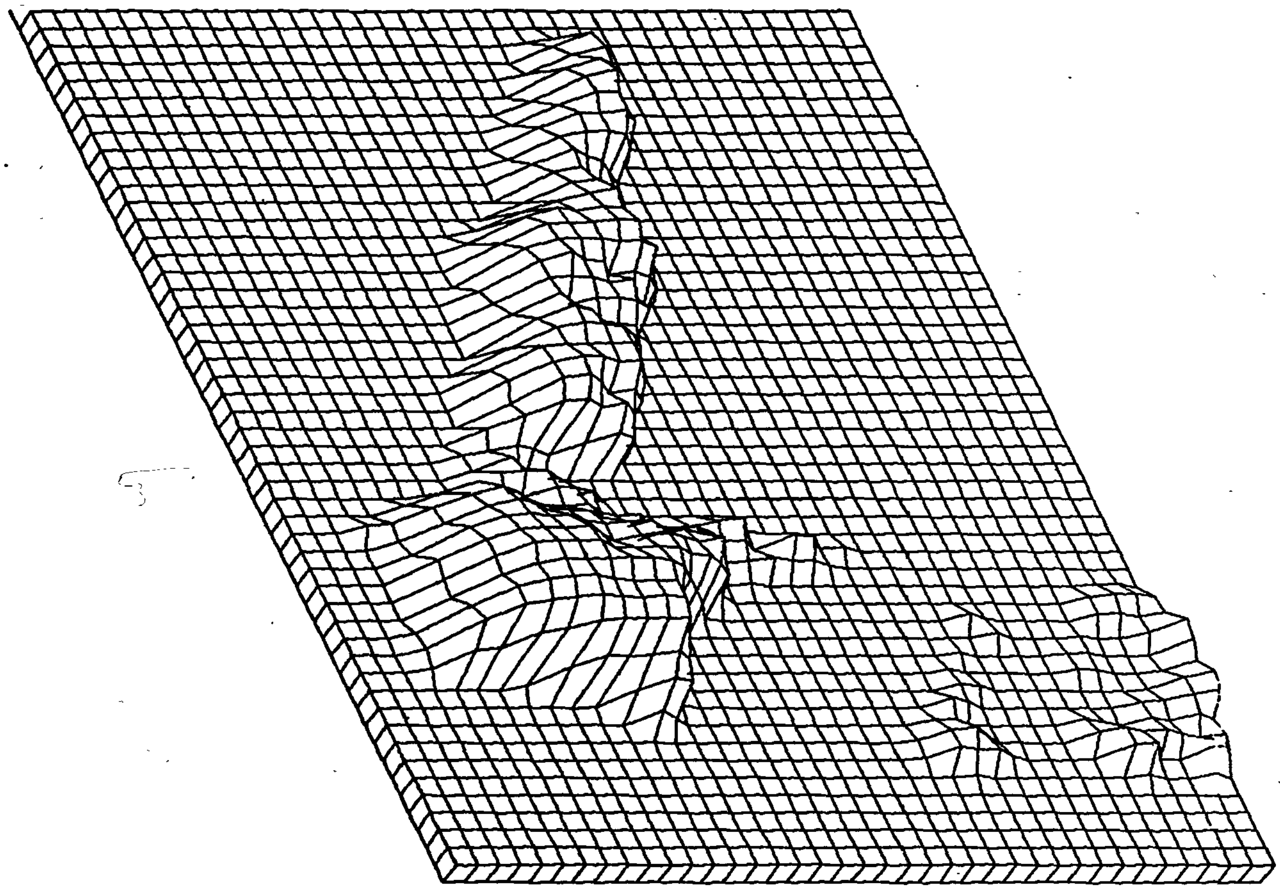

Figure 45. 3D projection of SAR X_{HH} returns of Pass 5 on November 3, 1978.

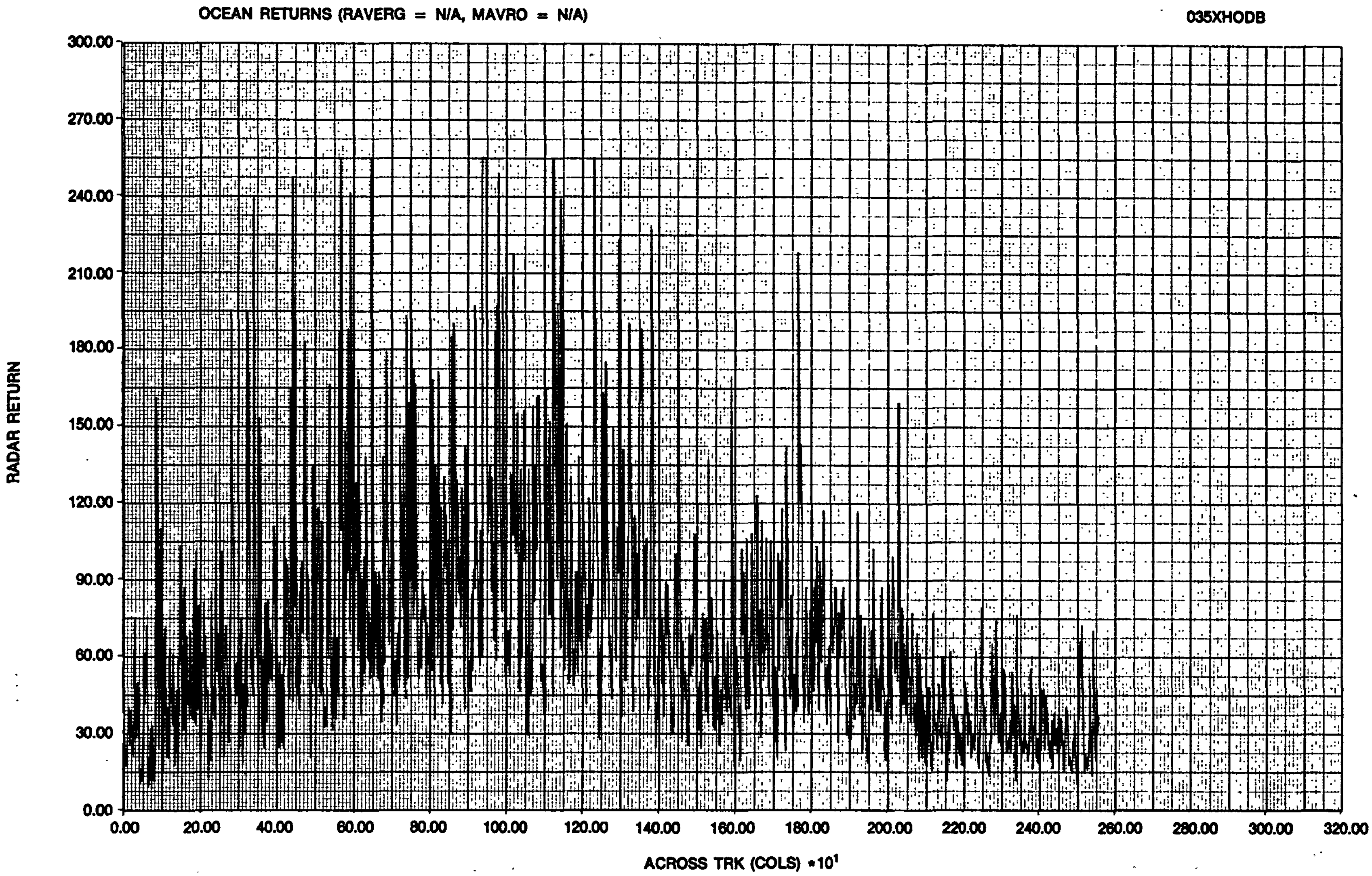

Figure 46. Unfiltered across track profile of ocean returns for SAR X_{HH} for Pass 5 on November 3, 1978.

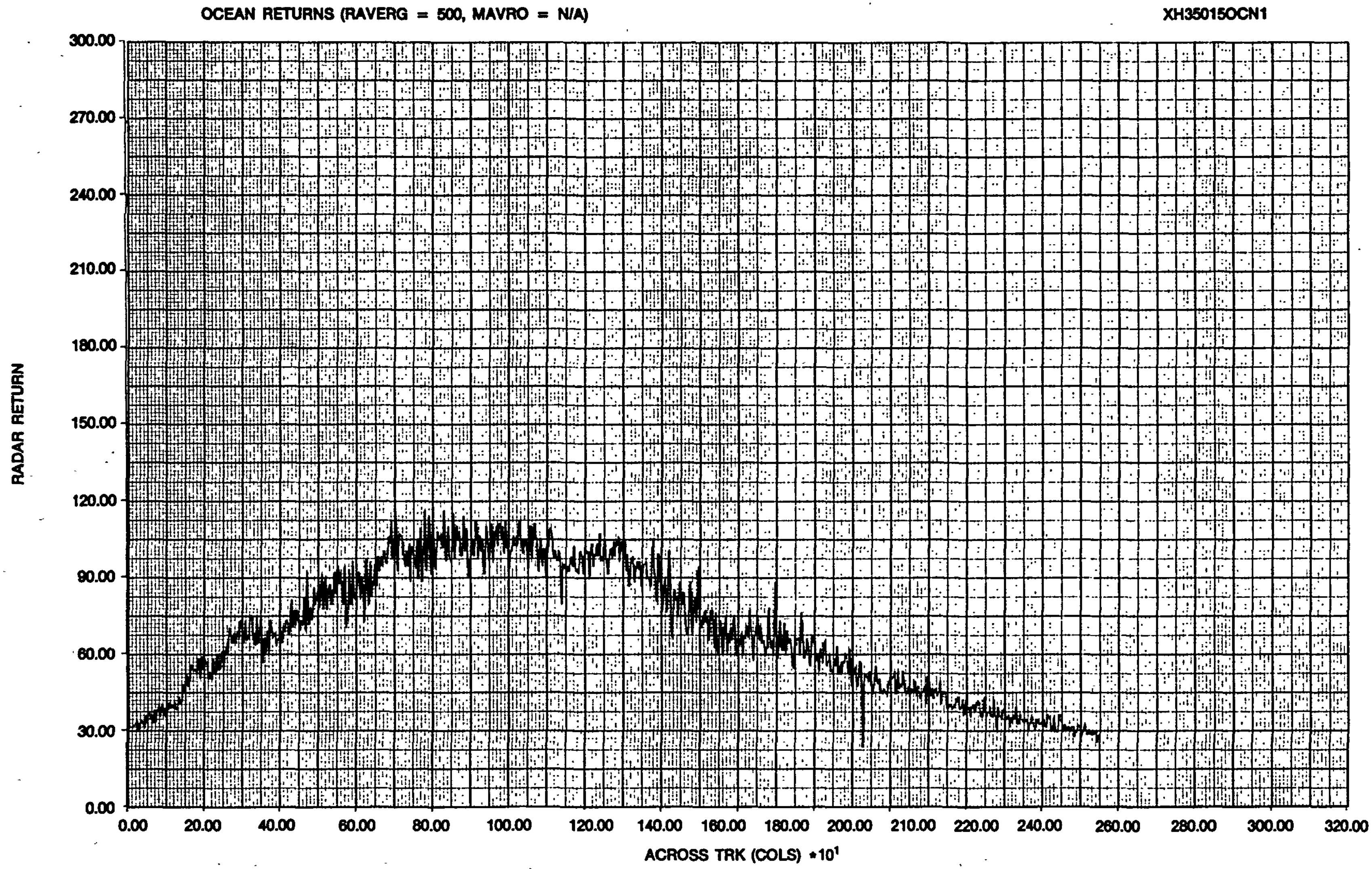

Figure 47. Filtered across track profile of ocean returns for SAR X_{HH} for Pass 5 on November 3, 1978.

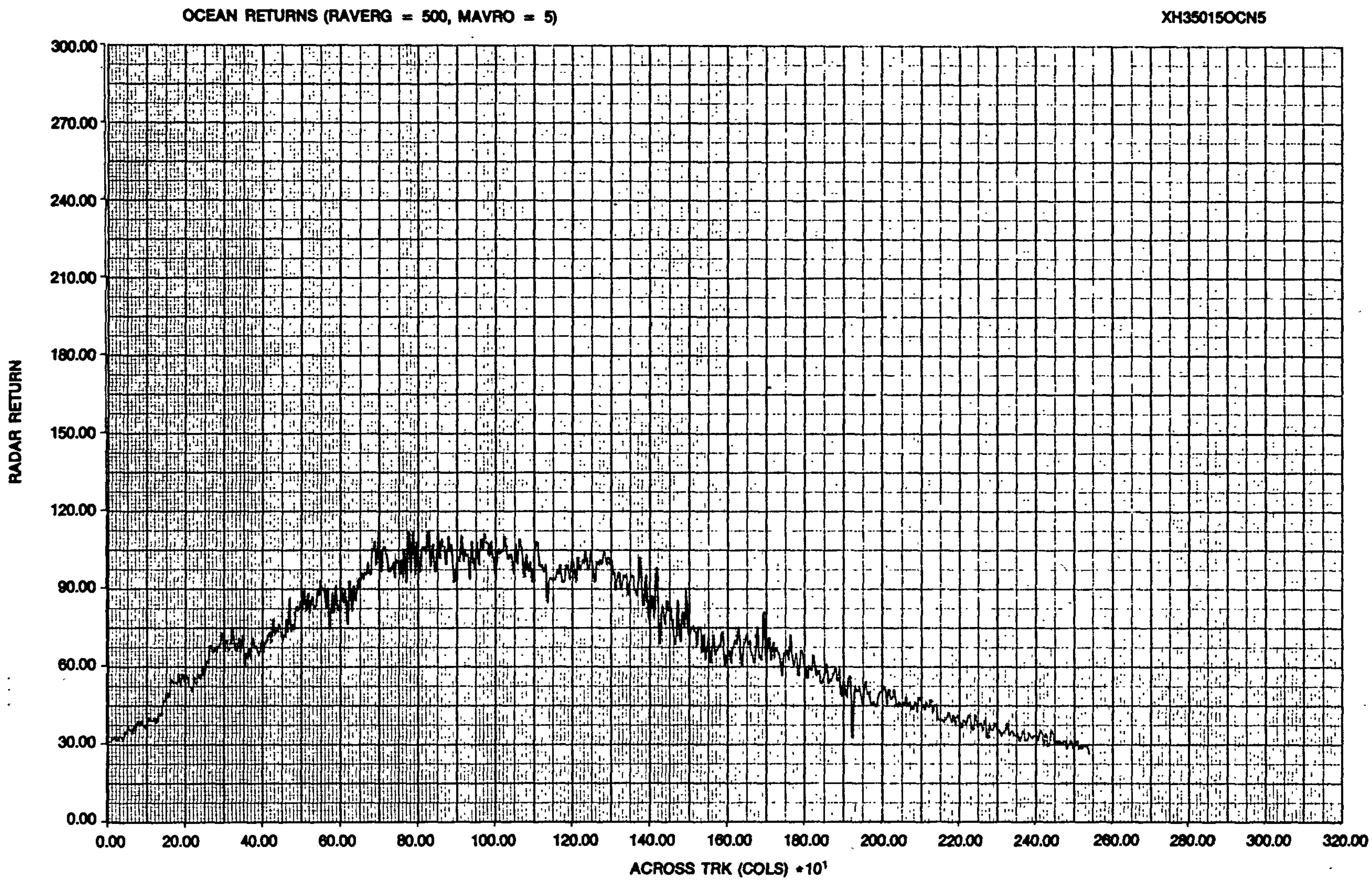

Figure 48. Filtered across track profile of ocean returns for SAR X_{HH} for Pass 5 on November 3, 1978.

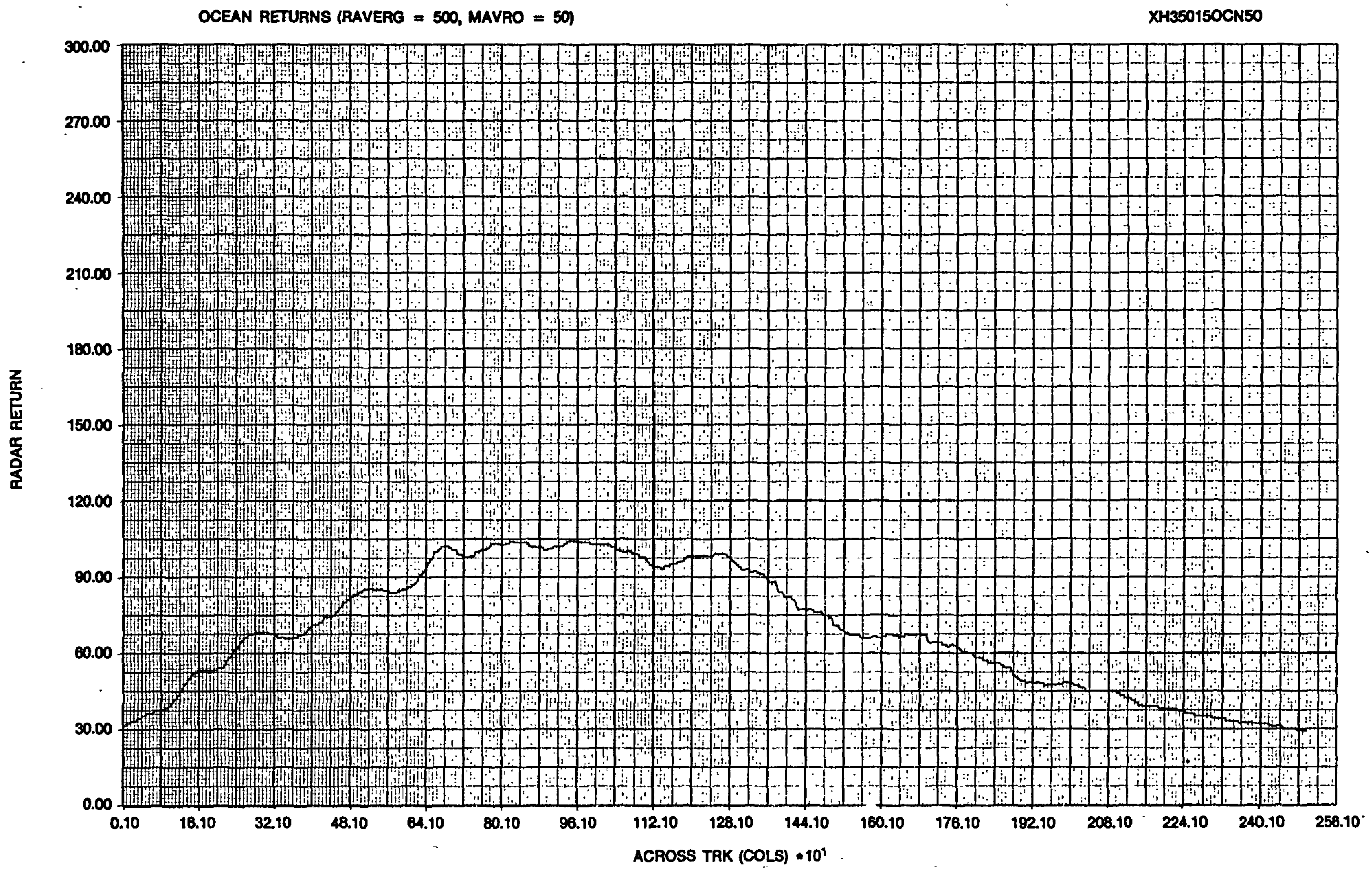

Figure 49. Filtered across track profile of ocean returns for SAR X_{HH} for Pass 5 on November 3, 1978.

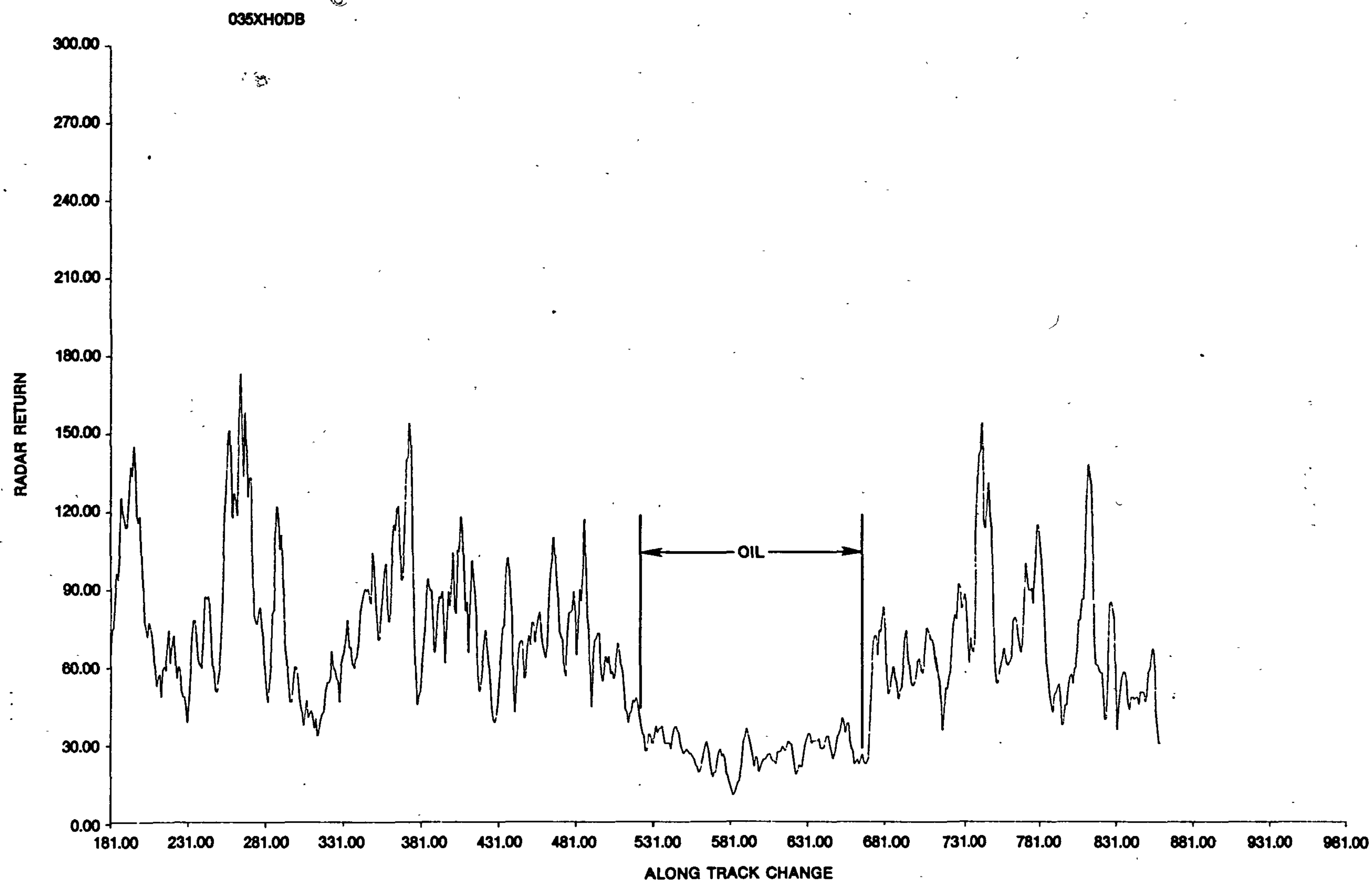

Figure 50. Filtered along track profile of SAR X_{HH} returns from oil and ocean for a depression angle of 47° for Pass 5 on November 3, 1978.

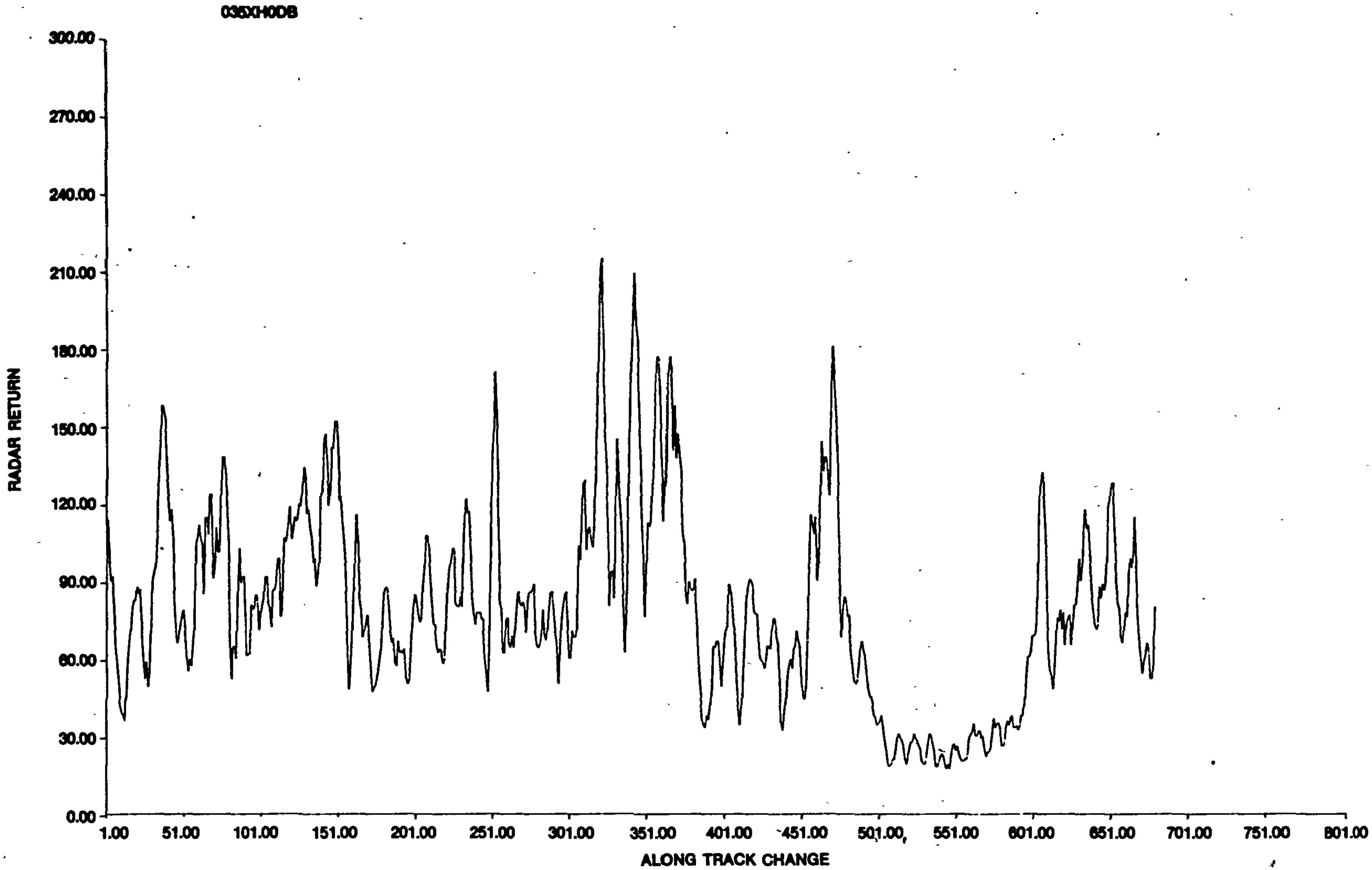

Figure 51. Filtered along track profile of SAR X_{HH} returns from oil and ocean for a depression angle of 43.5° for Pass 5 on November 3, 1978.

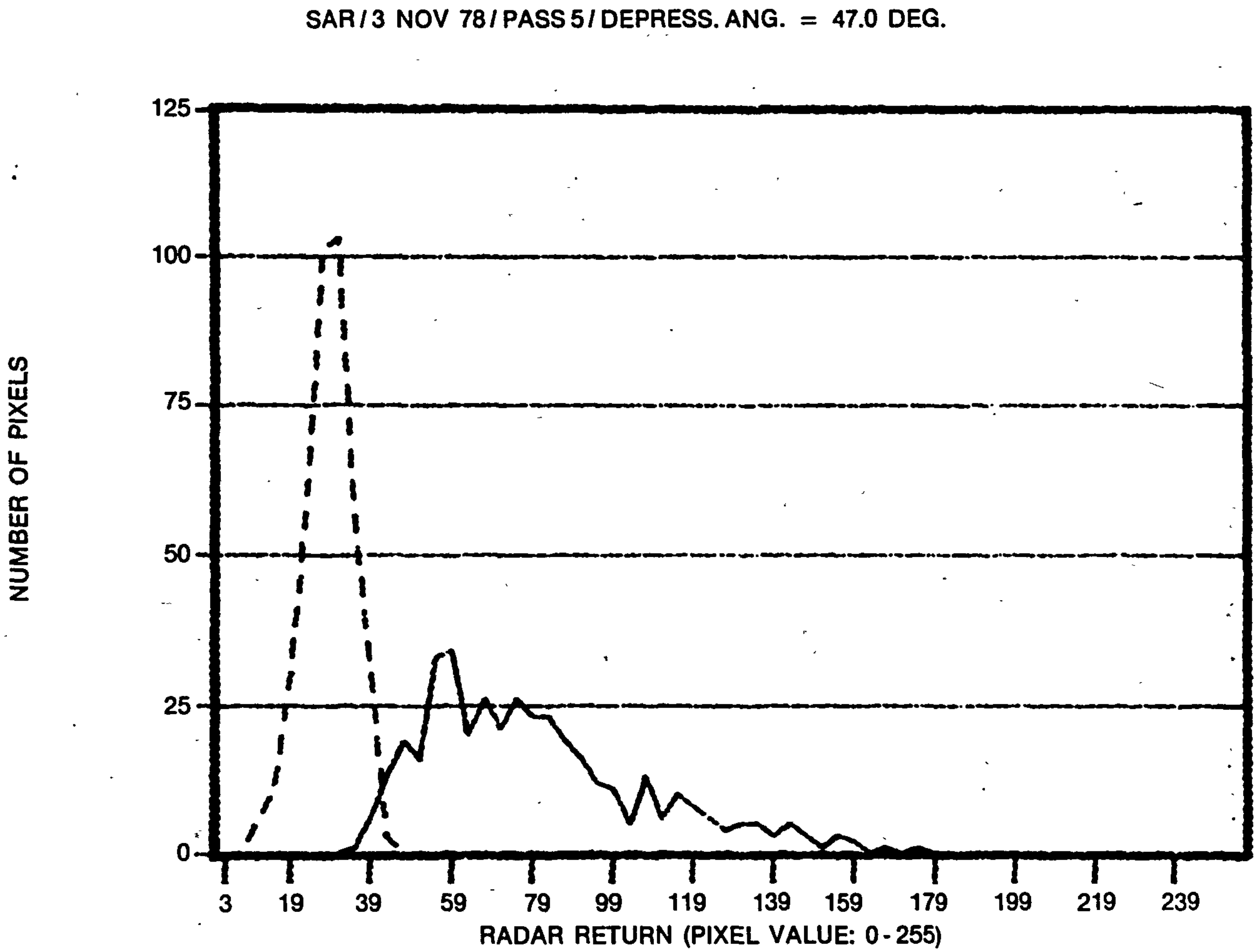

XH35DA5247

__________OCEAN: MEAN VALUE = 78.5: SAMPLE SIZE = 400

. . . . OIL: MEAN VALUE = 27.0: SAMPLE SIZE = 143 ADJUSTED TO 400

Figure 52. Histograms of SAR X_{HH} returns for oil and ocean at a depression angle of 47° for Pass 5 on November 3, 1978.

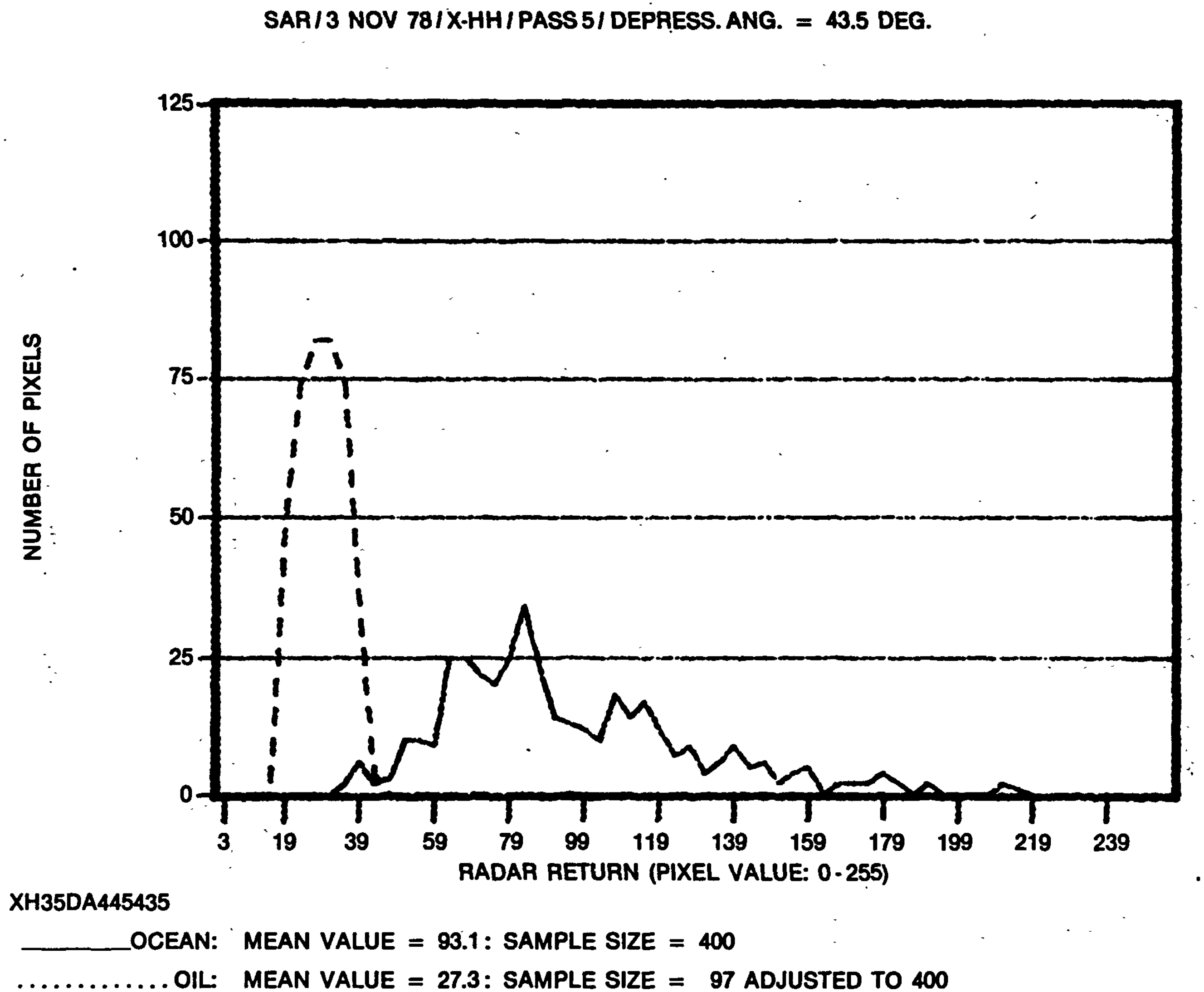

Figure 53. Histograms of SAR X_{HH} returns for oil and ocean at a depression angle of 43.5° for Pass 5 on November 3, 1978.

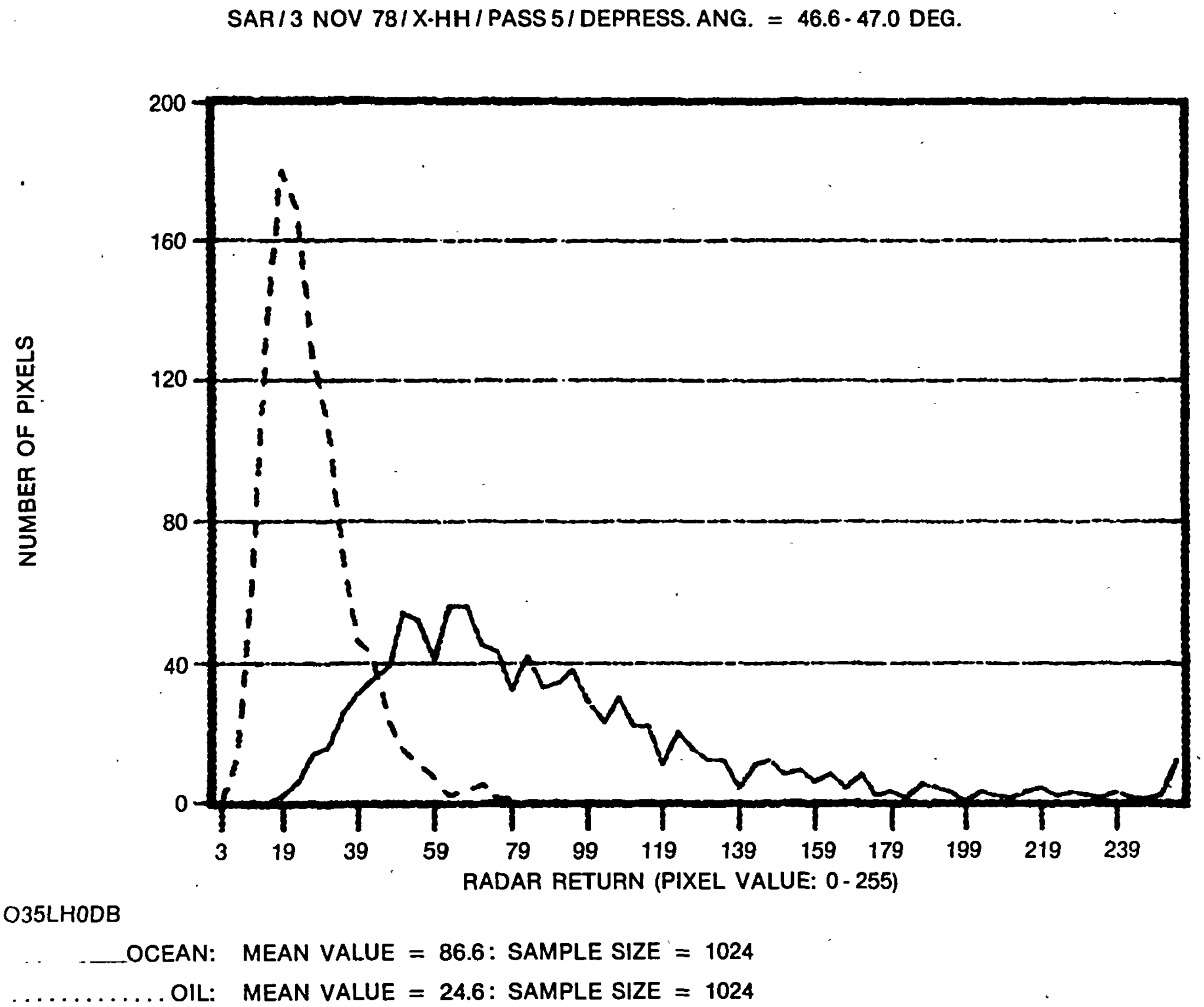

Figure 54. Histograms for SAR X_{HH} returns from areas of oil and ocean in the range of depression angles from 46.6° to 47° for Pass 5 on November 3, 1978.

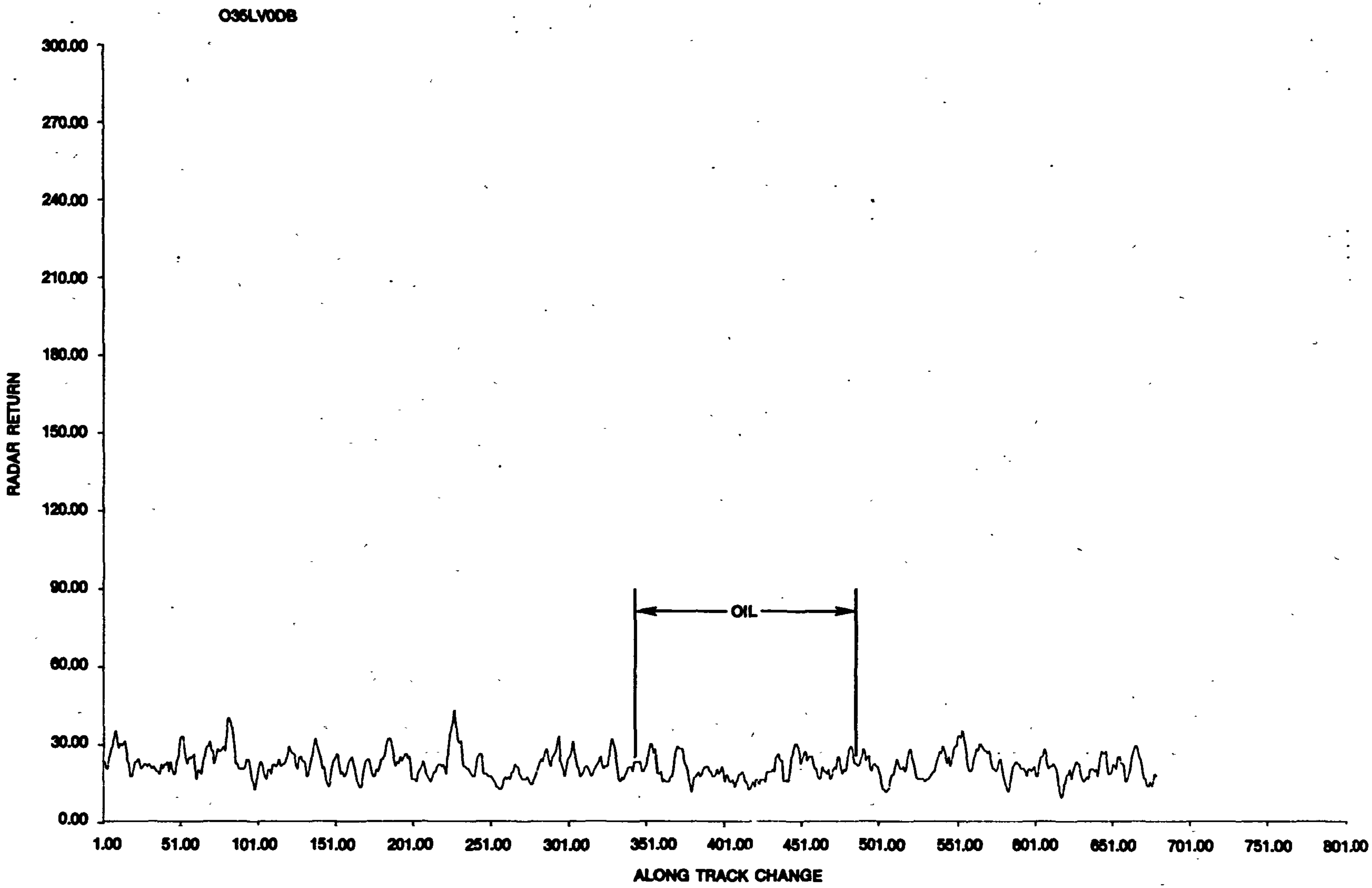

Figure 55. Filtered along track profile of SAR X_{HV} returns from oil and ocean for a depression angle of 47° for Pass 5 on November 3, 1978.

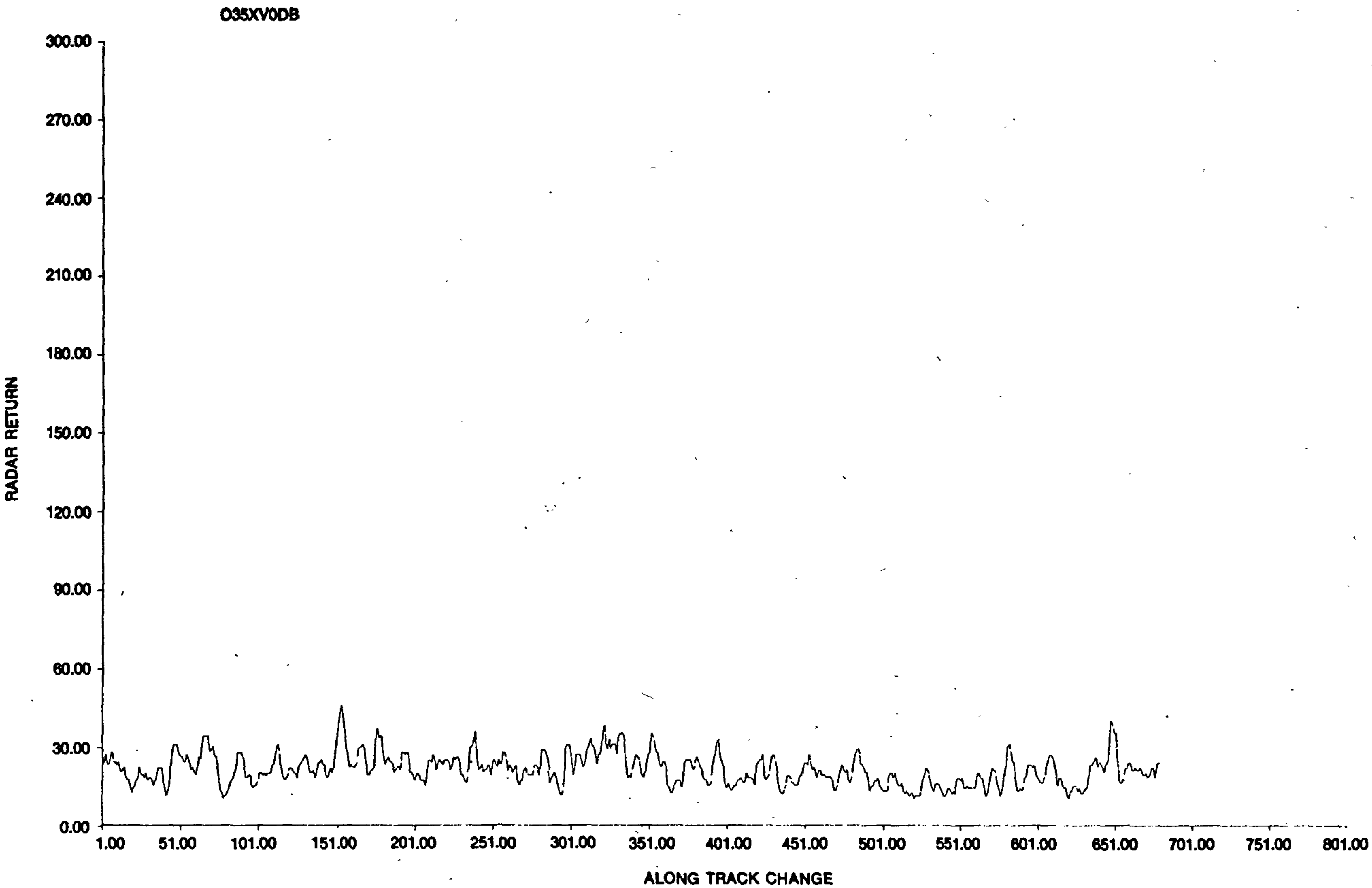

Figure 56. Filtered along track profile of SAR X_{HV} returns from oil and ocean for a depression angle of 43.5° for Pass 5 on November 3, 1978.

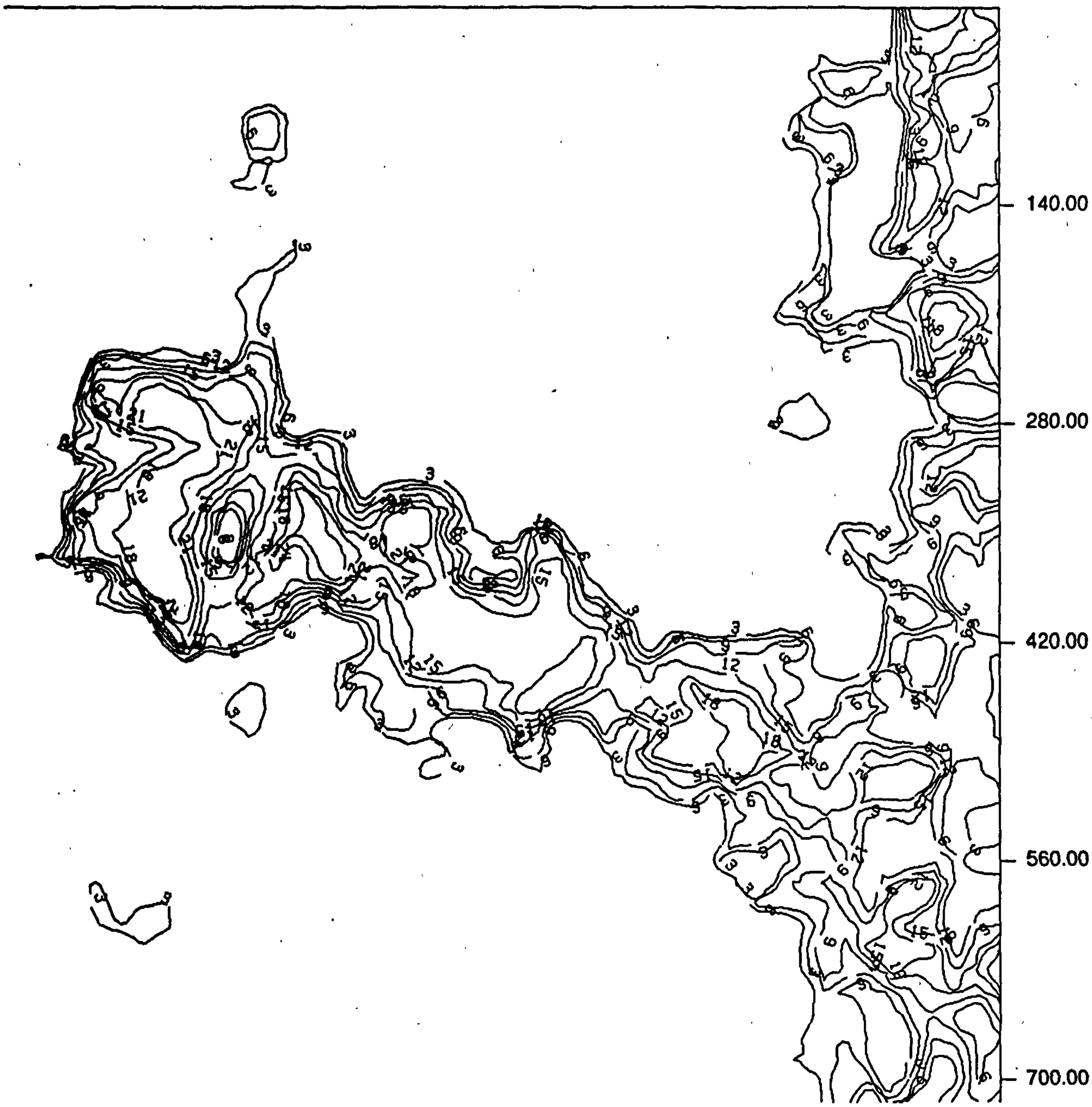

Figure 57. Contour plot of SAR L_{HH} returns for Pass 5 on November 3, 1978.

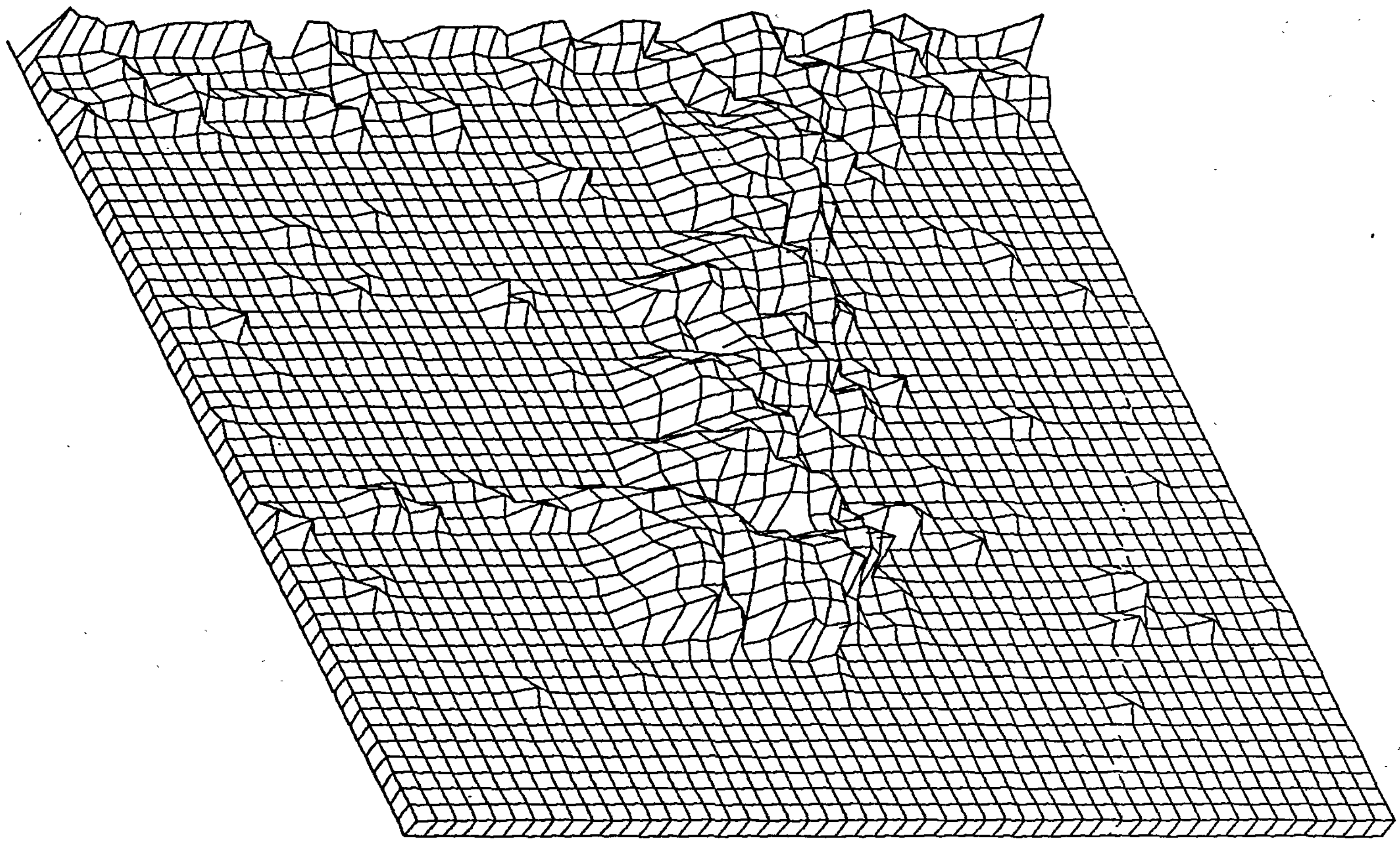

Figure 58. 3D projection of SAR L_{HH} returns for Pass 5 on November 3, 1978.

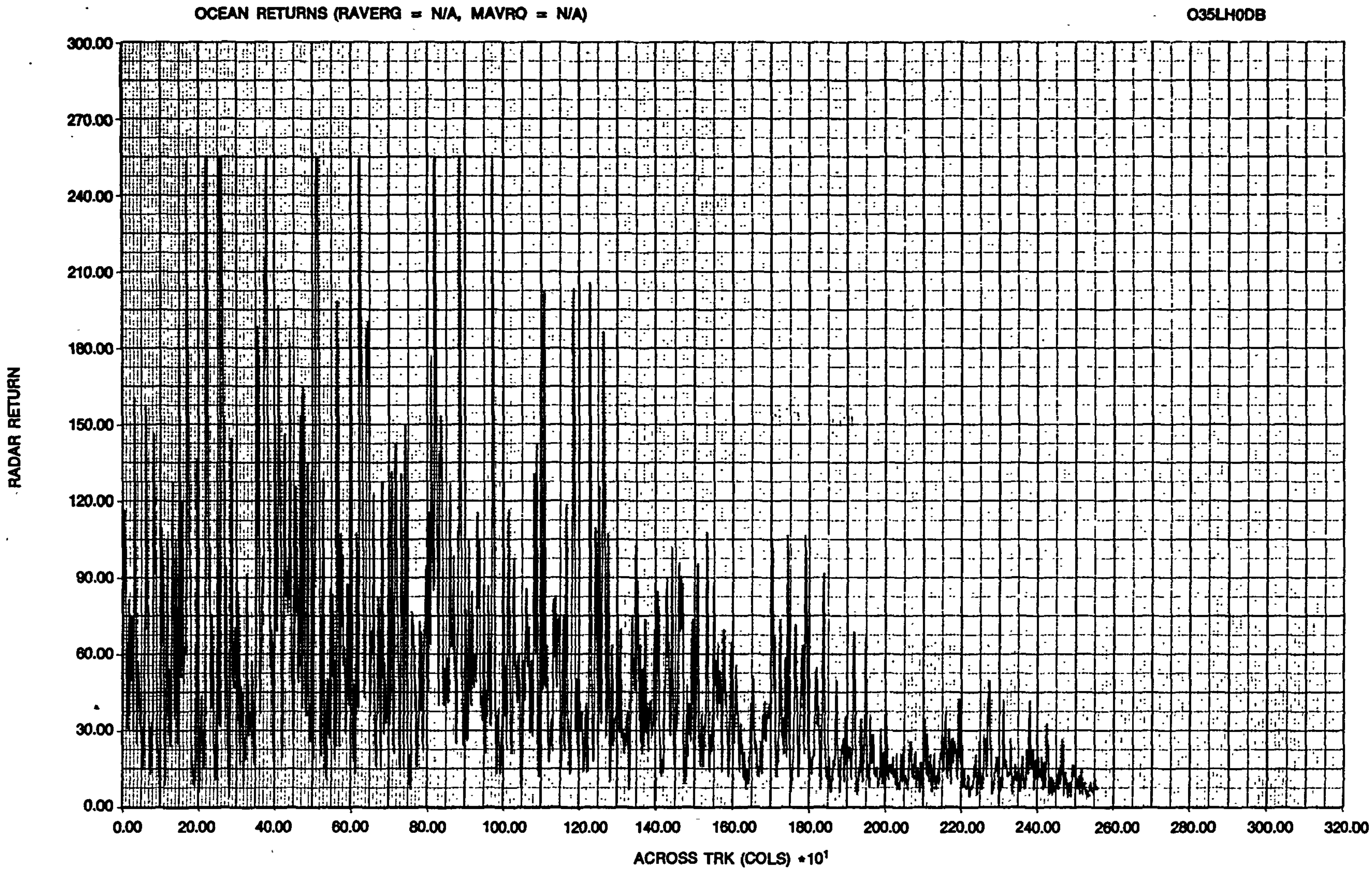

Figure 59. Unfiltered across track profile of SAR L_{HH} ocean returns for Pass 5 on November 3, 1978.

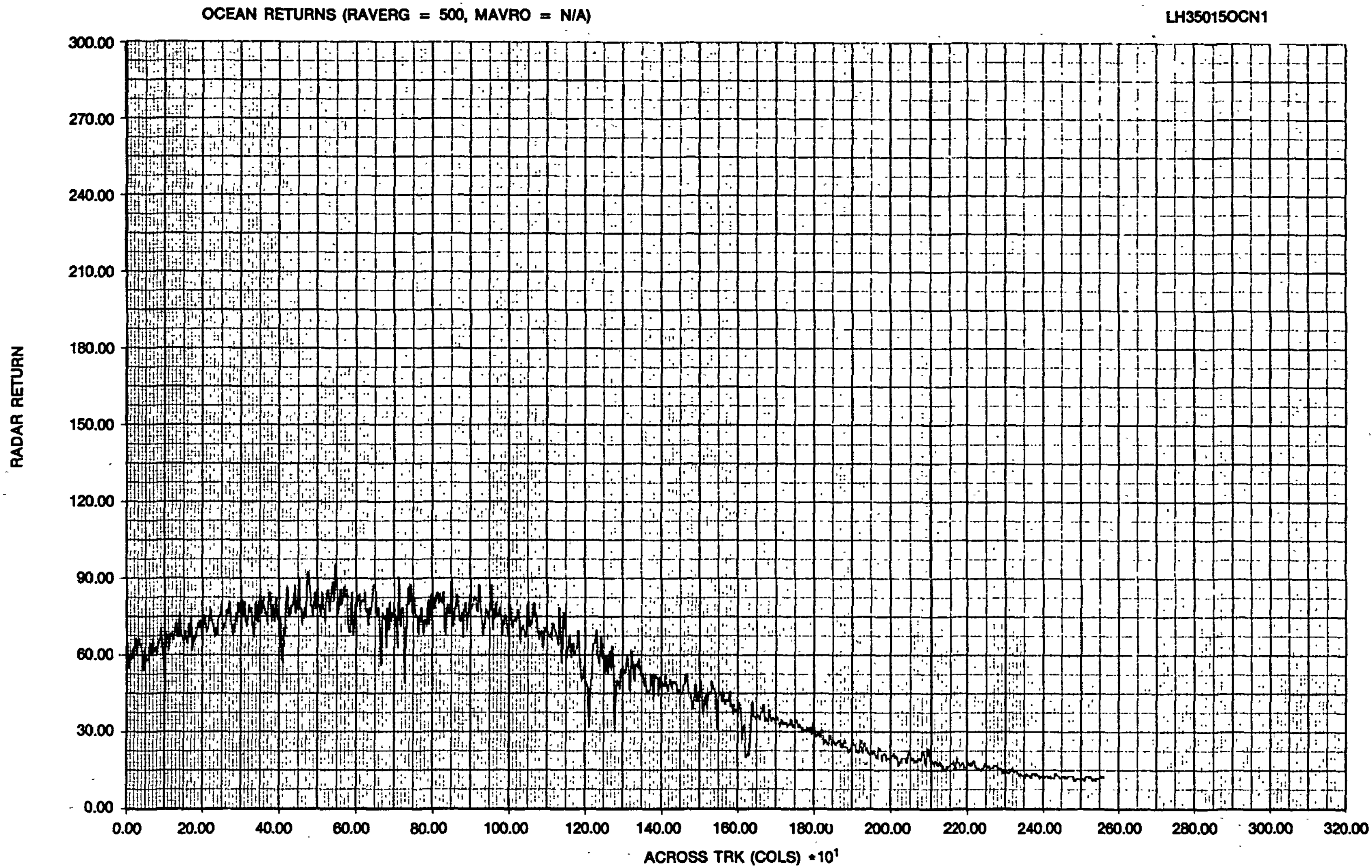

Figure 60. Filtered across track profile of SAR L_{HH} ocean returns for Pass 5 on November 3, 1978.

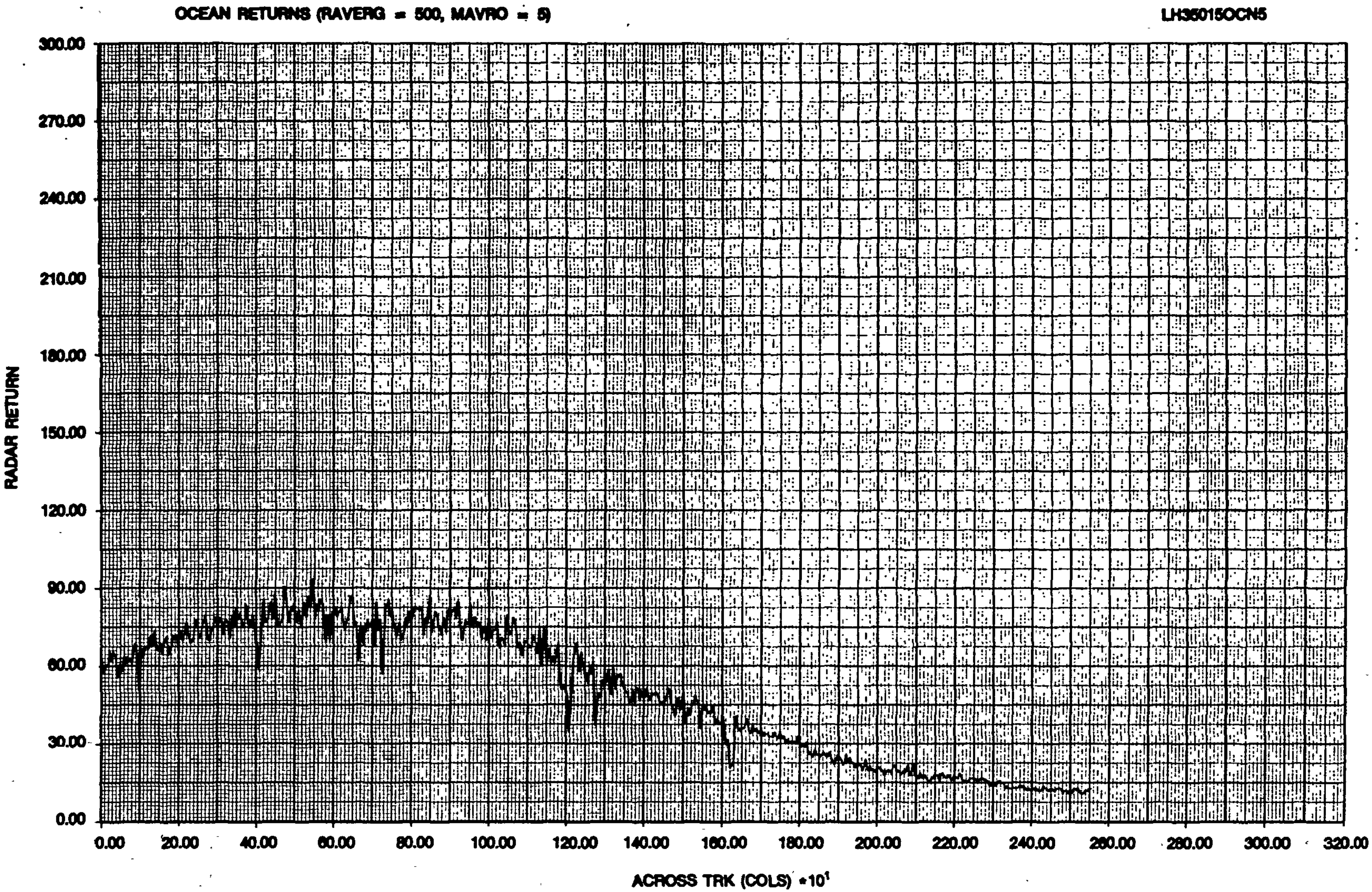

Figure 61. Filtered across track profile of SAR L_{HH} ocean returns for Pass 5 on November 3, 1978.

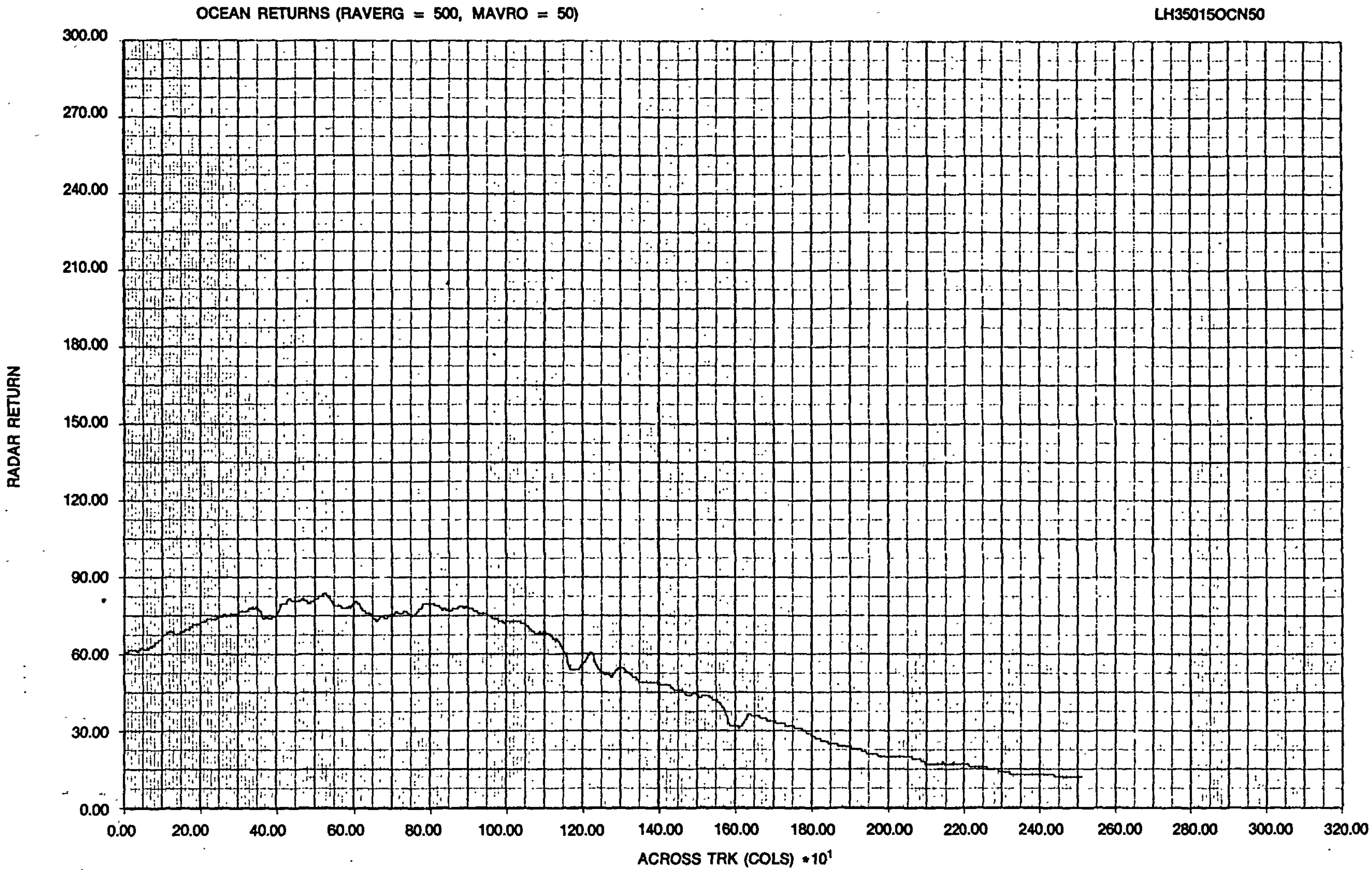

Figure 62. Filtered across track profile of SAR L_{HH} ocean returns for Pass 5 on November 3, 1978.

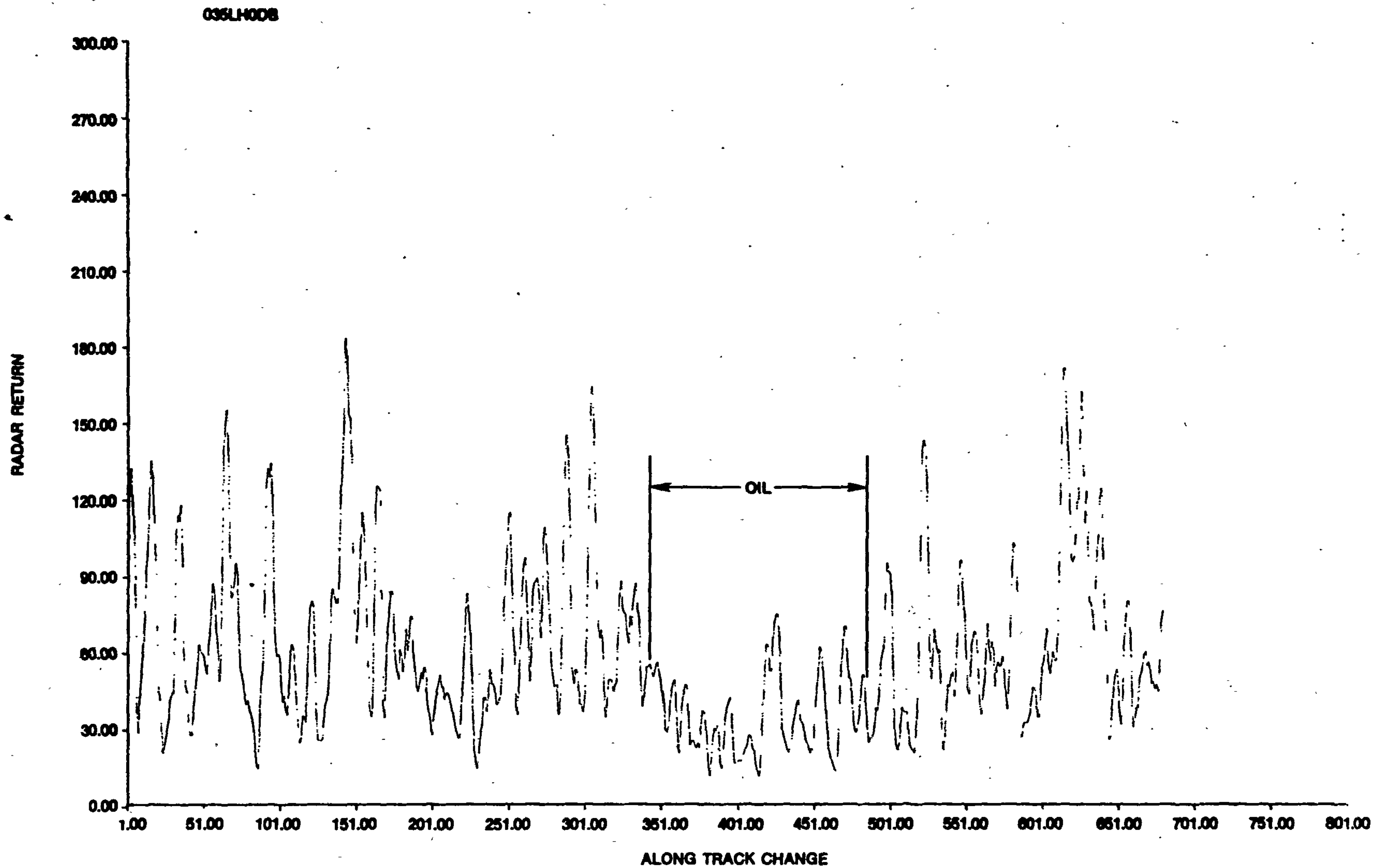

Figure 63. Filtered along track profile of SAR L_{HH} returns from oil and ocean for a depression angle of 47° for Pass 5 on November 3, 1978.

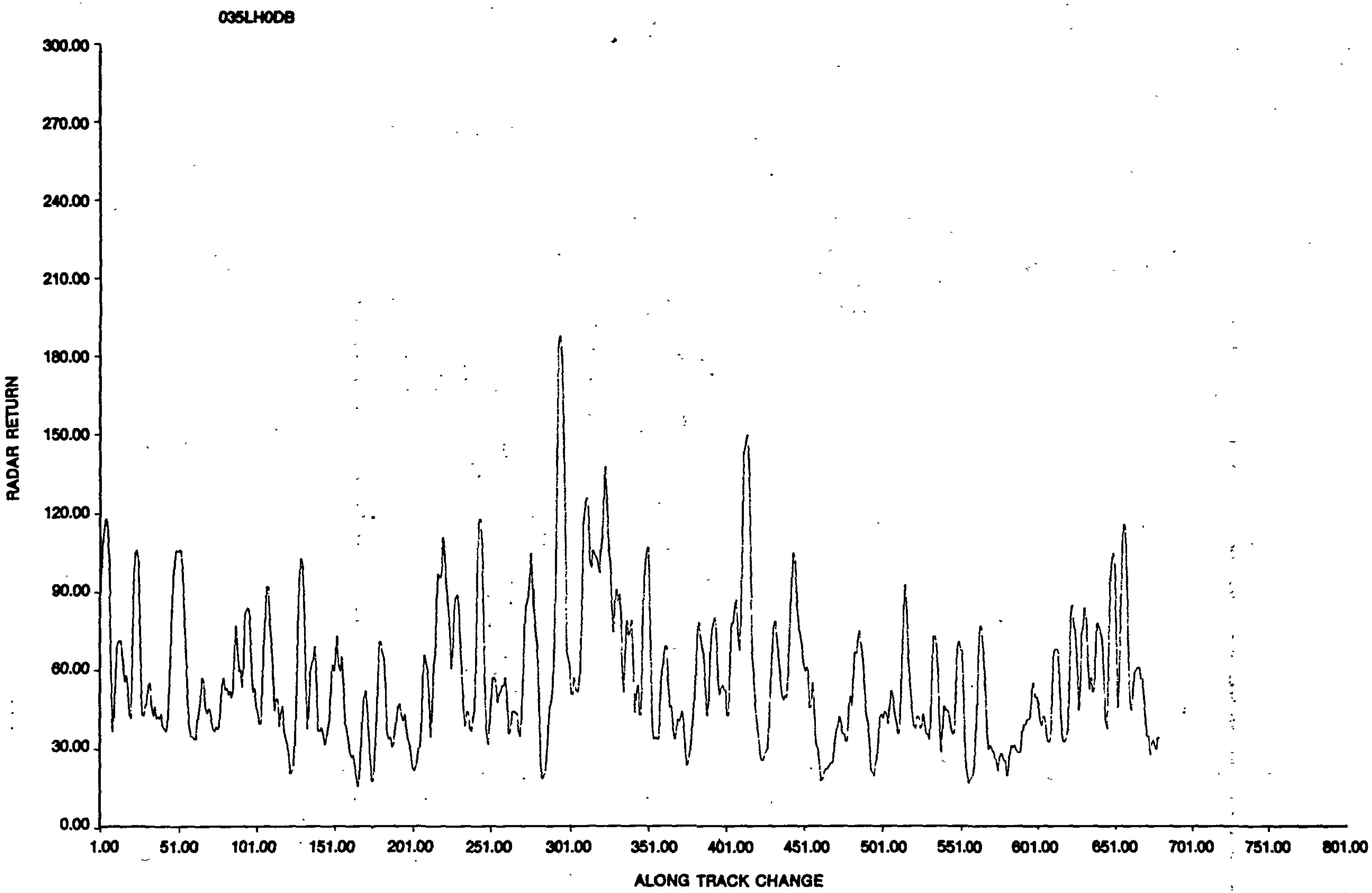

Figure 64. Filtered along track profile of SAR L_{HH} returns from oil and ocean for a depression angle of 43.5° for Pass 5 on November 3, 1978.

SAR / 3 NOV 78 / L-HH / PASS 5 / DEPRESS. ANG. = 47.0 DEG.

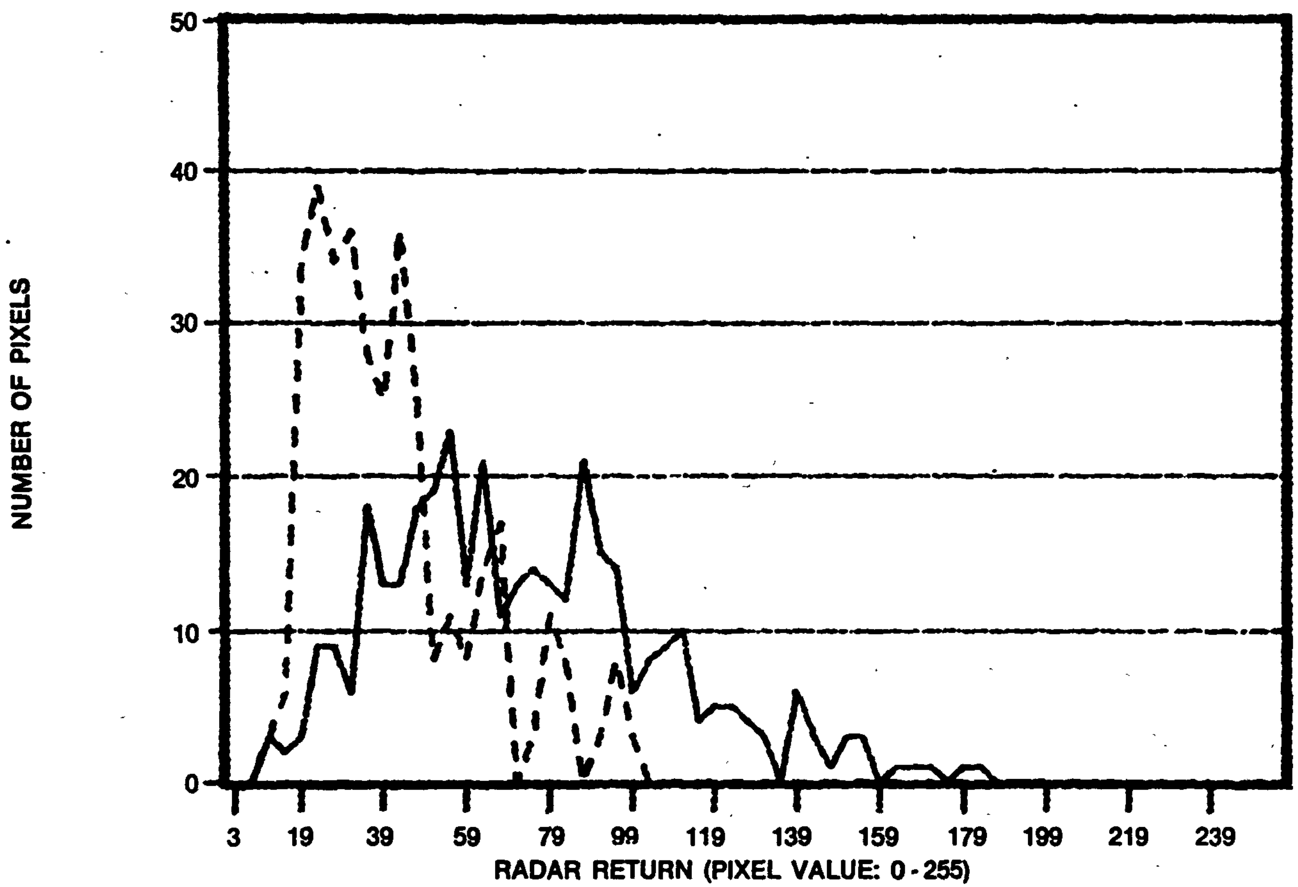

LH351DA475470

________OCEAN: MEAN VALUE = 71.3: SAMPLE SIZE = 361

.............OIL: MEAN VALUE = 40.4: SAMPLE SIZE = 129 ADJUSTED TO 361

Figure 65. Histograms of SAR L_{HH} returns for oil and ocean for a depression angle of 47° for Pass 5 on November 3, 1978.

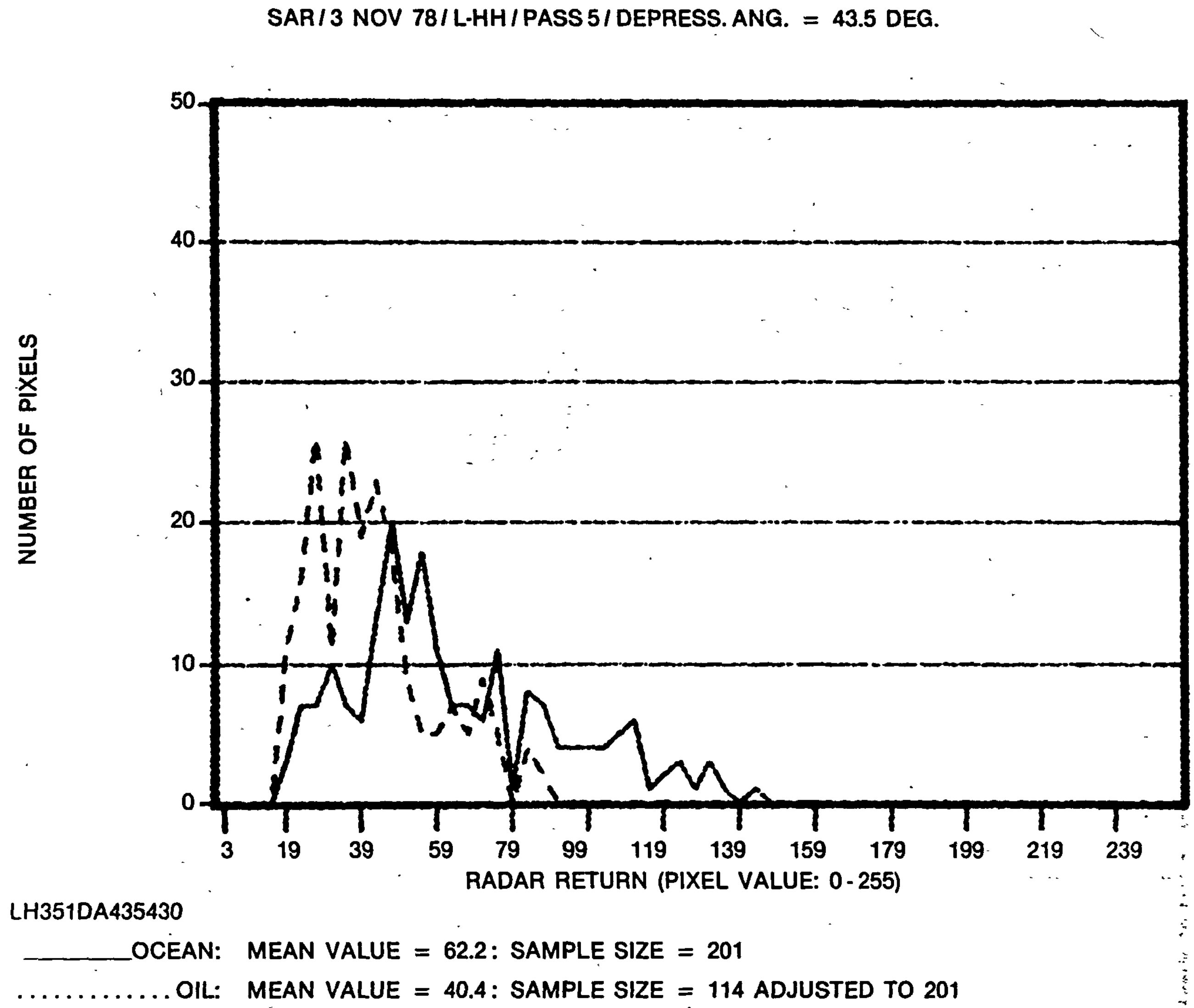

Figure 66. Histograms of SAR L_{HH} returns from oil and ocean for a depression angle of 43.5° for Pass 5 on November 3, 1978.

SAR / 3 NOV 78 / L-HH / PASS 5 / DEPRESS. ANG. = 46.0 - 46.5 DEG.

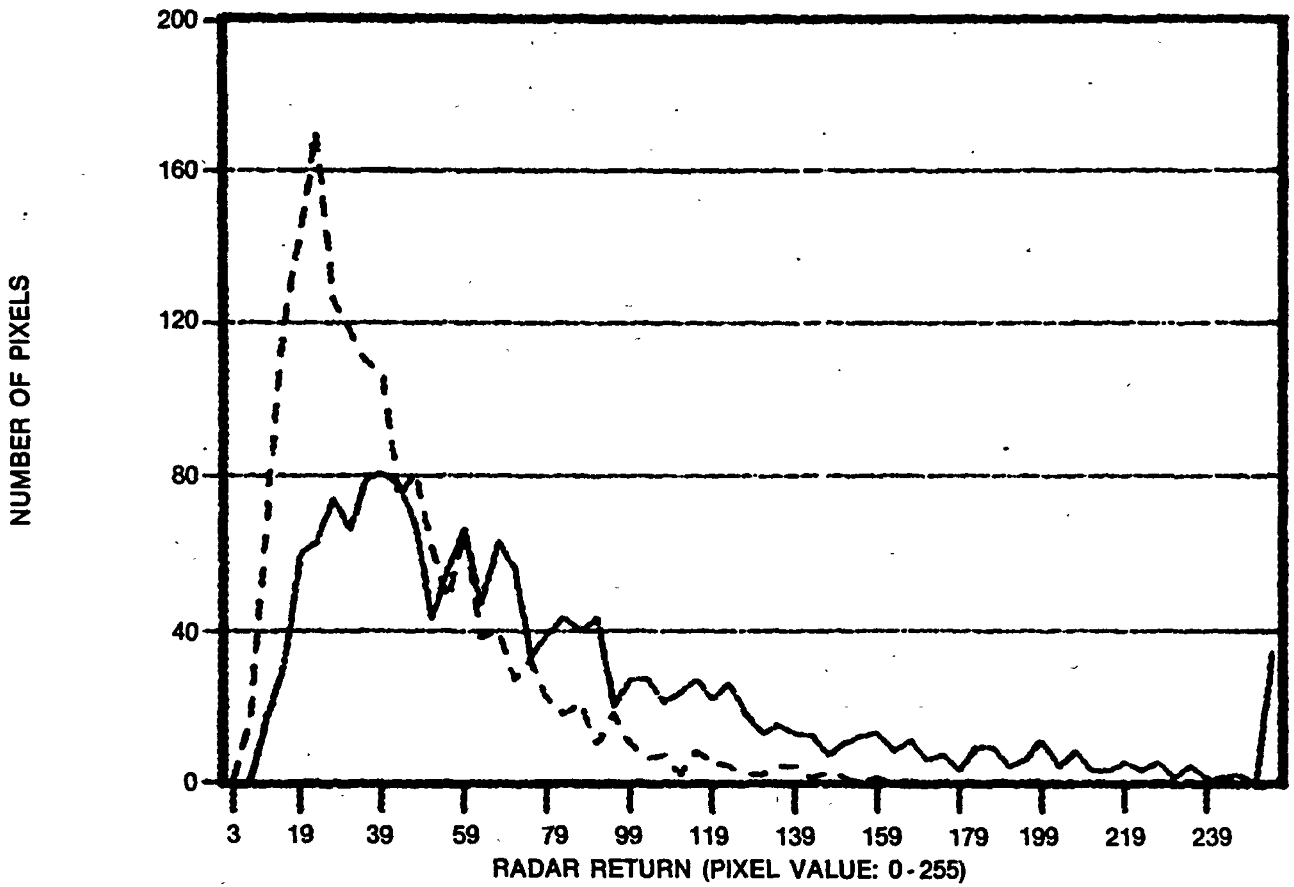

O35LH0DB

________OCEAN: MEAN VALUE = 76.3 : SAMPLE SIZE = 1600

.............OIL: MEAN VALUE = 39.1 : SAMPLE SIZE = 1600

Figure 67. Histograms of SAR L_{HH} returns from areas of oil and ocean in a range of depression angles from 46° to 46.5° for Pass 5 on November 3, 1978.

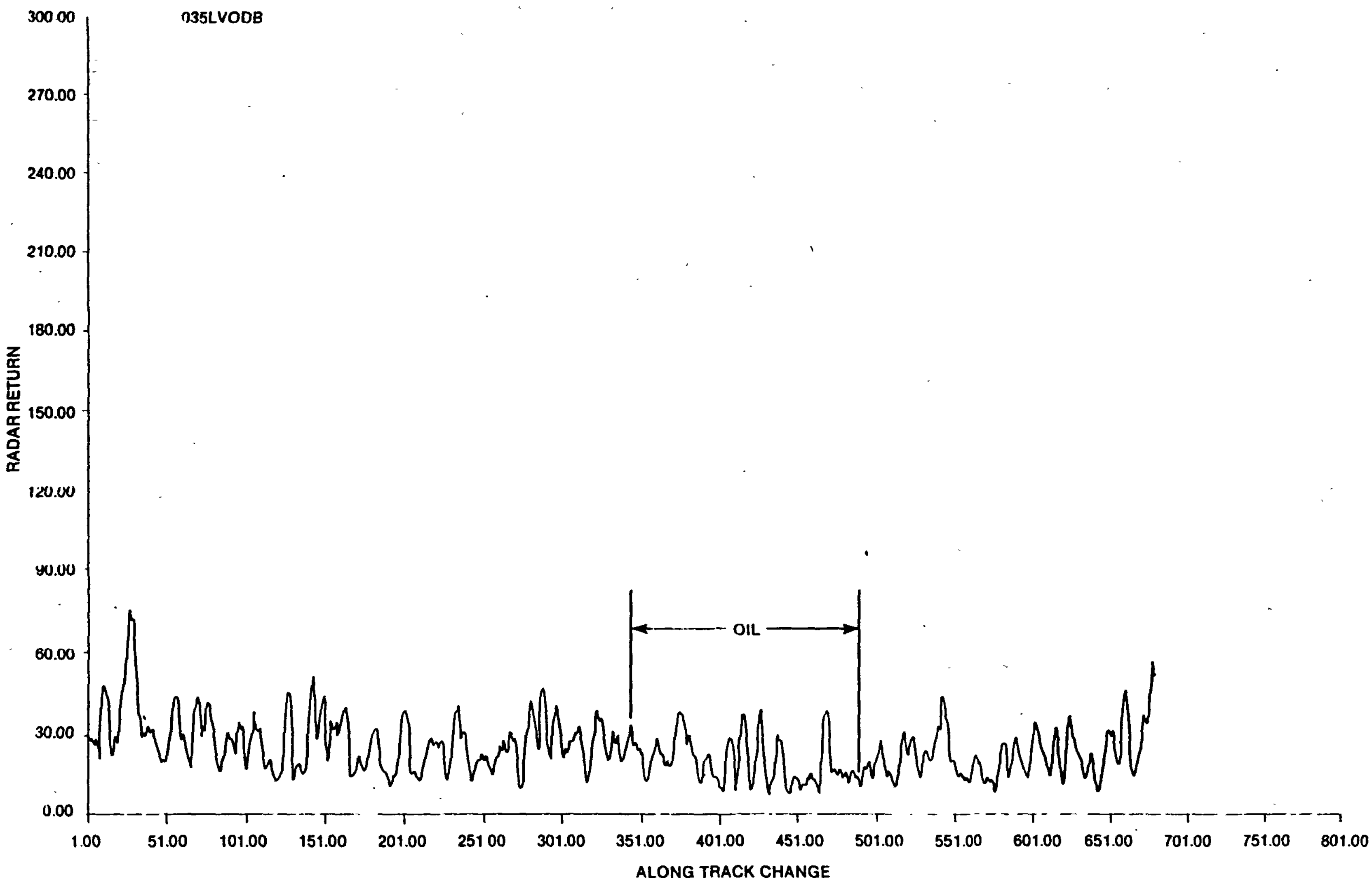

Figure 68. Filtered along track profile of SAR L_{HV} returns from oil and ocean for a depression angle of 47° for Pass 5 on November 3, 1978.

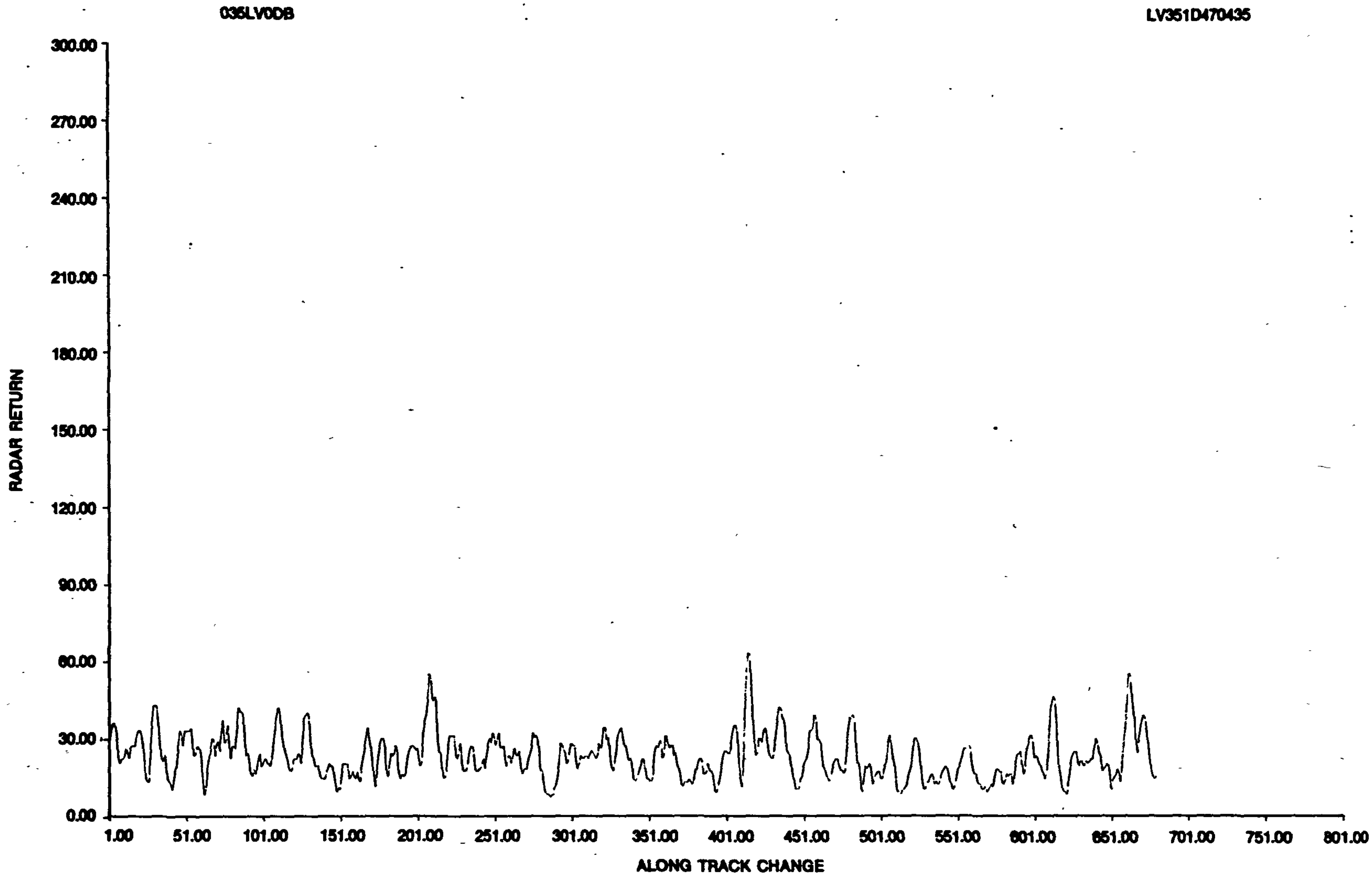

Figure 69. Filtered along track profile of SAR L_{HV} returns from oil and ocean for a depression angle of 43.5° for Pass 5 on November 3, 1978.

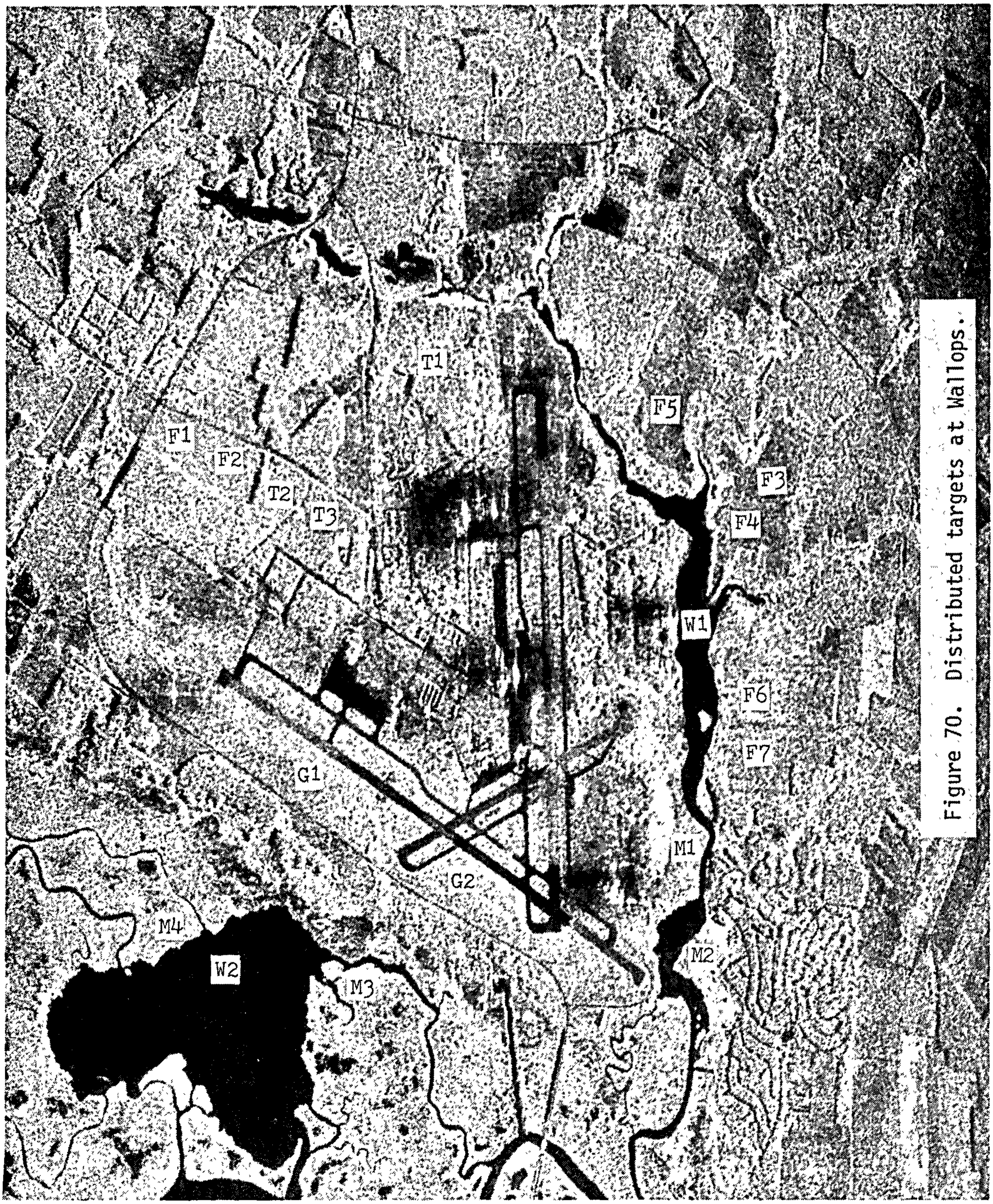

Figure 70. Distributed targets at Wallops.

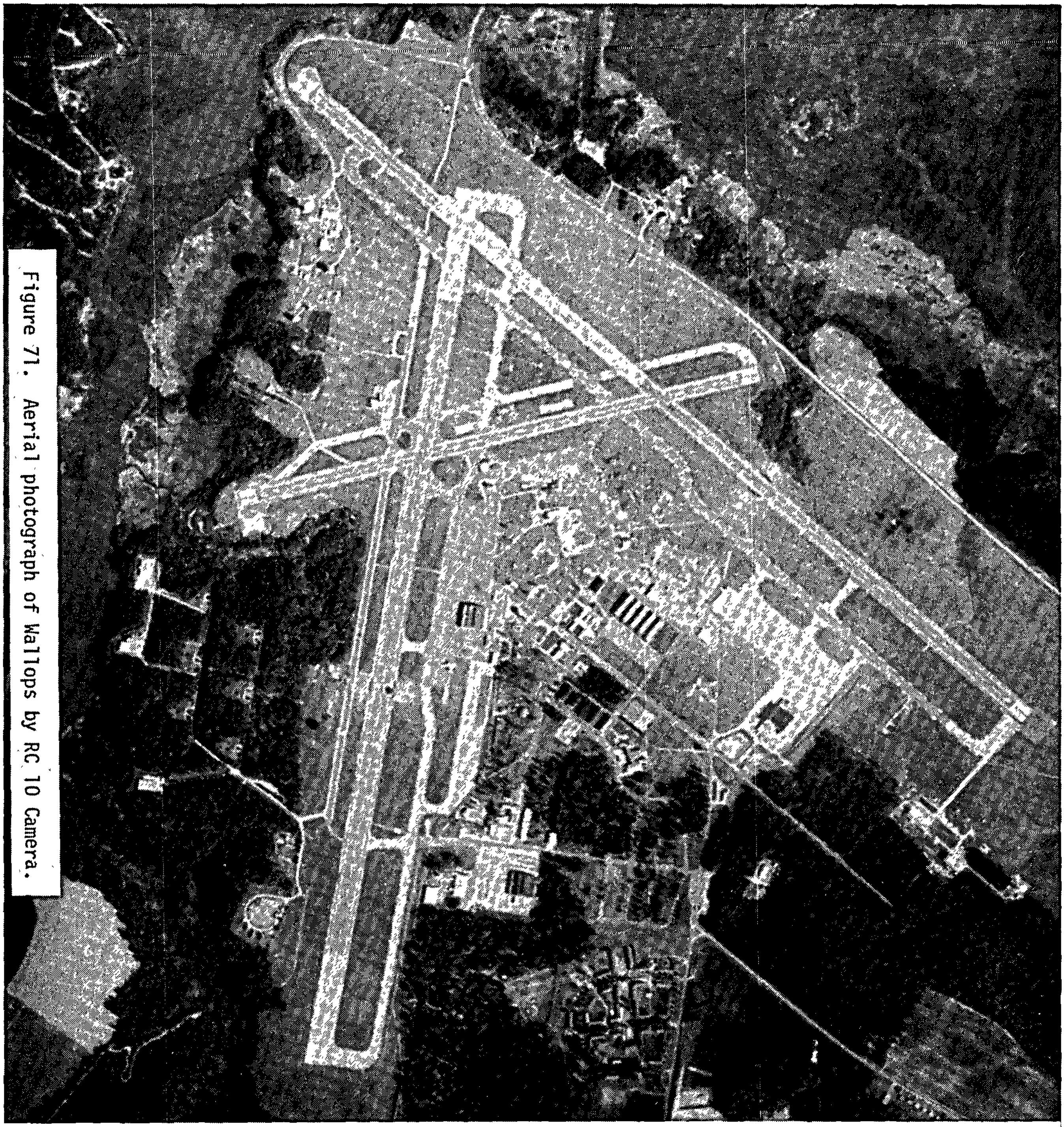

Figure 71. Aerial photograph of Wallops by RC 10 Camera.

GRASS - AREA G2 805

TAPE NO. = 4394 , SOURCE PROGRAM = ERIMSR

FIRST SCAN LINE = 2633 ** DATA SET NAME = W39KHODR
LAST SCAN LINE = 2716 ,SKIPPING 0 LINES, ** IMAGE(CHANNEL) = 1 OF 1
FIRST COLUMN = 1174 ** RADIANCE LEVELS = 256
LAST COLUMN = 1260 ,SKIPPING 0 COL'S, ** SPECTRAL RANGE = 31846.20 TO 31846.20 MICROMETERS

IMAGE 1

LEVEL	0	1	2	3	4	5	6	7	8	9	LN TOT	CUM TOT
30	0	0	0	0	1	0	0	0	1	0	2	2
40	3	0	2	1	1	4	4	3	5	5	28	30
50	5	7	5	4	7	9	8	4	12	3	64	94
60	10	11	13	9	13	11	17	14	14	15	127	221
70	21	23	19	22	25	29	13	25	37	24	238	459
80	13	21	23	32	23	24	36	24	44	33	273	732
90	30	38	27	26	31	45	34	41	47	37	356	1088
100	40	46	33	46	32	39	30	42	28	49	385	1473
110	43	51	43	46	48	46	47	44	39	36	443	1916
120	42	41	36	45	35	36	39	56	21	48	399	2315
130	43	41	40	47	26	58	46	30	44	55	430	2745
140	40	37	40	40	25	35	41	49	40	36	383	3128
150	40	40	38	39	38	54	47	21	37	52	406	3534
160	35	39	30	44	23	36	23	34	40	24	328	3862
170	45	34	32	29	35	31	27	31	26	30	320	4182
180	29	25	30	40	35	21	30	23	23	29	285	4467
190	25	32	13	23	21	34	26	26	20	23	243	4710
200	30	20	21	27	27	22	24	30	26	35	262	4972
210	21	20	21	30	15	25	20	21	18	24	215	5187
220	24	18	21	25	21	23	17	23	19	19	210	5397
230	25	19	20	20	18	19	15	16	17	29	198	5595
240	12	20	6	21	20	19	22	21	15	10	166	5761
250	17	22	20	24	12	1452					1547	7308

EQUAL AREA CUTOFF FOR 3 BINS ARE
132 206 255

STATISTICS	MEAN	VARIANCE	STANDARD DEVIATION
(N=1 WEIGHTING)	169.94	3845.38	62.01

Figure 72. SAR returns from subarea of Target G2.

HISTOGRAM OF DISTRIBUTION 805

DATA STARTS AT 30 AND ENDS AT 255
NUMBER OF CLASS INTERVALS 76
INTERVAL SIZE = 3

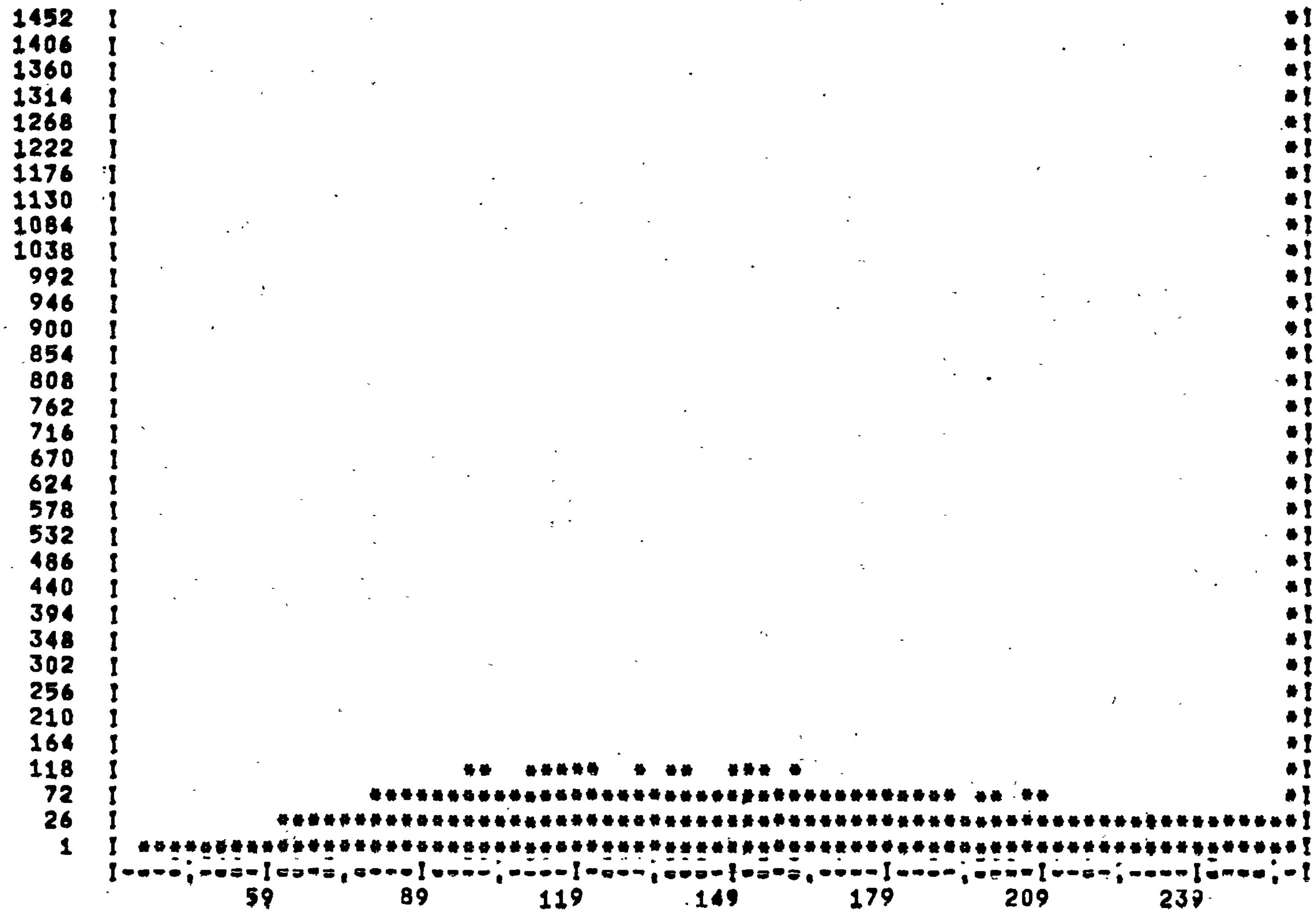

W39XHODB IMAGE 1

Figure 73. Histogram of SAR returns of Figure 72.

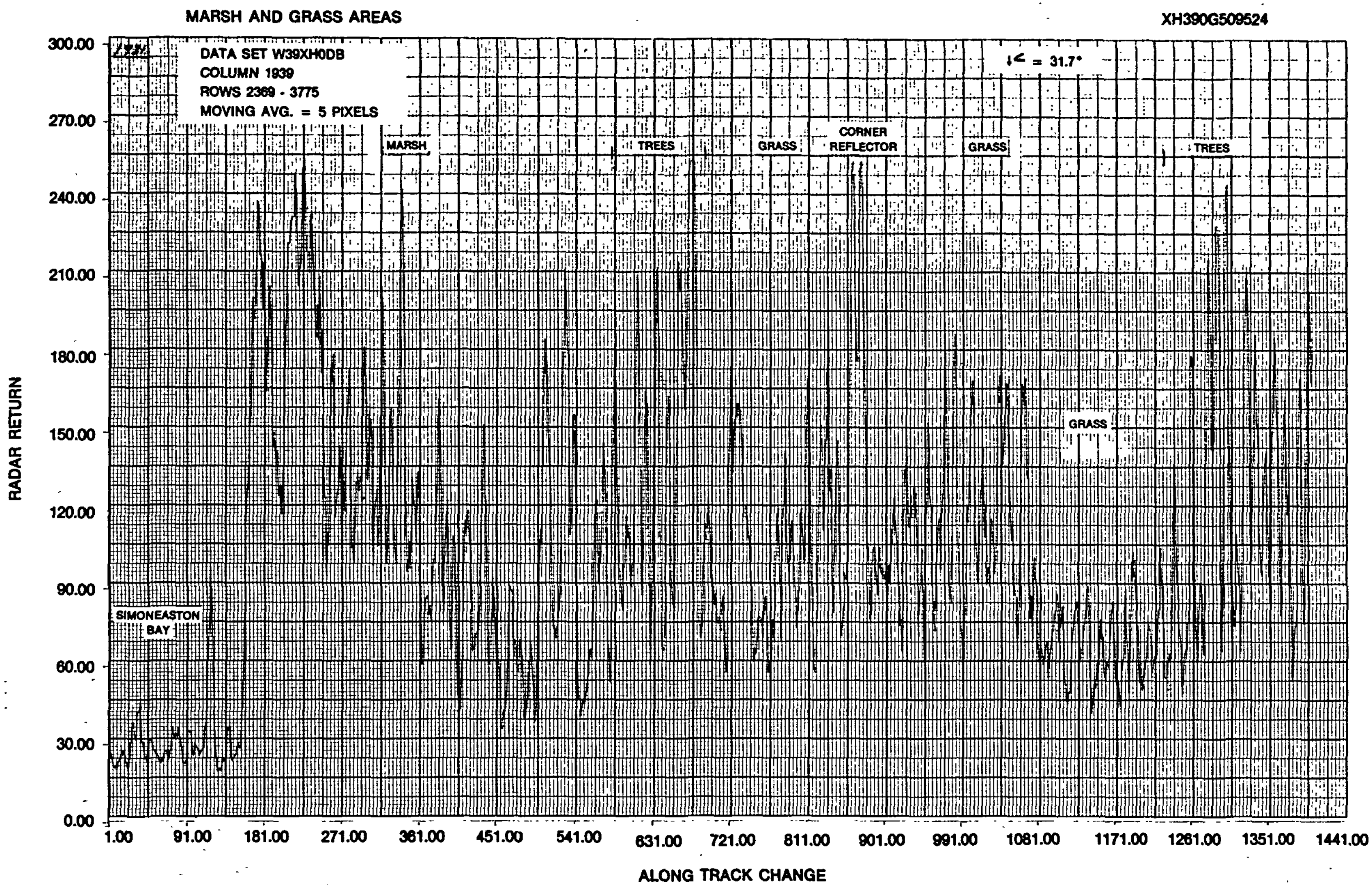

Figure 74. Filtered along track profile of SAR X_{HH} returns from distributed targets at Wallops at a depression angle of 31.7° for Pass 9 on November 3, 1978.

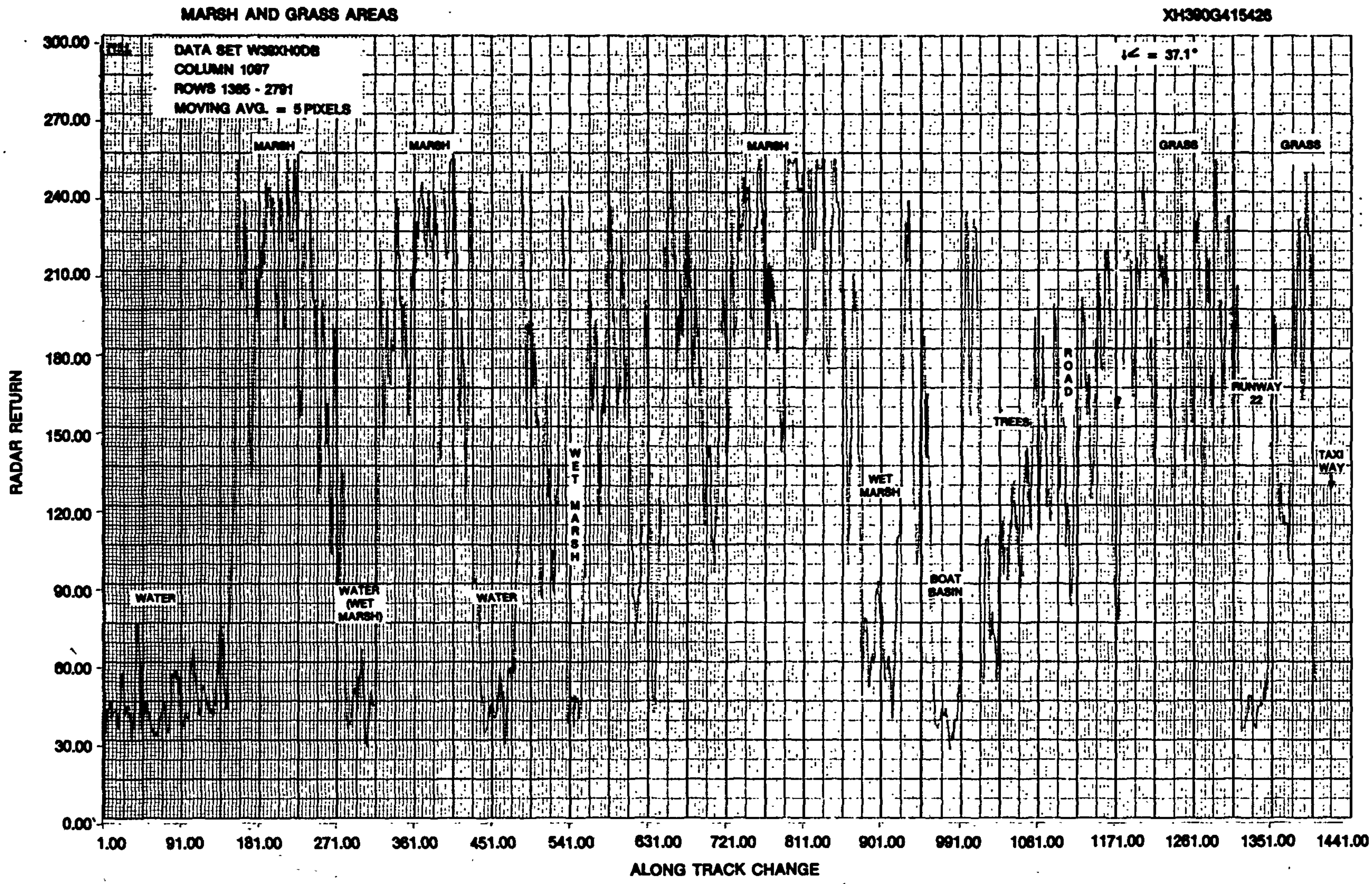

Figure 75. Filtered along track profile of SAR X_{HH} returns from distributed targets at Wallops at a depression angle of 37.1° for Pass 9 on November 3, 1978.

1. Report No. NASA TM-84419	2. Government Accession No.	3. Recipient's Catalog No.
4. Title and Subtitle AN ATLAS OF NOVEMBER 1978 SYNTHETIC APERTURE RADAR DIGITIZED IMAGERY FOR OIL SPILL STUDIES		5. Report Date December 1982 6. Performing Organization Code
7. Author(s) H. E. Maurer (NASA Goddard Space Flight Center) W. Oderman (Computer Sciences Corporation) W. F. Croswell (Harris Corporation)		8. Performing Organization Report No.
9. Performing Organization Name and Address National Aeronautics and Space Administration Goddard Space Flight Center Wallops Flight Facility Wallops Island, VA 23337		10. Work Unit No. 11. Contract or Grant No.
12. Sponsoring Agency Name and Address National Aeronautics and Space Administration Washington, DC 20546		13. Type of Report and Period Covered NASA Technical Memorandum 14. Sponsoring Agency Code
15. Supplementary Notes		

16. Abstract

A data set is described which consists of digitized synthetic aperture radar (SAR) imagery plus correlative data and some preliminary analysis results. This data set should be of value to experimenters who are interested in the SAR instrument and its application to the detection and monitoring of oil on water and other distributed targets. The SAR imagery was acquired during field experiments conducted during November 2 and 3, 1978.

17. Key Words (Suggested by Author(s))	18. Distribution Statement
Oil Slicks Remote Sensors Synthetic Aperture Radar	Unclassified - Unlimited STAR Category 15

19. Security Classif. (of this report)	20. Security Classif. (of this page)	21. No. of Pages	22. Price*
Unclassified	Unclassified	106	

*For sale by the National Technical Information Service, Springfield, Virginia 22151

National Aeronautics and
Space Administration

Goddard Space Flight Center
Wallops Flight Facility
Wallops Island, Virginia 23337

Official Business
Penalty for Private Use, $300

SPECIAL FOURTH CLASS MAIL
BOOK

Postage and Fees Paid
National Aeronautics and
Space Administration
NASA-451

U.S.MAIL

NASA

POSTMASTER: If Undeliverable (Section 158
Postal Manual) Do Not Return